Norges miljø- og
biovitenskapelige
universitet

Master thesis 2017 60 credits

Department of chemistry, biotechnology and food science
Supervisor: Vincent Eijsink

Eggshell membrane as an extracellular matrix environment for enhancing wound healing

Christian R. Wilhelmsen
Master in biotechnologi, molecular biology

Acknowledgements

The work presented in this thesis was done from February 2017 to December 2017 at Nofima AS, commodity and process department. Supervisors at Nofima have been Mona E. Pedersen and Sissel B. Rønning. Supervisor at NMBU has been Vincent Eijsink. The project is a collaboration between Nofima AS and Biovotec AS and has received financial support from forskningsrådet (NFR 235545).

My most sincere gratitude to my two Nofima supervisors, Mona E. Pedersen and Sissel B. Rønning for their continuous supervision, guidance and advice in the course of this master thesis. My warmest thanks to everyone at Nofima AS and especially to Ragnhild S. Berg and Vibeke Høst for brilliant advice, patient teaching and enduring support throughout the whole process. I would also like to express my gratitude to my NMBU supervisor Vincent Eijsink for guidance and availability during the conduct of this master thesis. Further, sincere thanks to the coffee machine at Nofima for its fundamental contribution in maintaining alertness and focus throughout the thesis. I have learned so much from this project, and I am deeply thankful to all of you. A special thank you also goes out to my parents and siblings for continuous support, and my friends for disrupting my work when a break was sorely needed. Last but not least, my warmest thanks go to Dr. Linn Nathalie Støme and Dr. Feter Mellbye for their excellent and enlightening comments to the structure and language of this Master thesis.

Norges miljø- og biovitenskapelige universitet

Ås, 12.12.2017

_____

Christian R. Wilhelmsen

Sammendrag

Kroniske sår og behandling av disse utgjør en av de største utgiftene innenfor medisin i dag. Diabetes resulterer ofte i kroniske sår, og med en økende eldre befolkning med diabetes, vil det økonomiske presset kun fortsette å stige. En måte å motvirke dette på er å utvikle nye og bedre lavkostnadsprodukter til behandling av sår som kan komme ut på markedet. Bruken av eggeskall-membran til sårheling har vært kjent i østlig medisin i flere hundre år, og nyere forskning har demonstrert en positiv effekt på sårheling. På grunn av dette er det et insentiv for å videreføre denne forskningen, og forstå hvilke effekter eggeskall-membran som ingrediens kan ha i en sårhelingsprosess, og i hvilken form eller type produkt det bør inngå i.

Målet med denne oppgaven er å undersøke effekten av prosessert eggeskallmembran-pulver (PEP) på fibroblastceller fra hud.

Eksperimenter ble gjennomført i 2D og 3D miljøer. I 2D ble humane dermale fibroblast celler sådd ut i celle kulturer og stimulert med PEP. Forsøk ble gjennomført med forskjellige konsentrasjoner og ved ulike tidspunkter, og deretter ble celleresponsen undersøkt ved å studere levedyktighet, cellevekst og spesialisering, cytotoksisitet, samt real-time PCR og western blotting av ulike cellemarkører. Ulike typer scaffolds som var implementert med eggeskall-membran, kollagen eller PEGDA ble karakterisert med tanke på struktur. Disse scaffoldene ble også brukt til å undersøke cellevekst.

Våre resultater viste at fibroblastcellene var levedyktige ved lave doser av PEP behandling, mens levedyktigheten ble redusert ettersom PEP-konsentrasjonen økte. Videre fant vi at PEP behandling stimulerte celleveksten og stress respons i fibroblast cellene. Ulike typer scaffold, produsert med varierende mengder ESM ble karakterisert ved hjelp av scanning electron mikroskopi, og ved hjelp av denne metoden var vi i stand til å vise hvordan inkludering av de forskjellige komponentene påvirket den strukturelle integriteten. Til sist brukte vi fluorescens mikroskopering for å undersøke cellevekst i de ulike scaffoldene.

Våre resultater viser at ESM og PEP har gunstige effekter på fibroblaster, både i 2D og 3, og at dette materialet har stort potensiale som ingrediens i scaffold brukt vevsregenerering

Abstract

Treatment of chronic wounds is one of the largest expenses in medicinal practice today. With increased accounts of diabetes which often results in chronic wounds, and a growing elderly population with diabetes, this economic pressure will only continue to grow. One way to prevent this is to bring new and improved low-cost products to the marked. The use of eggshell membranes for wound healing has been found in eastern medicine for hundreds of years, and recent scientific reports have demonstrated its positive effect on wound healing. As such, there is an incentive to further study the effect eggshell membranes may have in a wound healing process, and to find type of product it may be incorporated into.

The goal of this thesis is to study the effect of processed eggshell membrane powder (PEP) on fibroblast cells derived from human skin.

Experimentation was conducted in 2D and 3D environments. For 2D, human dermal fibroblast cells were seeded into cultures and stimulated with PEP. Using different concentrations and time periods of treatment, the cell response was studied through cell viability, growth and specialization, cytotoxicity, in addition to real-time PCR and western blotting of different markers. Different types of scaffolds containing collagen, eggshell membrane or PEGDA was characterized by structure. These scaffolds were also used to study cell growth in a 3D environment.

Our results show that fibroblast cells maintained a suitable level of viability when treated with lower doses of PEP. Cell viability was reduced with increasing PEP concentrations. Further, we found that PEP treatment stimulated cell growth and stress response in fibroblast cells. Different types of scaffolds produced with variable concentrations of ESM was characterized using scanning electron microscopy. Using this method, we were able to show how the different components introduced affected the scaffolds structural integrity. Finally, we used fluorescent microscopy to study cell growth in the different scaffolds.

Our results show that ESM and PEP provides favourable effects to fibroblast cells, both in 2D and 3D environments. ESM shows great potential as an ingredient in tissue regeneration.

Abbreviations

2D	2-Dimensional
3D	3-Dimensional
α-SMA	Alpha smooth muscle actin
AEBSF	4-(2-aminoethlyl) benzenesulfonyl fluoride hydrochloride
ATP	Adenosine triphosphate
Au/Pd	Gold/Palladium
BSA	Bovine Serum albumin
$CaCl_2$	Calcium chloride
CREMPs	Cysteine-rich eggshell membrane proteins
CS	Chondroitin Sulphate
CY3	Carbocyanine 3
dH2O	Distilled water
DMEM	Dulbecco Modified Eagle Medium
DMSO	Dimethyl sulfoxide
D-PBS	Dulbecco's phosphate-Buffered Saline
ECM	Extracellular Matrix
EDTA	Ethylenediaminetetraacetic acid
Ef-1α	Elongation factor-1alpha
ESM	Eggshell Membrane
EthD-1	Ethidium Homodimer-1
EtOH	Ethanol
FBS	Fetal Bovine Serum
GAG	Glycosaminoglycan
HA	Hyaluronic acid
HCl	Hydrogen chloride
Hsp70	Heat shock protein 70
Ki67	Kiel 67
LAF-bench	Laminar flow cabinet
LDH	Lactate dehydrogenase
MgCl2	Magnesium chloride
MMP	Matrix metalloproteinase

NaCl	Sodium chloride
NaF	Sodium fluoride
PEGDA	Synthetic macromer polyethylene glycol diacrylate
PenStrep	Penicillin Streptomycin
PEP	Powdered eggshell membrane
PIPES	Piperazine-N,N'-bis(2-ethanesulfonic acid)
RT- PCR	Real-time polymerase chain reaction
RIPA	Radioimmunoprecipitation assay buffer
RPM	Rounds per minute
RT	Room temperature
SDS	Sodium dodecyl sulphate
SEM (1)	Scanning electron microscopy
SEM (2)	Standard error of the mean
TBS-T	Trisbuffered saline with Tween 20
TGF	Transforming growth factor
TIMP	Tissue inhibitor of metalloproteinase

Table of contents

1. Introduction

The economic cost of wound care to society is tremendous. On a world-wide scale, it is considered a multibillion-dollar problem. In the UK alone, the cost of chronic wound treatment accounted for more than 5% of the entire National Health Services (NHS) budget of 2017. In the US, the cost of chronic wound treatment accounts for ~$20 billion annually. (Järbrink et al., 2017). In 2007 it was reported that this number was more than $3 billion each year, which suggests a rapidly growing trend (Menke, Ward, Witten, Bonchev, & Diegelmann, 2007). In Norway, chronic leg ulcers accounted for 600 million NOK in 2012 (Rønsen, 2012). People suffering from chronic wounds have a reduced life quality caused by physical discomfort, functional limitations and physical distress, and chronical wounds can in worse cases lead to amputations and shorter life-span (Augustin, 2013; Järbrink et al., 2017). Diabetes is one of the leading causes of chronic wounds, and the number of people suffering from this illness has seen an alarming increase over the last decades, incrementing with almost 400% from 1980 to 2014 (World Health Organization, 2017). In addition to relevant illnesses, the risk of chronic wounds increases with age. At this time, products available for wound healing are expensive, so then facing an aging population, together with an increased incidence of diabetes (and related acute and chronic wounds), the wound care marked is set for continued growth (Gould et al., 2015). But to cope with these challenges as a society under restricted health budgets, there is an apparent need to develop efficacious, low cost products for treating chronic wounds.

1.1 The anatomy of human skin

The human skin consist of three layers (figure 1.1); the outer epidermis layer, the dermis which makes up the majority of the skin, and the hypodermis located deep in the tissue (Rittiè, 2016). The epidermis is a stratified epithelium that functions as barrier to avoid mechanical stress, dehydration and the infection of microorganisms (Sotiropoulou & Blanpain, 2012). The dermis consists of connective tissue made up from connective tissue proteins such as various types of collagens and elastin. This tissue provides the skin with mechanical strength and elasticity. The dermis functions as a supportive tissue that contains numerous blood vessels set to provide nutrients and oxygen to the keratinocytes, melanocytes and other cells located in the epidermis layer. The hypodermis, or subcutis, consists primarily of adipose fat cells. The subcutis layer stores nutrients, but also provides isolation and shock absorption to the body (Wyller, 2016). The cells that form the tissues maintains mechanical strength through the production of an extracellular matrix (ECM) that functions as a scaffold (Frantz, Stewart, & Weaver, 2010). ECM consists of fibre- and non-fibre-forming structural molecules, as well as matri-cellular proteins important for cell-matrix interactions (Tracy, Minasian, & Caterson, 2016).

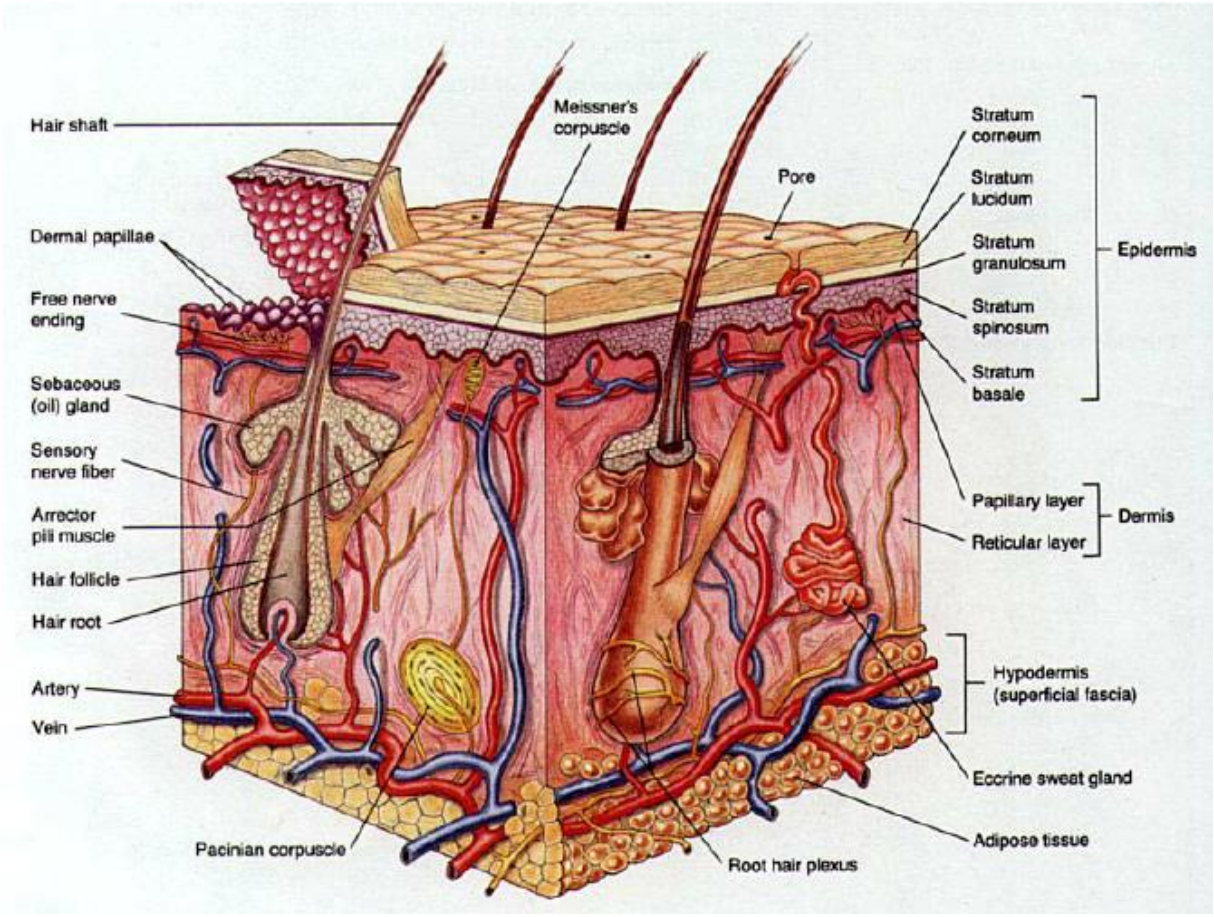

Figure 1.1: The structure of human skin. *Displays the constitution of mammalian skin structure. Included are the three layers of the skin; epidermis which consists five thin layers or strata, the dermis which consists of two layers; the papillary layer and reticular layer, and finally the hypodermis (subcutis) which consists of adipose fat tissue. Additional components of the skin are also included, such as the location of hair follicles and roots, and where arteries are situated in the skin. Figure is reproduced from (Dario et al., 2003).*

1.2 Wound healing

Any damage to the skin, as a cut, through burning or other causes, will cause an activation of the epidermal healing process latent in the human skin. During wound healing, the epidermis is restored through nutrients, mechanical support and progenitor cells supplied from the inner layers (Rittiè, 2016). This process of repairing damaged tissue is commonly divided into three overlapping phases; namely inflammation, tissue formation and remodelling (figure 1.2) (Darby, Laverdet, Bonté, & Desmoulière, 2014; Hu et al., 2014; Rittiè, 2016; Tracy et al., 2016).

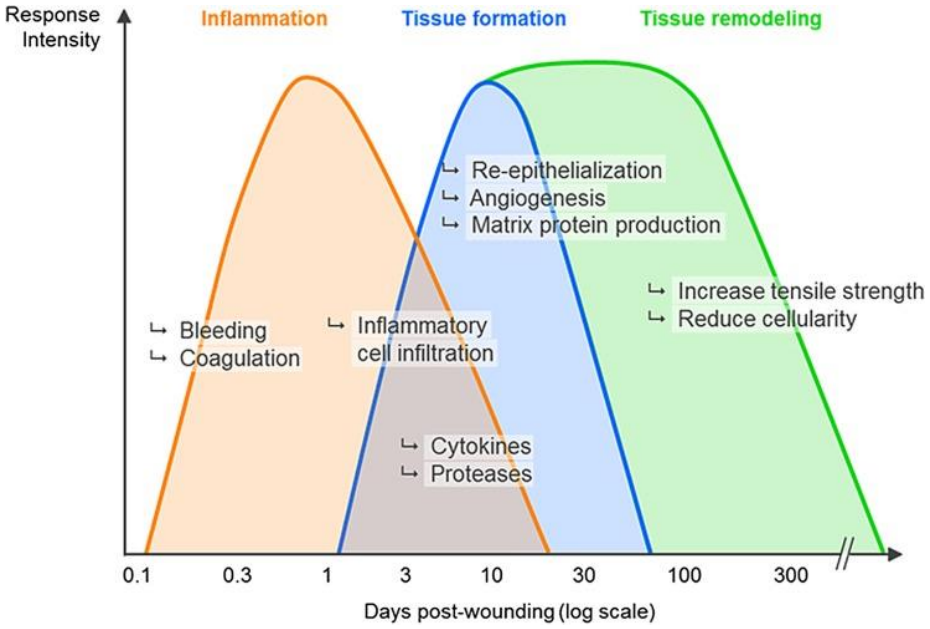

Figure 1.2: The various phases of wound healing. *The process begins with hemostasis, followed by the inflammatory response where the wound is cleansed. The tissue formation phase consists of repairing the wound site. The tissue remodelling phase gradually turns off the different processes that were used in the previous phases, and normalises the wound site. As can be seen in the graph, these phases strongly overlap. Figure is reproduced from (Rittiè, 2016).*

1.2.1 Inflammation

The inflammatory phase is the initial response to damage to the capillaries, which results in the removal of any foreign cells and molecules from the wound (Darby et al., 2014; Rittiè, 2016). The inflammation causes platelet activation that leads to an increase of fibrin and fibronectin at the targeted location (Rittiè, 2016). This accumulation results in the formation of a blood clot that provides the damaged area with a temporary defence against foreign substances, as well as enabling a suitable provisional matrix for cell movement during repair (Darby et al., 2014; Martin, 1997). The activated platelets initiate a release of a large number of chemokines that assist in recruiting a variety of innate immune cells required for the tissue repair, such as inflammatory cells, neutrophils, phagocytes, macrophages and T lymphocytes (Darby et al., 2014; Su & Richmond, 2015).

1.2.2 Tissue formation

As the different phases in wound healing are largely overlapping, certain components included in one phase also holds importance for another. One example of this is the macrophages. As briefly touched upon in the previous section, during the inflammatory phase the macrophages releases cytokines and thereby assist in promoting inflammation. Another task they perform is to remove any cell destined for apoptosis, thereby assisting in the reduction of inflammation during the tissue formation stage (Guo & DiPietro, 2010). As the healing process moves from the inflammation stage into the tissue

formation stage, the macrophages are phenotypically transformed into a state where their secreted cytokines react with keratinocytes, fibroblasts and endothelial cells to promote angiogenesis and tissue regeneration to restore the vascular perfusion (Darby et al., 2014; Guo & DiPietro, 2010). Epithelial proliferation and migration occurs across the provisional matrix within the wound, while at the same time in the dermis, endothelial cells will support capillary growth. Meanwhile, fibroblast cells will colonize the provisional matrix through secretion of ECM-cleaving matrix metalloproteinases (MMPs) and produce immature ECM variants, in the form of collagen- and cellular fibronectin-rich components (Bielefeld, Amini-Nik, & Alman, 2013). This initiates the formation of the granulation tissue at the wound site, which consists of fibroblast cells and small capillaries in a loose ECM. The initial granulation tissue is loosely built, but over time it will grow stronger following collagen secretion by the fibroblast cells (Krafts, 2010). As the granulation tissue progresses during the wound healing process, the change in composition promotes differentiation of resident fibroblast cells into myofibroblasts through a feedback mechanism (Rittiè, 2016). Once the granulation tissue is populated with myofibroblasts, wound contraction will occur (Hinz, Mastrangelo, Iselin, Chaponnier, & Gabbiani, 2001).

1.2.3 Remodeling

During the final phase, all the processes required in the previous phases are gradually switched off. This phase attempts to normalize the wound site to mimic the composition as close as possible to how it was prior to wounding (Rittiè, 2016). The granulation tissue is remodelled and is further used as a substrate for ECM formation. Synthesis of ECM components are reduced, while at the same time the already synthesized components are modified into the matrix. Collagen III, which is a major component of the granulation tissue, is replaced with Collagen I (Krafts, 2010). Elastin, which is absent in the granulation tissue during the earlier stages, is synthesized and secreted by fibroblast cells to provide skin elasticity (Mithieux & Weiss, 2005). The number of vascular cells and myofibroblast cells is reduced through apoptosis (Darby et al., 2014). The success of wound healing may depend on the age and physical constitution of the patient, as well as the type of tissue damaged (Hu et al., 2014). There are many factors which may inhibit proper wound healing, but the three most common causes are diabetes, ulcers and venous stasis. Although these conditions differ in the specifics, the common denominator is that degradation of tissue is higher than the synthesis, resulting in impaired wound healing. Restoring the balance between these two factors is an important aspect to include when designing any wound healing product (Menke et al., 2007).

1.3 Fibroblast and myofibroblast cells

Fibroblast cells are the most abundant cell type found the human dermis (Tracy et al., 2016). These cells are present in uninjured tissue where they regulate the turnover of ECM (Li & Wang, 2011). They are largely heterogenous and can differ greatly depending on what tissue they are located in (Rittiè, 2016). One factor that may vary is the expression of collagen I and III proteins. These structural proteins may differ both in quantity and ratio depending on how deep into the dermis the fibroblasts are located, the type of tissue they are expressed in and the developmental stage of the wounded organism (Hu et al., 2014; Krafts, 2010; Tracy et al., 2016). Fibroblast cells are considered to be one of the most important cellular factors in wound healing. They are responsible for breaking down the fibrin clot by producing various metalloproteinases (MPPs) and replacing it with collagen and elastin, or other ECM structures (Bainbridge, 2013). Fibroblast cells also generate and deposit suitable types of growth factors depending on the endogenous stimuli presented to them, as well as promoting wound contraction after differentiation (Hinz, Mastrangelo, et al., 2001; Hu et al., 2014).

1.3.1 Fibroblast & Myofibroblast Activity

The fibroblast cells migrate to the wounded area during the end of the inflammation phase (24-48 hours following injury) through attraction to chemo-attractants resident in the provisional matrix or produced by other cells during the inflammatory phase. Fibroblast cells attaches to fibrous proteins on the ECM through stimulation from transforming growth factors (TGF-β1 & TGF-β2). These TGF-β's activates the fibroblasts and causes them to differentiate into the intermediate phenotype promyofibroblast cells. Promyofibroblast cells increase adhesion to the ECM and begin to express and lay down the initial collagen bundles (Rittiè, 2016). Following exposure to the transforming growth factors, promyofibroblast cells are further differentiated into myofibroblasts (Bainbridge, 2013). Once differentiated, the myofibroblast cells begin synthesizing ECM components such as Collagen I-IV and XVIII, glycoproteins and proteoglycans that play an important role in growth differentiation and wound repair (figure 1.3) (Guo & DiPietro, 2010; Li & Wang, 2011). Myofibroblast cells also contribute by synthesising and secreting glycosaminoglycans (GAG) most notably the Hyaluronic acid (HA) which plays an important role in ECM structure, as well as matrix-modifying proteins like matrix metalloproteinases (MMPs) and the MMP tissue inhibitors (TIMPs) (Hu et al., 2014; Li & Wang, 2011).

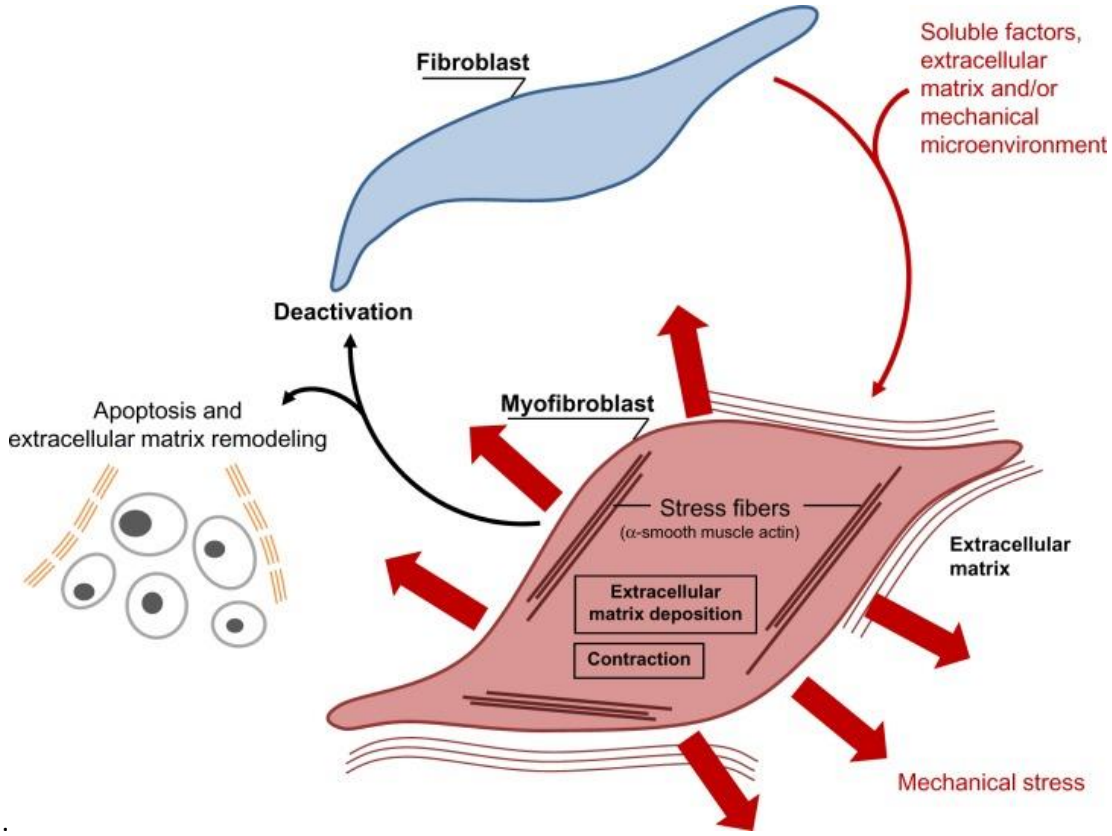

.

Figure 1.3: Schematic illustration of fibroblast activation and differentiation into myofibroblast cells. *Differentiation from fibroblast to myofibroblast involves the intermediate phenotype promyofibroblast. The myofibroblast is downregulated through apoptosis or deactivation into fibroblast. The latter has not been clearly demonstrated in vivo. Figure is reproduced from (Darby et al., 2014).*

Myofibroblasts are characterized by their expression of α-smooth muscle actin (α-SMA), which helps the cell to form cell-matrix and cell-cell adherins, in addition to providing it with increased contractile power compared to normal fibroblasts located in healthy tissue. α-SMA, in addition to actin filaments expressed during differentiation are vital for both migration and contraction of the wound during the final stages of wound healing (Bainbridge, 2013). Wound contraction is caused by promyofibroblast- and myofibroblast-containing granulation tissue generating contractile forces through shortening and compacting collagen fibres. These forces are proportional to the volume of the granulation tissue, meaning that large wounds will have a higher contraction rate than smaller wounds (Rittiè, 2016). During the end of the wound healing process, myofibroblasts are meant to go through apoptosis. This is an important aspect of the process, because the persistence of myofibroblast cells may lead to over-production of ECM and excessive scarring (Darby et al., 2014; Li & Wang, 2011).

1.4 Stress indication in cells during wound healing

During wound healing, cells present in skin tissue will exhibit reactive stress indications as a result of the situation. One of these indications involve the increased expression of heat shock proteins (HSP). These proteins appear in an abundance of different phenotypes, and respond to a wide variety of

cellular stress, including apoptosis inhibition, reducing oxidative damage and supressing the inflammatory response. During normal conditions, the role of HSPs involve acting as molecular chaperones, facilitating protein folding, preventing protein aggregation, and degradation targeting. The HSP proteins are expressed in low amounts during normal physiological conditions, but will show a dramatic increase when cells are exposed to stressful conditions, such as tissue damage. During tissue injury, these proteins may assist in maintaining synthesis and proper conformation of proteins, as well as repairing damaged proteins and promote tissue healing with its anti-inflammatory and pro-proliferative effects (Atalay et al., 2009). Hsp70 is an important member of the HSP family and is commonly involved in wound healing, where they show a large increase in protein expression. However, when observing expression in chronic wounds there is little to no expression (Oberringer et al., 1995).

1.5 Extra cellular matrix (ECM)

The ECM is secreted by an abundance of cells and provides a scaffold for cells to further proliferate and migrate into the healing wound. The ECM consists of various building blocks that provide mechanical strength, as well as a charged, dynamic and active space suitable for the cells. There are receptors as integrin and syndecan on the cell surface that interact with the ECM through signalling (figure 1.4) (Tracy et al., 2016).

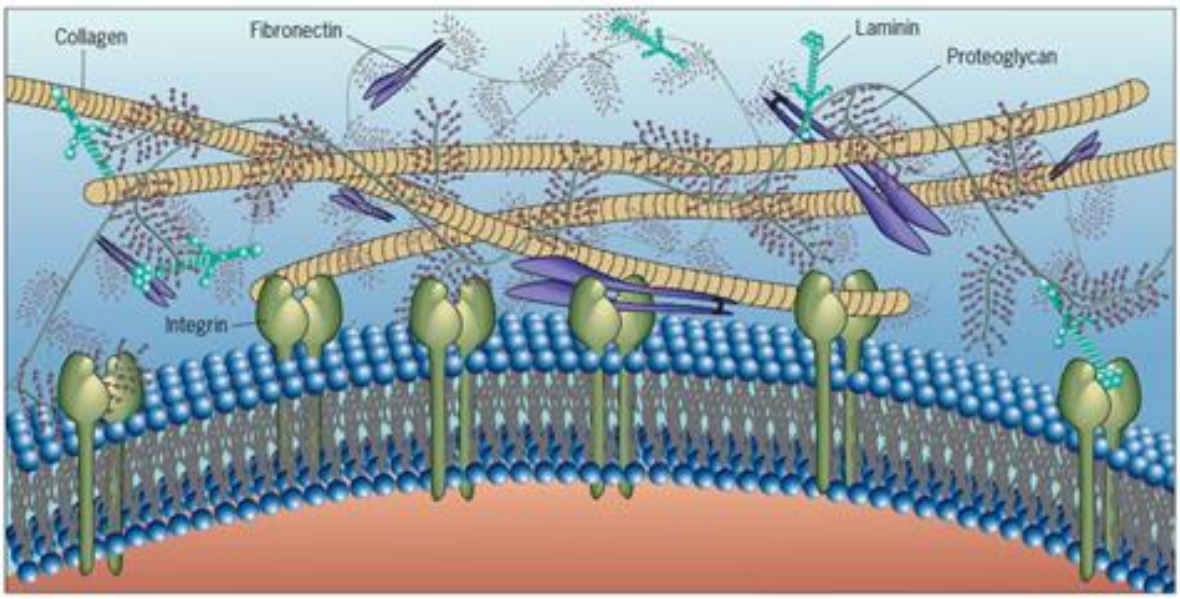

Figure 1.4: Constitution of extracellular matrix. *An overview of how the ECM components are situated in comparison to each other and towards the cells they encircle. Fibronectin, collagen and laminin each have binding sites for each other. They also contain binding sites for receptors located at the cell surface. Proteoglycans are large polysaccharide complexes that occupy the majority of the extracellular space. Figure is reproduced from (Karp, 2010).*

1.5.1 ECM components

Collagens

Collagen proteins are defined by a triple-helical organization of component pro-α-chains that provides the proteins with their unique physical properties (Rozario & DeSimone, 2010). They assist the ECM structure with tensile strength, regulating the cells adhesion to the ECM, support chemotaxis and migration, and regulate tissue development (Frantz et al., 2010). Collagen proteins are the most abundant in the human body and are found as a major component in bone, cartilage, skin, ligament and tendon (Hu et al., 2014). 28 different types of collagen proteins have been identified, but only a handful of these are present in the skin. Collagen I and III are by far the most abundant, accounting for about 90% and 10% of the total amount, respectively. Collagen V accounts for about 2%, while some others (collagen IV, VII and XVII) may be present in lower concentrations (Tracy et al., 2016). It should be noted that the ratio between collagen I & III displays a far higher proportion of collagen III in fetal skin. Fetal wounds results in scarless repair, and it has been speculated that this shift in ratio might be partly responsible (Hu et al., 2014).

Fibrillar collagens

Collagens are broadly divided into fibrillar and non-fibrillar families (Rozario & DeSimone, 2010; Tracy et al., 2016). Collagen I-III & V are part of the fibrillar family and responsible for fibroblast function and mechanical stress. The presence, absence and ratio of these collagens may affect scar forming, wound contraction and structural abnormality in collagen fibrils. The different types of these fibrillar collagens may regulate the synthesis and assembly of the others. Tracy *et al*. state that collagen III and V may regulate the synthesis and assembly of collagen I, respectively (Tracy et al., 2016).

Non-fibrillar collagens

Collagen IV, VI-VIII and XIV are part of the non-fibrillar collagen family. Instead of forming fibrils, they compose reticular nets that connect cells to the basement membrane or aid in the organization and fibre-size of other collagens fibres, thereby regulating the strength of the fibrillar collagens (Tracy et al., 2016).

Elastin

Collagen and other fibre-forming proteins provide the ECM with its rigid morphology important for maintaining the integrity of the scaffold. However, it is also important for the ECM to maintain a certain level of flexibility and elasticity to respond to physical forces with elastic recoil (Rozario & DeSimone, 2010). Elastin is an extremely durable biopolymer formed through lysine-mediated crosslinking of its

precursor tropoelastin. Elastin fibres are arranged into long cross-linked structures that intertwine with collagen fibres in the ECM, and provides elasticity and resilience in tissues. Tropoelastin can promote fibroblast cells to attach, spread and proliferate throughout the ECM (Tracy et al., 2016). Elastin comprises about 90% of the dry weight of elastic fibres and form its internal core. In addition to providing elasticity to tissues, elastin is known to contain receptors responsible for facilitating fibroblast proliferation and chemotaxis (Mithieux & Weiss, 2005).

Fibrin

During the initial stage of wound healing, fibrin proteins form the fibrin clot. Inflammatory cells uses this clot to migrate into the wound site (Frantz et al., 2010). Following the inflammatory phase, fibroblast cells uses this provisional clot matrix to migrate into the wound site and remodelling it later in the process. During the proliferation stage, the fibrin clot is broken down and its components replaced with ECM proteins, causing it to progress into a granulation tissue (Tracy et al., 2016). Failure to break down the fibrin clot is a common reason for leg ulcers, where the provisional matrix becomes corrupted and no longer supports reepithelialisation or granulation tissue formation (Clark, 2001).

Fibronectin

Fibronectin is a dimeric glycoprotein containing numerous binding sites, which makes it a unique responder during tissue damage. It is expressed by multiple cell types (Pankov & Yamada, 2002). Fibronectin is found in a soluble form in the plasma, and in an insoluble form in the ECM. During the wound healing process, fibronectin will bind to integrin expressed by fibroblast cells, which stimulates their migration to the wound site. Fibronectin is also responsible to bind and stabilize fibrin. Fibronectin is vital for ECM organization and stability by regulating deposition of structural proteins into the ECM, such as collagen I (Tracy et al., 2016).

Proteoglycans

Proteoglycans are non-fibre-forming molecules found in the ECM that are responsible for force dispersion through a negatively charged and hydrophilic composition. They form hydrated gels that permeates the majority of the extracellular interstitial space within the tissue. Proteoglycans consist of a protein core substituted with a variable number of unbranched polysaccharide chains, named glycosaminoglycans (GAGs) (Tracy et al., 2016). GAGs are divided into different types depending on their sulphated structure (CD, DS, KS and HS) and non-sulphated Hyaluronan acid (HA) (Lindahl U, 2017). HA is the only type that is not attached to a core protein. With the exception of HA, proteoglycans consist of one core protein covalently bound to GAG side chains. Proteoglycans are

extremely hydrophilic which enables the matrices generated by them to withstand compressive forces to a high extent (Frantz et al., 2010). Proteoglycans are divided into three categories; small leucine-rich proteoglycans (SLRP), modular proteoglycans, and cell-surface proteoglycans. Proteoglycans are responsible for maintaining structural integrity in the ECM, and also have shown to perform regulatory functions in signal transduction in various cellular processes (Schaefer & Schaefer, 2010). HA is one of the most common GAGs found in the human skin and is an important polysaccharide present in connective tissues. As a major component of ECM, its structure differs from other GAGs as it does not occur naturally in a sulphated form (Hu et al., 2014; Tracy et al., 2016). HA is synthesized and deposited into the wound site by fibroblast cells on an early stage of wound repair (Frantz et al., 2010; Hu et al., 2014). Here it plays a key role in maintaining tissue hydration and osmotic balance by attracting water and promoting matrix swelling, which is an important factor in wound healing (Rozario & DeSimone, 2010; Tracy et al., 2016). By generating a porous coat that encircles the cells can HA also inhibit cell-cell adhesion (Haddon & Lewis, 1991). Furthermore, HA assists in collagen synthesis. A higher concentration of HA receptors on fibroblast cells enhances their migration without compromising fibroblast cells ability to produce additional HA. This migration may in turn result in an increase in collagen III & other ECM proteins that prompts a faster wound repair. This increase in HA receptors is commonly seen in fetal fibroblasts (Hu et al., 2014). Depending on the size of HA molecules, they will display conflicting effects. The larger (>500 kDa) versions will cause a decrease in inflammation, an increase in collagen III expression and increased anti-fibrotic TGF-β3 activity. The smaller versions (<400 kDa) will increase inflammation, increase collagen I expression, increase fibroblast proliferation and its differentiation into myofibroblasts. As such, the larger versions of HA display factors which might cause a reduction in scar formation, while the smaller ones may show an increase (Hu et al., 2014; Tracy et al., 2016).

1.6 Treatment of wounds

1.6.1 Scaffolds and tissue engineering

Chronic wounds are a result of a combination of factors that overwhelm the healing response in patients. Factors that may influence the ability to heal wounds are tissue oxygenation (hypoxia) and an altered cellular and systemic stress response (Mustoe, O'Shaughnessy, & Kloeters, 2006). Hypoxia is found in normal healing wounds as vascular perfusion is disrupted by initial injury. Hypoxia signalling can be beneficial for wound healing as it induces several beneficial growth factors. However, for a prolonged period of time, as is seen in chronic wounds, hypoxia will lead to reduced collagen synthesis and α-SMA expression. Alterations in cellular and systemic stress response in chronic wounds can be identified by a hyperproliferative activity, without showing any reduction to the wound margin. The

wound site shows high amounts of inflammatory products. An imbalanced ratio of MMPs and their inhibitors is also present, which breaks down ECM (Werdin, Tennenhaus, Schaller, & Rennekampff, 2009). There are many advanced methods of therapy available for treating chronic wounds. These include negative pressure wound therapy, hyperbaric oxygen therapy, biophysical modalities and biological and bioengineered therapies. However, the majority lack definite proof of their efficacy, and as such further research is required (Frykberg & Banks, 2015). One method for treating chronic wounds which has seen several advancements over the years is skin tissue engineering, which introduces suitable scaffold matrices to the wound area to facilitate the process. Scaffolds are typically made of polymeric biomaterials, and provide the structural support for cell attachment, resulting in a suitable addition to tissue development (Chan & Leong, 2008). Research has been performed on an abundance of different types of scaffolds, and the method is showing great potential, as several of the scaffolds has provided remarkable success in skin tissue repair and wound healing. However, there are several factors to account for in regards to optimizing a scaffold. The scaffold must provide a suitable 3D environment for the cells, and maintain an optimal porosity to enable nutrient and oxygen supply. Mechanical strength, biocompatibility and biodegradability also need to be addressed. Further, different tissue shows enhanced response to different scaffolds. Both natural biomaterials and synthetic biomaterials have been tested, where the former tends to provide a better biodegradability and biocompatibility, while the latter provides a stronger mechanical strength (Chaudhari et al., 2016). One important factor in scaffold production is to include different components which suggests advantageous effects to wound healing. Collagens are frequently incorporated, as they are major components in the ECM and important for a series of vital roles in developmental processes and tissue homeostasis (Ahmed, Suso, & Hincke, 2017; Chaudhari et al., 2016). Attempts have also been made to incorporate synthetic macromer polyethylene glycol diacrylate (PEGDA) into cryogel scaffolds. Cryogels are interconnected supermacroporous gels that are prepared using sub-zero temperatures, resulting in a 3-dimensional networks based on a mixture of polysaccharides (dextran, HA and chitosan) and proteins (collagen or gelatine) (Kumar, Mishra, Reinwald, & Bhat, 2010). The incorporation of PEGDA to these scaffolds increase mechanical stability, inter-connecting porosity and encourage in vitro cytocompatibility (Wartenberg et al., 2017). Synthesized cryogels are a cross between natural and synthetic biomaterials, and appear to show promising suitability for use as wound dressings. However, there is need for further testing to determine whether cryogels with the inclusion of PEGDA holds an advantage over other scaffold compositions.

1.6.2 Eggshell Membrane

Eggshell membrane (ESM) is a natural scaffold, which may be a potentially beneficial component in skin tissue engineering. As ESM is currently considered a waste material, large quantities go to waste

every year. In 2007, annual global egg production exceeded 60 million tons, resulting in a substantial waste generation which has a strong negative effects both environmentally and financially (Jia, Guo, Yu, & Duan, 2011). To find a use for ESM would prove highly beneficial at a global scale. In eastern medicine ESM has been used for a variety of purposes over centuries (Sah & Rath, 2016). In Chinese traditional medicine, ESM has been an ingredient in what is called a "phoenix cloth" which is a dressing material used for treating burn wounds, different types of ulcers and tympanic perforation (Jia et al., 2011). In Japan, ESM is used as a natural remedy for injuries by sumo wrestlers. In addition to the above mentioned, the use of ESM as a natural treatment appears in several settings, suggesting that ESM has a positive effect on wound healing (Ohto-Fujita et al., 2011). However, these traditional examples have trouble providing any definite proof of effect, and although the use of ESM as an externally applicable equivalent of ECM, that might promote wound healing is becoming a widespread subject of research, the molecular mechanism is still somewhat unknown (Ohto-Fujita et al., 2011). In avian eggs during embryo development, the ESM is an equivalent of ECM, and consist of many of the same compounds as ECM. The ESM is a two-layered insoluble sheet found between the shell and the egg white, and acts as a scaffold for biomineralization of the egg shell (Ohto-Fujita et al., 2011). The ESM consists of two membranes, where the outer membrane has a thickness of 50-70 µm, and the inner membrane 15-26 µm (Ahmed et al., 2017). The ESM consists of mainly proteins, and small amounts of carbohydrates (~2-10%) and lipids (~1-3%) (Ahmed et al., 2017; Wartenberg et al., 2017). There is presence of collagen I, V and X within a highly cross-linked fibrous meshwork, structurally similar to that of ECM, which protects the egg against pathogen invasion, but could also prove useful for mechanical strength as a scaffold component (Ahmed et al., 2017; Rose & Hincke, 2009). The fibrous network of ESM also includes GAGs (most notably HA) and fibronectin, which can also be found in skin tissue ECM, and provides a positive environment for cells (Ohto-Fujita et al., 2011; Sah & Rath, 2016; Tracy et al., 2016). ESM also include high amounts cysteine-rich eggshell membrane protein (CREMPS) which may hold properties important for wound healing (Tram T. Vuong et al., 2017). Previous studies has shown that fragmented ESM fibres, reduced to a powdered form (PEP) maintains their structural abilities, closely resembling a scaffold (figure 1.5) (Tram T. Vuong et al., 2017). ESM is also highly degradable, and could potentially provide many of the qualities required in tissue engineering.

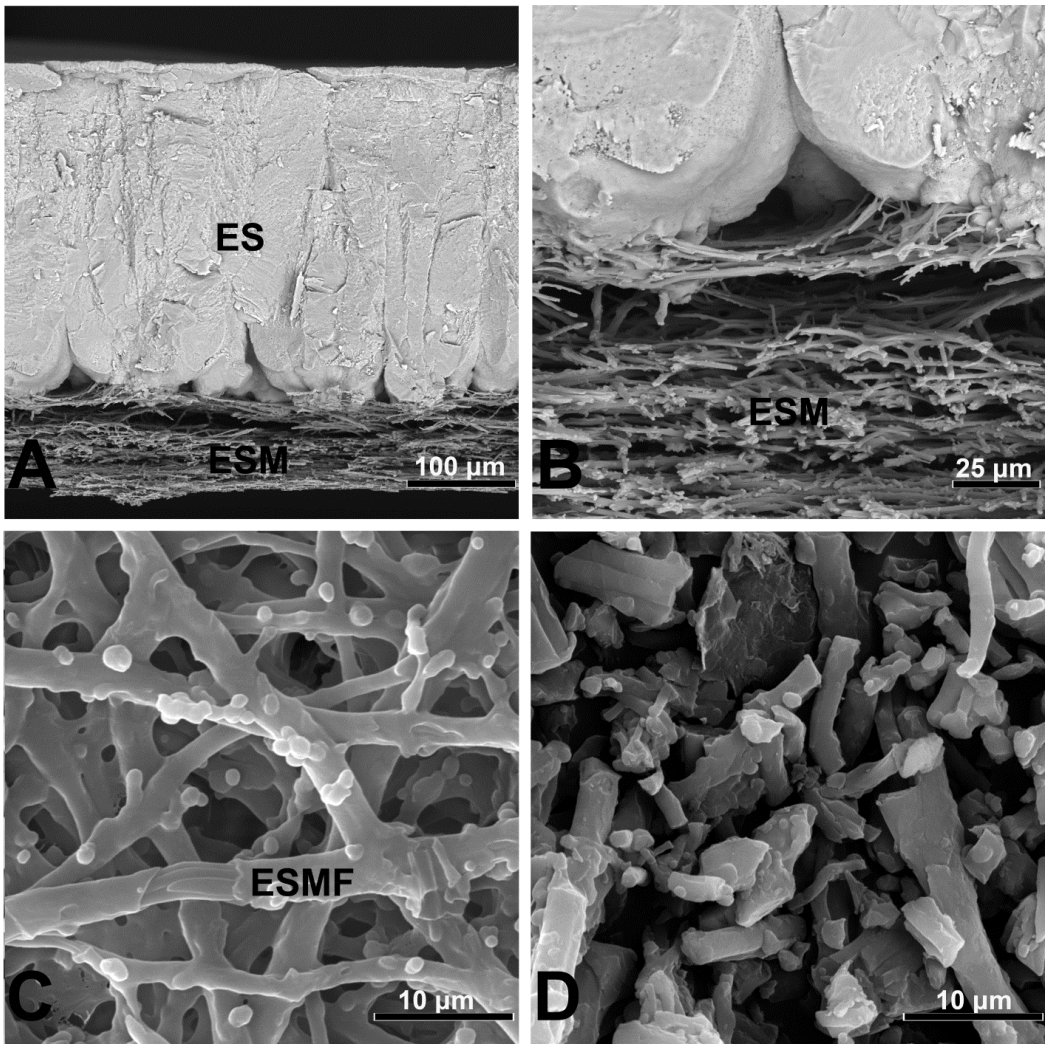

Figure 1.5: Eggshell and membrane structural image taken using SEM imaging. *A) shows how ESM is distributed in comparison to the eggshell. B) shows the relationship at a higher magnification. C) shows the organisation of the fibrous network in ESM. D) shows processed fragmented ESM fibres. Figure is reproduced from (Ahmed et al., 2017)*

2. Aim of Study

The inclusion of ESM to promote wound healing can be performed in different ways. In a powdered form, ESM may be incorporated into a plaster used for superficial wound healing, or in a scaffold component to generate a pad used for deeper and more serious wounds. The powdered ESM (PEP) is composed of collagens, glycol- and antibacterial proteins as well as carbohydrates. Ha is the primary form of GAG present (81%), with a small amount of chondroitin sulphate (CS) (Tram T. Vuong et al., 2017).

This thesis will attempt to observe how fibroblast cells react to exposure to ESM in a powdery substance, in a 2D environment, and study fibroblast cells response to exposure to a scaffold environment with the inclusion of ESM.

This thesis aims to determine the effect different concentrations of ESM has on fibroblast cells ability to proliferate, differentiate and produce extracellular matrix components in an attempt to determine whether it holds properties advantageous for wound healing. Experiments will also be conducted to observe how different concentrations of ESM affects fibroblast cell viability and the potential cytotoxic effect it may have. The thesis also aims to visualize how fibroblast cells adhere and proliferate in a 3D environment of different scaffold compositions, in an attempt to determine whether ESM may hold merit for inclusion in a 3D scaffold.

This thesis may therefore be divided into two separate parts:

- Observing the 2D effect different concentrations of ESM has on fibroblast cells.
- Observing how fibroblast cells may respond when exposed to a 3D scaffold containing ESM.

3. Materials

3.1 Laboratory equipment & instruments

3.1.1 Laboratory equipment

Equipment	Supplier
1.5 ml Eppendorf tubes	Eppendorf
15 ml and 50 ml tubes	Sarstedt
2 ml, 5 ml, 10 ml & 25 ml Serological Pipettes	Sarstedt and VWR
Accurpette	VWR
Biopsy Punch	Kai Medical
Black- & White Tissue Cell Culture Plate, 96-well	Thermo Scientific Nunclon™
Blotting Roller	Invitrogen
Cell culture Multiflask TC, 3-layer 525 cm^2	Falcon
Countess™ cell counting chamber slides	Invitrogen
CryoTube™ Vials	Thermo Scientific
FinnPipette®F2	Thermo Scientific
Glass vials with plastic snap-cap	Assistent
Nitrile powderfree disposable gloves	VWR
NuPAGE™ 10% Bis-Tris Gel	Invitrogen
Parafilm	Parafilm®
Pipette tips	Sarstedt, Sartorius, Biosphere
Pipettes	BIOHIT and Thermo Scientific
QIAshredder Mini Spin Columns	Qiagen
Stainless steel surgical blade	Swann-Morton
Standard 6-well Cell culture plate	Sarstedt
Standard Tissue Cell Culture Plate, 96-well	Falcon®
TC-Cell flask T75	Sarstedt

3.1.2 Instruments

Instrument	Supplier
Avanti™J-301 Centrifuge	Beckman Coulter™
Axio Observer Z1 Microscope, Jena, Germany	Zeiss
Bal-Tech CPD 030	Bal-Tech AG
Countess™ Automated Cell Counter	Invitrogen
Digital Heatblock	VWR
Digital IR Vortex Mixer	VELP Scientifica
Eppendorf centrifuge 5430	Eppendorf AG
EVO 50 EP Scanning Electron Microscope	Zeiss
G:Box	Syngene
Galaxy 170R Thermostatic cabinet	New Brunswick
Gel electrophoresis apparatus; Powerease™ 500	Invitrogen
GeneAmp®PCR System 9700	Applied Biosystems
iBlot™ Device	Invitrogen
InoLab pH7110	WTW
Laboratory Centrifuge, Micro Star 17R	VWR
LAF-bench: Biohazard safety cabinet class II	ScanLaf

Leica DMIL LED Microscope w/ Canon EOS 550D	Leica Microsystems Canon inc.
Nanodrop®ND-100 Spectrophotometer	Thermo Scientific
Polaron SC 7640	Quorum Technologies Ltd.
QuantStudio5™ Real-Time PCR instrument	ThermoFisher Scientific
See-saw rocker SSL4	Stuart
SW22 Heated Water Bath	Julabo
Synergy|H1 Microplate Reader	BioTek
Vacusafe	Integra Biosciences AG
YellowLine TTS2 Shaker	IKA®Works Inc.

3.1.3 Software

Software	Supplier
Excel	Microsoft
G:Box Chemi-XX6	GeneSys
Gen5 V3.02 Microplate and Imager Software	BioTek instruments inc.
GeneTools	Syngene
GraphPad Prism 7	GraphPad Software, Inc.
ImageJ 1.51n	Java
NanoDrop ND-100 V3.81	Thermo Scientific
Microsoft Paint v.1607 for Windows 10	Microsoft Corporation
QuantStudio™ Design & Analysis Software v1.4.1	Applied BioSystems, Thermo Fisher Scientific
SmartSEM	Zeiss
ZEN Lite (Blue edition)	Carl Zeiss Microscopy

3.2 Chemicals

Chemical	Supplier
AEBSF	Sigma-Aldrich
BSA – Protein assay standard	Bio-Rad
Dulbecco's Phosphate-Buffered Saline, [-] $CaCL_2$, [-] $MgCl_2$	Life technologies
ECL Prime™ Blocking Agent	GE Healthcare
ECL™ Plex Fluorescent Rainbow Marker, Full	GE Healthcare
Formaldehyde Solution 38% (in H_2O)	Sigma Life Science
Glutardialdehyde, 25% aqueous solution	Merck
O.C.T. Compound, Embedding Medium	Tissue-Tek®
PIPES-disodium salt	Sigma-Aldrich
Sodium Chloride	Millipore
TaqMan® Gene Expression Master Mix	Applied Biosystems
Triton™ X-100	Sigma-Aldrich
Trizma® base	Sigma-Aldrich
Trypan Blue Stain 0.4%	Invitrogen
TWEEN® 20	Sigma-Aldrich

3.3 Cell growth medium

Medium	Components	Supplier

Proliferation Medium	DMEM (1X) - GlutaMAX™-I, [+] 1 g/L D-Glucose, [+] Pyruvate 10% Fetal Bovine Serum 1:10.000 PenStrep 1:10.000 Fungizone	Life Technologies Life Sciences Life Technologies Life Technologies
Starvation Medium	DMEM (1X) - GlutaMAX™-I, [+] 1 g/L D-Glucose, [+] Pyruvate 2% Fetal Bovine Serum 1:10.000 PenStrep 1:10.000 Fungizone	Life Technologies Life Sciences Life Technologies Life Technologies

3.4 Primers and probes for real-time PCR

Primer/probe	Catalogue Number	Supplier
Collagen 1	Hs01028939_gl	Applied BioSystems
Collagen 3	Hs00943809_m1 COL3AI	Applied BioSystems
Ef-1α	Hs00265885_g1 EEF1AI	Applied BioSystems
Elastin	Hs00355783_m1 ELN	Applied BioSystems
Hsp70	Hs00745797_s1 HSPA2	Applied BioSystems
Ki67	Hs04260396_m1 MKI67	Applied BioSystems
SMA	Hs00909449_1 ACTA2	Applied BioSystems

3.5 Antibodies for western blot

Antibody	Mixing Ratio	Supplier	Product number
CY3, mouse	1:2500	GE Healthcare	PA43009V
Hsp70, mouse	1:1000	Abcam	AB2787
SMA, mouse	1:200	Abcam	AB7817
α-tubulin, mouse	1:10000	Sigma	T5168

3.6 Kit

Kit	Contents	Supplier
CellTiter-Glo®Luminescent Cell Viability Assay	CellTiter-Glo® Buffer CellTiter-Glo® Substrate (liophilized)	Promega
CyQuant® Proliferation Assay Kit	CyQuant GR dye, comp. A, 1:400 Cell-lysis buffer, comp B, 1:20	Invitrogen
DC Protein Assay	RC Reagent I RC Reagent II Reagent A Reagent B	BIO-RAD
iBlot® Gel Transfer Stacks Nitrocellulose, Regular	Anode Stack (containing nitrocellulose membrane) iBlot™ Filter Paper Cathode Stack Disposable sponge w/ metal contact	Invitrogen

Live/Dead™ Viability/Cytotoxicity Kit	EthD-1 CalceinAM	ThermoFisher Scientific
NuPAGE sample preparation kit for Western Blotting	NuPAGE®LDS Sample Buffer (4x) NuPAGE®Reducing Agent (10x) NuPAGE® MOPS SDS Running buffer (20x) NuPAGE®Antioxidant	Novex, by Life Technologies
RNase-Free DNase Set	RNase-free Water DNase I, RNase-Free (lyophilized) Buffer RDD	Qiagen
RNeasy® Mini Kit	Buffer RLT Buffer RW1 Buffer RPE RNase-free Water	Qiagen
Roche® Cytotoxicity Detection Kit (LDH)	Dye Solution: INT and Sodium Lactate Catalyst: Diaphorase/NAD+ mixture	Sigma-Aldrich
TaqMan®Rt-PCR kit	10x RT Buffer $MgCl_2$ (25 mM) Deoxy NTP's Hexamer RNase inhibitor Multiscribe	Applied Biosystems
XCell SureLock™ Mini-Cell	Buffer Dam Gel Tension Wedge Mini-Cell Lid	ThermoFisher Scientific

3.7 Buffers and solutions

Buffer/Solution	Components
PIPES-buffer 0.1 M	0.1 M PIPES disodium salt Dissolved in dH_2O pH adjusted to 7.2
RIPA-Buffer	0.5 M Tris base, pH 6.8 0.5 M EDTA, pH 8.0 5 mM NaF 5 mM Na-pyrophosphate ($Na_4P_2O_7$) 2% SDS Solved in dH_2O
TBS 10x (concentrated Tris-buffered saline)	0.2 M Trizma base 1.5 M NaCl Dissolved in dH_2O pH to 7.6 with 6 N HCl
TBS-Tween 1x	1:10 TBS 10x Dissolved in dH_2O 1:1.000 Tween 20

3.8 Scaffolds

Scaffold	Notable Components/Concentrations	Supplier
Biovotec Control	0.75% Collagen	Biovotec AS, Dublin
Biovotec ESM	0.75% Collagen 3% ESM	Biovotec AS, Dublin
Cryogel 5	200 mg/ml PEGDA 2 mg/ml Collagen 50 mg/ml ESM	Innovent, Jena, Germany
Cryogel 6	200 mg/ml PEGDA 2 mg/ml Collagen 12.5 mg/ml ESM	Innovent e.V
Cryogel 8	200 mg/ml PEGDA 2 mg/ml Collagen	Innovent e.V

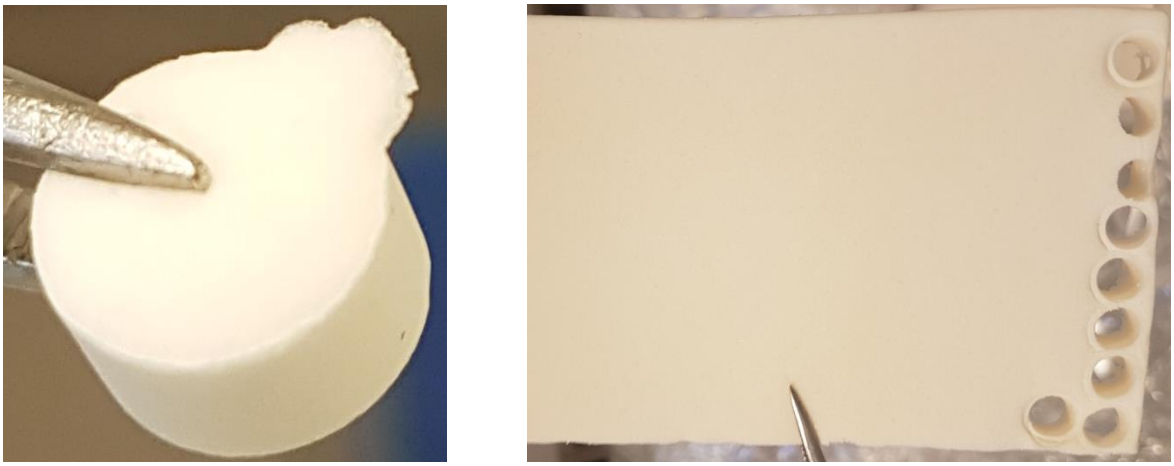

Figure 3.1: Scaffolds. *The structure of scaffolds as delivered from their respective suppliers. Left image is a representative image of cryogels (Cryogel 5 displayed) supplied by Innovent. Right image is a representative image of scaffold sheets (Biovotec ESM displayed) delivered from Biovotec AS. The holes in the sheets are scaffolds cut out for testing.*

3.9 Intervention

Primary Dermal Fibroblasts; Normal, Human, Adult (HDFa) (ATCC®PCS-201-012™).	ATCC
Powdered ESM (PEP), < 100 µ in size, containing similar components as ESM, has a fibrillar structure.	Supplied by Nortura, processed by Biovotec AS, Dublin

4. Methods

4.1 Making of ESM

The ESM originated from flakes of eggshells, provided by the egg breaking company *Nortura*, situated in Norway. Through a patented process owned by *Biovotec*, the ESM was processed and harvested from the eggshells, and further treated and pulverized into a powdery substance (PEP) (patent number: WO 2015/058790 A1) (Tram T. Vuong et al., 2017). Different concentrations of PEP were used in the experiments. ESM has a highly cross-linked fibrous-like structure, and is known to contain an abundance of different proteins and carbohydrates (Ahmed et al., 2017; Tram T. Vuong et al., 2017). The carbohydrate fraction of ESM contains glycosaminoglycans (GAGs) imbedded into its structural network. The GAGs consist mainly of two subtypes; Hyaluronic acid (HA) which consist of ~81%, and as well as a minor amount of Chondroitin Sulphate (CS) (Tram T. Vuong et al., 2017). The protein fraction of ESM consists of a large variety of protein families, including collagens, Cysteine-rich eggshell membrane proteins (CREMPs), histones, avian beta defensins (AvBDs) and Ovocalyxin-36 (OCX36). These proteins help maintaining mechanical integrity of ESM, assisting in its natural role as protective barrier against pathogens (Ahmed et al., 2017).

A stock solution of 10 mg/ml PEP was mixed and was further used to generate the desired concentrations used in this experiment. It should be noted that PEP would easily precipitate, and as such a continuous mixing was required to ensure the same amount/concentration of PEP was added to the cells.

The ESM was either introduced to fibroblast cells as PEP, where the cells were cultured in 2D, or cultured in 3D scaffolds with ESM imbedded. The scaffolds consist of different structural components such as collagen, ESM and PEGDA. They were manufactured by either *Biovotec*, or the company *Innovent*. The content differing between them is displayed in chapter 3.8.

4.2 Cell Treatment with PEP

The cells used in this thesis were primary human dermal fibroblasts, taken from skin tissue of adult humans. To avoid any contamination to the cells, every experiment was performed in a sterile environment. As such, all equipment and workplace environment were thoroughly washed with 70% EtOH before and after use. The experiments conducted focused primarily on observing how different concentrations of PEP would affect the fibroblast cells over time. Fibroblast cells that were not treated with PEP were used as a negative control.

To observe any effect ESM would have on fibroblast cells, different dose-response concentrations of PEP was performed. To ensure the fibroblast cells had a synchronized cell cycle, they were treated with starvation medium. The starvation medium contained a reduced amount of FBS, although a small amount was required to avoid cell death. PEP was thoroughly mixed into this medium prior to exposure to the cells.

Procedure:

- A stock solution of 10 mg/ml of ESM was prepared in starvation medium.
- The desired lower concentrations were then generated from this stock solution through dilution with additional starvation medium.
- Control cells received starvation medium only.

4.3 Handling fibroblast cells

4.3.1 Thawing

Prior to use, the cells were stored in a liquid nitrogen-tank. To ensure the cells were not destroyed during freezing, DMSO was added to protect the cells from lysing by preserving the plasma membrane. However, the DMSO is toxic to cells, and as such, it had to be rapidly separated from the cells once thawing was initiated.

Procedure:

- Proliferation medium was pre-heated in a water-tank to 37˚C.
- Once removed from the tank, the tube content was thawed using a water tank at 37˚C.
- The tube was sterilized using 70% EtOH prior to bringing it into the LAF-bench.
- 1 ml of cell suspension was transferred to 9 ml of proliferation medium.
- The cell suspension was centrifuged at 550 rpm for 6 minutes.
- The supernatant was discarded and the pellet was resuspended in 2 ml of proliferation medium.
- A cell count was performed (see chapter 4.3.3).
- Using this number of cells, one can measure how much time is needed before the cells must be divided, to ensure they do not grow too densely.
- The 2 ml of cell suspension was transferred to T75 cell culture flask(s) containing 12 ml of proliferation medium. The cell count would determine the number of flasks required, to achieve cell density of 5.000-10.000 cells/cm^2.
- The flask(s) were then incubated in a thermostatic cabinet, set to 37˚C, 5% CO_2 and 19% O_2.

4.3.2 Cell splitting

Once the fibroblasts were placed in proliferation medium and surrounded by suitable environmental conditions that closely resembles their *in vivo* standard living conditions, they resumed a steady proliferation process. The cells continued to proliferate until they ran out of nutrients or space. It is therefore important to regularly change the medium at a ~3 days interval. Once the cells reached a 70%-90% confluence, they would start to differentiate into myofibroblast cells. Because this is undesirable in the following experiments, they were split into smaller cultures prior to reaching this level of confluence. Trypsin-EDTA was used to loosen cells from their surface area. When utilizing this enzyme degrading protein solution, it is important to expose the cells to it for the shortest amount of time possible, as it may cause cell death.

Procedure:

- Proliferation medium and Trypsin-EDTA was preheated to 37˚C in a water bath.
- The cell media was discarded, and any excess medium was washed away using D-PBS.
- To loosen the cells from their adherent surface, the cells were exposed to Trypsin-EDTA and incubated in a thermostatic cabinet for ~6 minutes. To ensure they were loosened from the flask, they were observed in a microscopy. As the fibroblasts not only can be seen move around, but also display a conformational change in shape, from stretched adherent cells along the flask surface into spherical shaped non-adherent cells, this was easy to observe.
- After detachment, additional medium was added to the cell/Trypsin solution to lower the concentration of Trypsin-EDTA and reduce toxicity.
- The solution was transferred to a falcon tube, and centrifuged at 550 rpm for 5 minutes to separate the cells from the trypsin/medium solution.
- The supernatant was discarded, and the pellet resuspended in a suitable amount of medium before cell counting.

4.3.3 Cell counting

This method used Trypan Blue stain, a compound that is unable to penetrate the membrane of living cells. Through this trait, the cell counter is able to differentiate between living and dead cells through a distinctive bright centre of any living cell, in contrast to a dark, fully stained centre in dead cells. Using the number of living- and dead cells on the cell counting chamber slide, the automated cell counter quantifies this amount, and is able to make an estimate of the cell concentration in a sample.

Procedure:

- 10µl of the cell suspension was transferred to an Eppendorf tube.

- 10µl of Trypan Blue stain 0.4% was added to the cell suspension and mixed thoroughly.
- 10 µl of this mixture was placed on a cell counting chamber slide and inserted into cell counter.
- This Cell counter displayed the concentration of cells/ml.

4.3.4 Seeding

Once the cell number was determined, this amount was resuspended in proliferation medium to achieve the desired concentration of cells/ml for the given experiment. The desired concentration was added to the designated wells, and the plate(s) were incubated overnight in a thermostatic cabinet to ensure cell adhesion. Table 4.1 below displays the approximate number of cells to medium ratio for the different plate types utilized.

Table 4.1: *The concentration of cells in the wells used.*

Plate type	Concentration (cells/well)
96 well plate (200 µl)	5.000
6 well plate (2 ml)	200.000

4.4 Cell proliferation

In order to measure the effect of different PEP concentrations on cell proliferation, the CyQuant® Cell Proliferation Assay Kit was used. The CyQuant® GR dye binds to cellular nucleic acids. When bound, the natural fluorescence latent in the dye will be activated, and exhibit a signal. This notable fluorescence can be measured to determine the number of cells in the sample, since the amount of cellular DNA is proportional to the number of cells. To ensure that the fluorescence dye could properly permeate the plasma membrane and reach the nucleic acids, a cell-lysis buffer was also included. Living fibroblast adhere naturally to the well, while dead cells appear floating freely in the medium. As such, removing the medium was done prior to adding kit components, in addition to properly washing the wells with PBS, to ensure a minimal number of dead cells present in the samples, that would otherwise result in false quantification.

Materials:

- *CyQuant Proliferation Assay Kit* from *Invitrogen*
    - CyQuant GR dye, component A
    - Cell-lysis buffer, component B
- PEP
- Black Tissue Cell Culture Plate, 96-well

- Proliferation Medium
- Starvation Medium
- Instrument: Synergy|H1 Microplate Reader from BioTek
- Software: Gen5 V3.02 Microplate and Imager Software & Microsoft Excel

Method:

- 200 µl medium containing appropriate concentration of cells were inserted into the designated wells on a black 96-well plate (*see table 4.1*) and incubated at 37˚C in a thermostatic cabinet overnight, to ensure adhesion to the well.
- The following day, the cells were treated with PEP.
    - The experiment was conducted on five different concentrations; 1 mg/ml, 2 mg/ml, 3 mg/ml, 4 mg/ml and 5 mg/ml.
    - Each concentration was seeded out in triplicates.
    - A negative control (cells left untreated) was also included.
- Cells were treated with PEP for 1 and 3 days.
- Following conclusion of treatment period, the medium was carefully removed.
- The wells were carefully washed with D-PBS to remove any remaining medium.
- The plate were wrapped in parafilm, and frozen at -80˚C to ensure efficient lysis.
- The kit reagents were thawed at RT, while avoiding any light exposure.
- The cell-lysis buffer stock solution was diluted 1:20 in distilled water.
- The GR dye was then added to the 1x cell-lysis buffer, in a 1:400 dilution.
- Each well was supplied with 200 µl of the assay reagent, and the plate was incubated at room temperature for 10 minutes, while avoiding light exposure.
- The fluorescence of each well was then measured using the Synergy|H1 Microplate Reader.
- The data was obtained through the Gen5 V3.02 Microplate and Imager Software, and exported to Microsoft excel for further analysis.
- Through normalisation of the negative control, each measurement was calculated. An average amount for each concentration was then determined.
- The final results were calculated from 3 independent cell experiments performed in triplicates.

4.5 Viability

In order to measure cell viability when exposed to different concentrations of PEP the CellTiter-Glo® Luminescent Cell Viability Assay (Promega) was used. This method utilizes a thermostable luciferase

(Ultra-Glo™ Recombinant Luciferase) that reacts with ATP, while also inhibiting enzymes which degrades ATP during cell lysis, such as ATPases.

$$\text{Beetle Luciferin} + \text{ATP} + O_2 \xrightarrow{\text{Ultra-Glo™ Recombinant Luciferase + Mg2+}} \text{Oxyluciferin} + \text{AMP} + PP_i + CO_2 + \text{Light})$$

As the amount of ATP in the sample is proportional to the number of living/metabolically active cells, this method is suitable for determining the effect different concentrations of PEP would have to the viability of fibroblasts.

Materials:

- *CellTiter-Glo®Luminescent Cell Viability Assay* from *Promega*
    - CellTiter-Glo® Buffer
    - CellTiter-Glo® Substrate (lyophilized)
- PEP
- White Tissue Cell Culture Plate, 96-well
- Proliferation Medium
- Starvation Medium
- Instrument: Synergy|H1 Microplate Reader from BioTek
- Software: Gen5 V3.02 Microplate and Imager Software & Microsoft Excel

Method:

- 200 µl medium containing the appropriate number of cells were seeded into the designated wells on the white 96-well plate (*see table 4.1*) and incubated at 37˚C in a thermostatic cabinet overnight, to ensure adhesion to the well.
- The following day, the cells were treated with PEP.
    - The experiment was conducted on five different concentrations; 1 mg/ml, 2 mg/ml, 3 mg/ml, 4 mg/ml and 5 mg/ml.
    - Each concentration was seeded out in triplicates.
    - A negative control (cells left untreated) was also included.
- Cells were treated with PEP for at 1 and 3 days.
- The CellTiter-Glo® Buffer andd CellTiter-Glo® Substrate was thawed and equilibrated to RT prior to mixing.
- The appropriate volume of buffer was added to the substrate bottle, and vortexed until the substrate was dissolved and homogenized into the buffer solution, resulting in the kit reagent.

- 100 µl medium was removed from each well on the plate, to ensure that 100 µl was remaining.
- 100 µl of kit reagent was added to each well, and the plate was then incubated for 2 minutes on the See-saw rocker SSL4 while avoiding exposure to light.
- The plate was then incubated for 10 minutes at dark RT to stabilize the luminescence signal.
- The luminescence of each well was then measured using the Synergy|H1 Microplate Reader.
- The data was obtained through the Gen5 V3.02 Microplate and Imager Software, and exported to Microsoft excel for further analysis.
- Through normalisation of the negative control, each measurement was calculated. An average amount for each concentration was then determined.
- The final results were calculated from 3 independent cell experiments performed in triplicates.

4.6 Cytotoxicity

In order to measure a possible cytotoxic effect of PEP on fibroblast cells, different PEP concentrations were tested by the Roche® Cytotoxicity Detection Kit (LDH). This method uses LDH (Lactate dehydrogenase) as a measurement for cytotoxicity, a component that is released from cells during tissue damage. It is commonly used as an unspecific indicator for cell damage, as it is present in the cytoplasm of all cells in the human body (Thomas, Marwood, Parsons, & Parsons, 2015). LDH facilitates the transition of L-Lactate into Pyruvate as well as converting NAD^+ into NADH and vice versa.

Materials:

- Roche® Cytotoxicity Detection Kit (LDH)
    - Dye Solution: INT and Sodium Lactate
    - Catalyst: Diaphorase/NAD+ mixture
- PEP
- Blank Tissue Culture Plate, 96-well
- Triton X (2%) – *cytotoxic agent used for positive control*
- Proliferation Medium
- Starvation Medium
- Instrument: Synergy|H1 Microplate Reader from BioTek
- Software: Gen5 V3.02 Microplate and Imager Software & Microsoft Excel

Method:

- 200 µl medium containing the appropriate number of cells were seeded into the designated wells on the blank 96-well plate (*see table 4.1*) and incubated at 37˚C in a thermostatic cabinet overnight, to ensure adhesion to the well.
- The following day, the cells were treated with PEP.
    - The experiment was conducted on five different concentrations; 1 mg/ml, 2 mg/ml, 3 mg/ml, 4 mg/ml and 5 mg/ml.
    - Each concentration was seeded out in triplicates.
    - A negative control (cells left untreated) was also included.
    - A positive control designated for 2% Triton X (*cytotoxic agent*) was also included.
    - A blank was also included, in the form of starvation medium only.
- Cells were treated with PEP for at 1 and 3 days.
- Medium in the wells designated for positive control was exchanged with 100 µl of 2% Triton X.
- The plate was incubated in a thermostatic cabinet for ~2 hours.
- The medium in each well was carefully collected and transferred to a new 96-well blank tissue culture plate.
- The plate was wrapped in parafilm, and frozen at -80˚C to ensure efficient lysis.

Measurement:

- Both the plate and the kit reagents were thawed at RT.
- The reaction mix was generated using the dye solution- and catalyst kit components. See Table 4.2 below for exact values of the different components (displayed as amount per well).

Table 4.2: Roche®Cytotoxicity detection kit. *The mixing ratio of the assay reagents in the Roche®Cytotoxicity detection kit, for a single well.*

Total Volume	Dye Solution	Catalyst
115 µl	112.5 µl	25 µl

- 100µl of the sample was removed from each well.
- 100µl of the reagent mixture was added to the wells.
- The plate was then covered in foil to ensure minimal light exposure and incubated for 30 minutes.
- The absorbance of each well was then measured using the Synergy|H1 Microplate Reader.

- The data was obtained through the Gen5 V3.02 Microplate and Imager Software, and exported to Microsoft excel for further analysis.
- The average values measured of the blank samples was substracted for each measurement.
- Through normalisation of the negative control, each measurement was calculated. An average amount for each concentration was then determined.
- The final results were calculated from 3 independent cell experiments performed in triplicates.

4.7 Real-Time PCR

In order to observe genetic differentiation in fibroblastic cells when exposed to PEP, the method of quantitative real-time PCR was performed. The method is divided into two steps: In the first step, mRNA was isolated from fibroblastic cells, and transformed into cDNA through a reverse-transcriptase reaction. RNA is easily degraded and therefore the procedure was performed on ice, using RNase free equipment. Reverse transcription was performed by the enzyme reverse transcriptase that uses the RNA strand as template to generate a new cDNA strand. In the second step, the cDNA was amplified through a Polymerase Chain Reaction (PCR) with TaqMan polymerase. PCR is a repetitive process that performs a three-step program to amplify the genetic material (cDNA) on a logarithmic scale. The first step of this method causes the double stranded cDNA to break into single strands through exposure to high temperature. The second stage lowers the temperature substantially, and enables the gene-specific primers to bind to complementary sequences on the single strands. The third step uses the thermo-stable TaqPolymerase with an optimal temperature ~70 ˚C to polymerize the gene segment. As this process is repeated, any remaining cDNA not included by the addition of the primers will not be replicated, and finally result in such a low concentration that it will not tamper with the signal. To be able to quantify in real-time the relative expression, TaqMan (Hydrolysis) probes were included in the reaction. These probes consist of two connected parts where one is capable of emitting a fluorescent signal, commonly referred to as a *reporter*, while the other prevents it from emitting this signal, commonly referred to as a *quencher*. This probe binds to the target sequence with the reporter on the 5'end. During annealing, the reporter will be cleaved off, leaving the proximity of the quencher and can therefore emit its fluorescent signal (Heid, Stevens, Livak, & Williams, 1996). The accumulated strength of this signal can then be used to observe the amount of amplification in the sample throughout the reaction.

To properly observe differences between an untreated sample and samples exposed to different concentrations of ESM, the Elongation Factor 1α (Ef-1α) was chosen as a reference gene. Ef-1α is considered a housekeeping gene and should therefore display minor changes through exposure to PEP

(Nicot, Hausman, Hoffmann, & Evers, 2005). As such, Ef-1α may be used to properly calculate any transcriptional changes the other genes may display through PEP treatment.

To calculate these results, we observed the threshold cycle for real-time PCR (C_T), i.e. which PCR cycle the fluorescent signal exceeded a set threshold, to exclude any background noise, and ensure that the PCR had entered the exponential phase in the amplification. By substracting the C_T value of the reference gene from the target gene, the ΔC_T value was calculated. Standard deviation (SD) was calculated by substracting the SD of the reference gene from the target gene. To calculate the $\Delta\Delta C_T$ value, the ΔC_T value of the negative control sample was substracted from the ΔC_T value of the test sample. SD was calculated by substracting SD of the negative control sample from the SD of the test sample. To normalise the values, each value of the test samples was set into the equation $2^{-\Delta\Delta CT}$. The resulting value provided a normalised amount of RNA in the test samples compared to the negative control (Biosystems, 2008; Schmittgen & Livak, 2008).

4.7.1 RNA Isolation

We used RNeasy® Mini Kit to isolate RNA from the PEP treated cells. The method was performed according to the producer's protocol, with the inclusion of an additional re-appliance of 70% EtOH through the RNeasy Mini Spin Columns to increase yield. As such, the following method is a brief description of process.

Method:

- The cells were washed 2x with D-PBS.
- 350 µl RLT buffer was added to each well and thoroughly washed.
- The samples were centrifuged at 10.000 rpm for 5 minutes at 4˚C to separate any remaining ESM from the sample.
- 70% EtOH was added to the samples and thoroughly mixed.
- This solution was transferred to the RNeasy Mini Spin Columns and centrifuged at 10.000 rpm, at 4˚C, for 15 seconds. *This step was performed twice*.
- The columns were washed using the RW1 buffer.
- 1:8 concentrated RNase-free DNase (DNase:RDD-buffer) was added to remove remaining DNA, and the columns were incubated at RT for 15 minutes.
- The columns were washed with RW1 buffer and 2x with RPE buffer.
- The columns were washed with RNase-free water, and the supernatant was further measured for RNA using the NanoDrop ND-1000 Spectrophotometer.
- Using RNase-free water as a blank measurement, each sample was measured in ng/µl mRNA.
- Following measurement, the samples were stored at -80˚C until further analysis.

4.7.2 Generation of cDNA

Materials:

TaqMan®Rt-PCR kit

Method:

- The samples and the Multiscribe component were thawed on ice.
- The remaining components in the TaqMan®Rt-PCR kit were thawed at room temperature.
- The components were then mixed together to generate the TaqMan mix (*table 4.3*).

***Table 4.3: TaqMan Mix**. Displays the volume for each component of the TaqMan®Rt-PCR kit to be included to generate the TaqMan mix. The values displayed are intended for a single sample.*

Reagent	Volume
10xRT Buffer	2 µl
MgCl2 (25mM)	4.4 µl
Deoxy NTP's	4 µl
Hexamer	1 µl
RNase inhibitor	0.4 µl
Multiscribe	0.5 µl

- Each sample was diluted in RNase-free water to achieve a final concentration of 250 ng RNA.
- 12.3 µl of the TaqMan mix was added to each well to achieve to total volume of 20 µl.
- The plate was covered with a platic film.
- The plate was inserted into the GeneAmp PCR System 9700.
- The program settings run as follows:
  25˚C (10min), 48˚C (30min), 95˚C (5min), 4˚C (∞).
- Each sample was diluted to a total volume of 90 µl using RNase free water when the cDNA synthesis had ended, and frozen at -20˚C, until further analysis.

4.7.3 Real-Time PCR

Procedure:

- All reagents were thawed on ice prior to the experiment.
- Once thawed, the TaqMan-mastermix was prepared (*see table 4.4*).

Table 4.4: TaqMan-mastermix. *The reagents required for generating the TaqMan-mastermix used for Real-Time PCR. The values displayed are intended for single sample reaction.*

Reagent	Volume
TaqMan Gene Expression Master Mix	10 µl
dH_2O	5 µl
Primer/Probe	1 µl

- 16 µl of the TaqMan-mastermix was then transferred to their designated wells.
- 4 µl of the cDNA samples were added using a multi-pipette, to a total volume of 20 µl in each well.
- Each sample was run as a triplicate.
- The plate was sealed using a plastic film, and centrifuged for 1 minute at 1000 rpm.
- The plate was then inserted into the QuantStudio5 machine (see figure 4.1 for thermal profile) and the software QuantStudio™ Design & Analysis Software v1.4.1 was used for analysis.

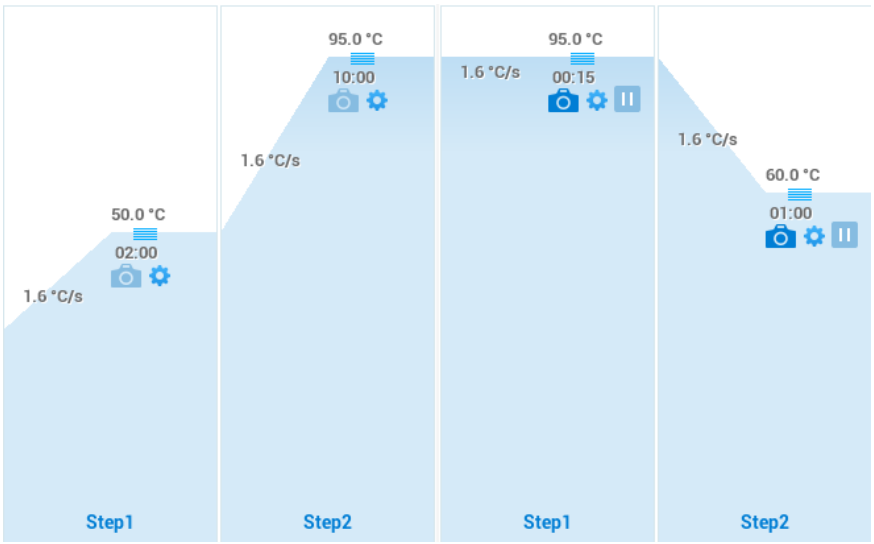

Figure 4.1: The thermal profile used in real-time PCR. *A single cycle of the Real-Time PCR run. Both temperature and time is stated on each step. Data was collected on Step1 and Step2 of the PCR stage (to the right).*

- Once the run had finished, the CT values were exported to Microsoft Excel, and further used to calculate the ΔCT and ΔΔCT values of the different genes.

4.8 Western Blotting

Real-time PCR provides information of how the gene expression may vary upon ESM treatments, however, gene expression and protein expression are not the same thing. Western blotting is

considered a method quite suitable for both protein identification and quantitation. The method involves a series of steps. First it uses gel electrophoresis to separate proteins by size. In the second step it will transfer the resulting bonds to a more solid substance, in this case the nitrocellulose membrane. Finally it visualizes the protein through primary- and secondary antibodies, in the process of immunoassay (Mahmood & Yang, 2012). Here the primary antibody will attach specifically to the protein in question, whereas the secondary antibody containing a fluorescence tag will attach to the primary and once bound, give off a fluorescent signal. Through a series of washing steps, unwanted proteins and unbound antibodies are removed, resulting in a pure reading of the desired protein. When observing the blot, the intensity of the bonds will give a good indication as to the amount of the specific protein in the given sample (Mahmood & Yang, 2012). The size of the protein can be determined through the addition of a ladder, containing components with known sizes. As quantification is the goal of this experiment, the reference protein *α-tubulin* is included in the analysis. As this protein should display minor effects to exposure of ESM, it can be used as a reference marker for normalization.

4.8.1 Cell lysis

Once the cells had reached their designated time point, they were exposed to a lysing buffer that is suitable to maintain any proteins present in the cell. As the cells contain enzymes that can cause protein degradation, this lysing buffer includes the protease inhibition cocktail (AEBSF-) and a phosphatase cocktail to inhibit these enzymes.

Method:

- The treated cells were washed twice in D-PBS before lysed in 250 µl Lysis Buffer (see table 4.5 for details) for 10 minutes, at 4˚C.
- The lysis was transferred to a QIAshredder Mini Spin Columns and centrifuged at 10.000 rpm for 5 minutes at 4˚C to separate any remaining ESM from the sample.
- The supernatant was then transferred carefully to designated Eppendorf-tubes.
- The samples were frozen at -20˚C before further analysis.

Table 4.5: Western blot lysis buffer. *The volume required to make the Western Blot Lysis Buffer, use solution. The values displayed are intended for 1 ml of reagent.*

Reagent	Volume
RIPA-buffer	1 ml
AEBSF	5 µl

Phosphatase Cocktail	10 µl

4.8.2 Protein Measurement

Prior to performing western blotting of the samples, it is important to ensure that the samples applied on the gel contain a similar amount of proteins. The amount of isolated protein in each sample was determined by the BIORAD Protein / Assay. This assay contains an acidic dye that binds to proteins, and measured using a spectrophotometer. For this assay, it is necessary to also include a protein of known concentration to generate a standard-curve. The standard-curve was generated using BSA as a protein standard, and measurements were performed in triplicated of both samples and BSA. A triplicate of blank sample containing dH_2O is also measured to exclude any background noise.

Materials:

- Kit: DC Protein Assay
    - RC Reagent I
    - RC Reagent II
    - Reagent A
    - Reagent B
- Instrument: Synergy|H1 Microplate Reader
- Software: Gen5 V3.02 Microplate and Imager Software & Microsoft Excel

Procedure:

- 5 µl of each sample is placed into a well on a 96-well plate.
- 25 µl of reagent A was added to each well.
- The plate was vortexed and further incubated for 5 minutes at RT.
- Following incubation, 200 µl of reagent B was added to each well.
- The plate was vortexed and incubated for 15 minutes.
- The plate absorbance at 750nm was then read using the Synergy|H1 Microplate Reader.
- The data was obtained through the Gen5 V3.02 Microplate and Imager Software, and exported to Microsoft excel for further analysis.
- The sample values were compared to a known standard curve to determine the amount of protein in each sample.

4.8.3 Sample preparation & SDS-gel electrophoresis

Prior to running the samples through gel electrophoresis, they were mixed with components from the NuPAGE sample preparation kit for Western Blotting.

Materials:

- NuPAGE sample preparation kit
- Digital Heatblock
- XCell SureLock® Mini-Cell
- NuPAGE™ 10% Bis-Tris Gel
- Powerease™ 500

Procedure:

- The sample was mixed with the NuPAGE® LDS sample buffer (4x) and the NuPAGE® Reducing Agent.
- The solution was vortexed, and heated at a Digital Heatblock to 70˚C for 10 minutes.
- The outer chamber of the electrophoresis apparatus was filled up with running buffer (950 ml Millipore water + 50 ml NuPAGE® MOPS SDS Running buffer (x20)).
- 500 µl of NuPAGE®Antioxidant was added to 200 ml running buffer and poured into the inner layer chamber of the electrophoresis apparatus.
- 1,5 µl of ECL™ Plex Fluorescent Rainbow Marker, Full was added to one well on each gel.
- 20 µl of the preheated sample mixture was added to designated wells.
- The Mini-Cell Lid was placed on top of the buffer dam and the Powerease™ 500 attached to the Mini-Cell Lid was turned on.
- The gel was run at 200V, 125mA for 1 hour.

4.8.4 Blotting

Materials:

- Kit: iBlot® Gel Transfer Stacks Nitrocellulose, Regular
- Instrument: iBlot™ Device
- Blotting Roller

Procedure:

- Following the gel electrophoresis, the anode stack with its tray included, was placed directly on the blotting surface.
- The gels were removed from their seals, and placed carefully on the nitrocellulose membrane on top of the anode stack.
- A pre-soaked IBlot™ filter paper was placed on top of the gels.
- The cathode stack was placed on top of the filter paper.
- For each step above, a blotting roller was utilized to remove any air bubbles.

- A disposable sponge was place with its metal contact on the upper right corner of the lid to connect with metal plate in the instrument.
- The lid was closed and the instrument ran at program 2 for 6 minutes to transfer the blot to the nitrocellulose membrane.

4.8.5 Antibody Staining

The entire segment was performed on a See-saw rocker SSL4, at room temperature.

Materials:

- TBS-Tween 1x
- ECL Prime™ Blocking Agent
- Primary Antibodies (see chapter 3.5)
- Secondary Antibody (see chapter 3.5)

Procedure:

- The nitrocellulose membranes were blocked using 2% ECL advanced blocking agent for 1 hour.
- The membranes were then incubated with the primary antibody diluted in 1% ECL blocking agent for 1.5 hours.
- The membranes were washed 3x10 minutes using TBS-Tween 1x, followed by 1 hour incubation with a secondary antibody.
- The membranes were washed 3x10 minutes using TBS-Tween.

The membranes were removed from the See-saw rocker SSL4, and dried at RT for ~1 hour without exposure to light.

4.8.6 Digitalization and Protein quantification

Materials:

- Instrument: G:Box
- Imaging Software: G:Box Chemi-XX6 GeneSys
- Quantification Software: GeneTools

Procedure:

- Each membrane was inserted into the G:Box.
- Using a green LED module and a Cy3 filter the membranes were digitalized.
- The bonds on each image were quantified and exported to Microsoft excel.
- The quantification value for each protein was divided to the reference protein value.

- The background noise value was subtracted.
- The quantification value for the samples containing ESM were normalised to the value of the negative control, to observe any increase or decrease in protein.

4.9 Culturing of fibroblast in 3-Dimensional Scaffolds

The experiments performed in the first part of this thesis have aimed to determine how the addition of ESM may affect fibroblastic cells in a two-dimensional environment, and PEP has been used in these experiments. However, as the research group aims to use this material in wound healing, it is also of interest to discover how ESM function as a material in a 3D substance that could be applied to a deeper wound. Such a 3D structure could function as a scaffold for the dermal fibroblast cells in the skin to proliferate and differentiate, and enable them to produce a new extracellular network within the scaffold. If this would prove successful, such a scaffold can be included in a variety of processes where rapid wound healing would prove to be of vital assistance. Examples of this could be everything from a pad to apply to shallow wounds, or to use in post-surgical wounds, where rapid healing could greatly benefit recovery rate. As such, companies that Nofima have close collaborations with, Biovotec AS and Innovent, have produced different types of 3D scaffolds containing a variety of ESM & collagen concentrations in order for us to discover what concentrations of these compounds are most optimal for the adhesion and growth of fibroblastic cells. For specified information as to what the scaffolds utilized in these experiments contains, see chapter 3.8.

4.9.1 Preparation of Scaffolds

Procedure:

- The different scaffolds produced were placed in 96 well plates and sterilized with 70% EtOH for 10 minutes.
- The EtOH was removed and the scaffolds were washed twice with D-PBS.
- The scaffolds were sliced into smaller fragments (~2mm thick) to ensure proper flow of nutrients.
- The Scaffolds were then placed in a thermostatic cabinet overnight to ensure they were properly dried prior to cell exposure.

4.9.2 Characterisation of scaffolds using Scanning Electron Microscopy

As the need for close-range observation of fibroblastic cells interaction with the scaffolds was of great importance for the thesis, the use of a SEM was apparent. A SEM may provide a far higher resolution and field of depth than the more common light microscopes, and can help obtain great topographical detail (Fischer, Hansen, Nair, Hoyt, & Dorward, 2012).

Prior to SEM imaging, the scaffolds were dehydrated. Although standard air drying may be used on certain substances, it may cause damage to the scaffold surface. As such a method was implemented that exchanges the water in the sample with gaseous CO_2.

Method:

- The process involves solvent dehydration to first exchange the water with ethanol, where the scaffolds were placed in glass vials and exposed to a series of dehydration steps. *All steps were conducted on a shaker*:
    - 3 x 10 minutes with PIPES buffer.
    - 1 x 10 minutes with 50% EtOH.
    - 1 x 10 minutes with 70% EtOH.
    - 1 x 10 minutes with 90% EtOH.
    - 1 x 10 minutes with 96% EtOH.
    - 4 x 10 minutes with 100% EtOH.

This step was followed by Critical Point Drying (CPD) that uses pressure and temperature to exchange the ethanol within the sample with CO_2 (Fischer et al., 2012).

Method:

- The samples were placed on a sample holder.
- The chamber in the CPD instrument was filled to about ¾ with 100% EtOH, and the sample holder was placed inside.
- The instrument was turned on and cooled to 10˚C.
- CO_2 was pumped into the chamber until filled.
- A mixture of EtOH and CO_2 was let out on the back of the instrument.
- This process was repeated until the liquid coming out of the instrument consisted only of CO_2 (indicated by that the liquid coming out consist only of dry ice).
- The sample chamber was heated to 40˚C and influx of CO_2 was stopped.
- The gas remaining in the sample chamber was gradually released.

Following the CPD, the samples were subject to Sputter Coating. Sputter Coating is the process of covering the sample in a thin layer of conductive material. This eliminated any difference of signalling through elemental weight throughout the composition of the sample, which helped obtain proper surface imaging. The coating used consisted of 80% Gold (Au) and 20% Palladium (Pd).

Method:

- The sample holder was placed into the sputter coater chamber.
- The instrument was turned on and the process initiated.
- Argon gas was pumped into the chamber.
- The sample functioned as an anode, and Au/Pd functioned as a cathode.
- The argon gas was ionized, and the argon ions were accelerated towards Au/Pd.
- Au/Pd atoms were released and attracted to the sample.
- The sample holder was continuously turned to ensure a smooth and even layer of atoms was applied on the whole sample.

Analysis and Digitalization

Table 4.6 displays the settings used for SEM imaging.

***Table 4.6: SEM image settings**. The settings used for Scanning Electron Microscopy. The settings displayed as generally "variable" is stated in each individual image.*

Vacuum	High Vacuum, HV
Detector mode	Secondary Electron Imaging (SEI)
Object lens aperture (OLA)	30 µm
EHT	10.00 kV
Spot Size	300
Working Distance (WD)	Variable
Magnification (Mag)	Mainly 50x, 100x and 500x (referencing images)
Brightness	~50%
Contrast	Variable

Each scaffold was observed at different magnifications to note how its components (see chapter 3.8) would affect the structural integrity of the scaffolds. SEM was also used to attempt to observe how the fibroblast cells would adhere, proliferate and differentiate within the scaffolds.

4.9.3 Cell seeding in scaffolds

To ensure the cells properly migrate into the scaffold, the process of applying them was performed in a slow, dropwise fashion. This ensures that the majority of the cells remain and later proliferate inside the scaffold.

Procedure:

- 400.000 cells were added on the top of each scaffold.
- Every 30 minutes, any fluid located in the well was reapplied to the top of the scaffold.

- After ~4 hours, the scaffolds were covered with proliferation medium.
- The plate was then incubated in a thermostatic cabinet for 2 weeks.
- Every 3rd day new proliferation medium was exchanged with the old one.

4.9.4 Live/Dead Staining

To observe whether fibroblast cells were able to grow in the scaffolds, the Live/Dead™ Viability/Cytotoxicity Kit was used. The kit consists of two fluorescent dyes that binds and emits a fluorescent signal for living and dead cells. The dye that binds living cells, calceinAM, is virtually nonfluorescent until it enters a living cell and converts to the highly green fluorescent calcein. EthD-1 may enter cells through damaged membranes and bind to nucleic acids. It will then undergo a conformational change in structure that enhances its fluorescence. As EthD-1 is unable to pass the plasma membrane of living cells, and calcein AM is unable to convert without the presence of naturally occurring ubiquitous intracellular esterase no longer functional in dead cells, these two dyes provide a suitable fluorescent contrast when observing through a fluorescent microscope.

Materials:

- Live/Dead™ Viability/Cytotoxicity Kit
    - EthD-1
    - CalceinAM
- Instrument: Axio Observer Z1 microscope, Jena, Germany
- Software: Zen lite

Procedure:

- The live/dead working solution was prepared, see table 4.7.

Table 4.7: Live/Dead™ Viability/Cytotoxicity working solution. *The reagents and volume required to mix the working solution used in the live/dead™ Viability/Cytotoxicity Kit. The values are balanced for 1 ml of final volume. For each addition in D-PBS a vortex step is required, starting with the addition of EthD-1. As the reagents are light sensitive, it is important the cover the tube in foil or other light excluding materials.*

Reagent	*Volume*
D-PBS	*1 ml*
EthD-1	*2 µl*
CalceinAM	*0,5 µl*

- The wells were thoroughly washed 3x with D-PBS.

- 200 µl of the live/dead working solution was added to each scaffold, ensuring that they were fully covered.
- The plate was then incubated at RT for 45 minutes, while avoiding light exposure.
- The live/dead working solution was removed from the wells and washed 2x with D-PBS.
- The scaffolds were then observed and recorded using fluorescence microscopy.

4.10 Statistics

The graphs presented in chapted 5 were created using Microsoft Excel. Error columns are included in each graph and represent the std. error of mean. Significant variance by treatments in comparison to the untreated sample was determined by one-sample two-tailed t-tests performed in GraphPad Prism Version 7. Differences were considered significant at $p<0.05$.

5. Results

5.1 Different PEP concentrations' effect on cell viability

Fibroblast cells were stimulated with different concentrations of PEP and cell viability was measured after 1 and 3 days of treatment (see figure 5.1). After both 1- and 3 days of treatment, the cell viability shows an increase at lower concentrations, and a steady decline as the PEP concentration increases. The experiment shows that low concentrations of PEP were beneficial to the cells, while higher concentrations of PEP gradually reduced the cell viability. This reduction appeared to show significant decrease around 4 mg/ml following 3 days of treatment, and at 5 mg/ml following 1 day of treatment.

A) B)

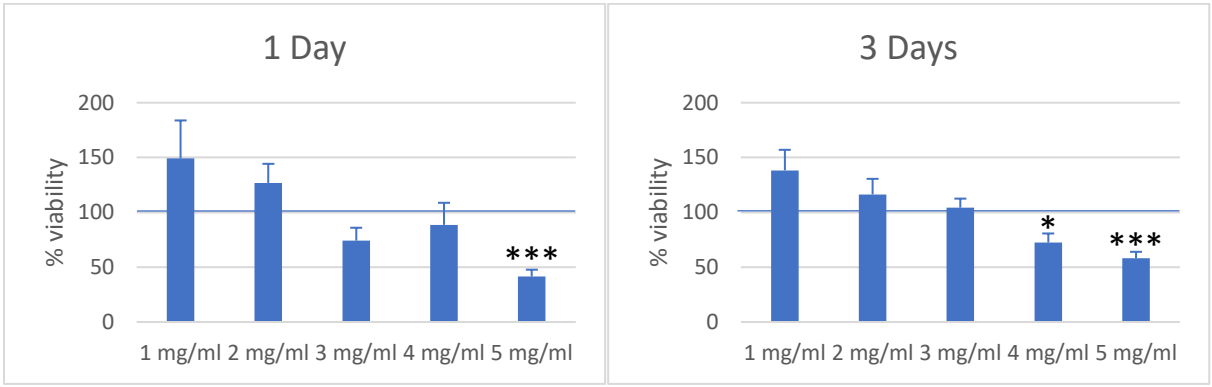

Figure 5.1: Different concentrations of PEP affect viability. *The cell viability after different concentration of PEP following A) 1 day of treatment, and B) 3 days of treatment. Cells with only starvation medium was used as a negative control, and each data was normalised to negative control (starvation medium only, which was set to 100% for the indicated time period baseline, indicated with line). The results are from 3 independent cell experiments performed in triplicates. Data is presented as mean + SEM. Asterisk denote show significant differences between control and PEP treated cells at the indicated time periods (*p < 0.05, ***p < 0.001).*

5.2 Different PEP concentrations' cytotoxic effect on fibroblast cells

Fibroblast cells were supplemented with different concentrations of PEP and cytotoxic effect was measured through LDH release. With the exception of 1 day treatment with 1 mg/ml PEP, all concentrations led to increased cytotoxicity (see figure 5.2). The lower concentrations led to modest cytotoxicity, which increased with higher concentration.

A) B)

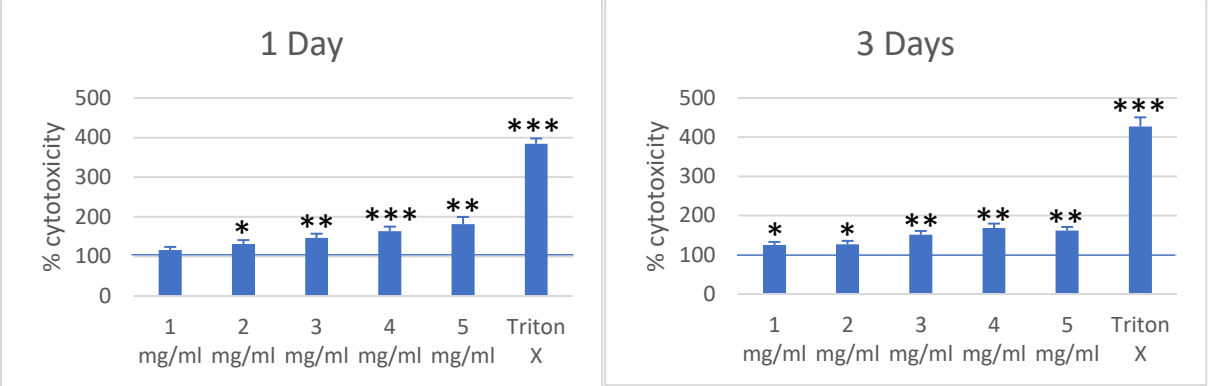

Figure 5.2: PEP cytotoxic effect on fibroblast cells. *The effects after different PEP supplementation after A) 1 day of treatment, and B) 3 days of treatment. Cells with only starvation medium was used as a negative control, and each data was normalised to negative control (starvation medium only, which was set to 100% for the indicated time period baseline, indicated with line). The cytotoxic agent Triton X was used as a positive control. The results are from 3 independent cell experiments performed in triplicates. Data is presented as mean + SEM. Asterisk denote show significant differences between control and PEP treated cells at the indicated time periods (*p < 0.05, **p < 0.01, ***p < 0.001).*

5.3 Different PEP concentrations' effect on cell proliferation

5.3.1 Fluorescence measurement of cell density

Fibroblast cells were supplemented with different concentrations of PEP and proliferation was measured after 1 and 3 days of treatment (see figure 5.3). PEP substantially increase cell proliferation at all concentrations tested compared to the untreated samples, even after just 1 day of treatment. The effect is more evident after 3 days of PEP treatment. After 3 days of treatment, higher concentrations of PEP show higher proliferation compared to the negative control, with the exception of 4 mg/ml.

A) B)

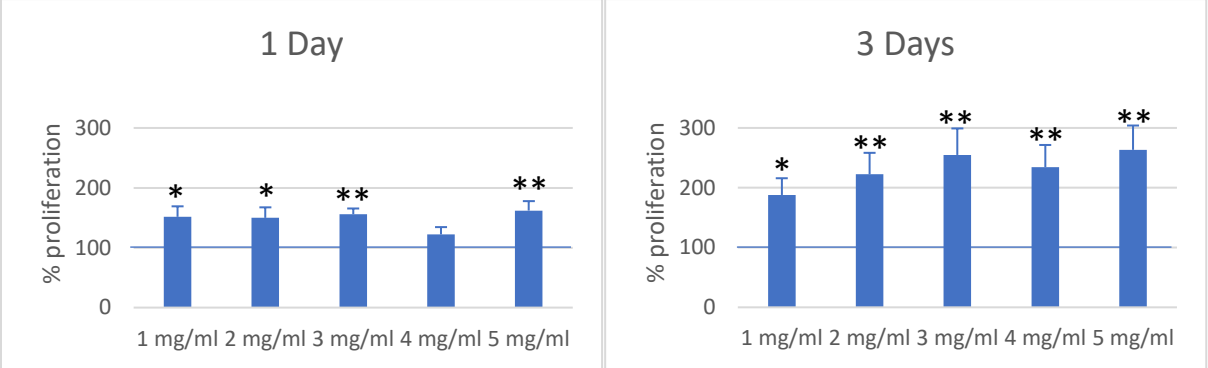

Figure 5.3: Different concentrations of PEP affect proliferation. *Cell proliferation after different concentration of PEP following A) 1 day of treatment, and B) 3 days of treatment. Cells with only starvation medium was used as a negative control, and each data was normalised to negative control (starvation medium only, which was set to 100% for the indicated time period baseline, indicated with line). The results are from 3 independent cell experiments performed in triplicates. Data is presented as mean + SEM. Asterisk denote show significant differences between control and PEP treated cells at the indicated time periods (*p < 0.05, **p < 0.01).*

Following the experiments performed above, it was decided that the ESM concentrations most favourable to work further with was 1 mg/ml and 3 mg/ml, which showed a high effect on cell proliferation, low cytotoxicity and no decrease in cell viability.

5.3.2 Relative gene expression of proliferation marker Ki67

Using real-time PCR, the effect PEP had on proliferation was further studied by using the proliferation marker *ki67* (see figure 5.4). In addition to the previously conducted time periods, *ki67* measurement was also performed after 10 days of treatment (see figure 5.4C), where there is no significant increase compared to the negative control. A western blot experiment was also conducted using Ki67 to measure protein expression, but this resulted in no bonds, and was therefore not included in this thesis.

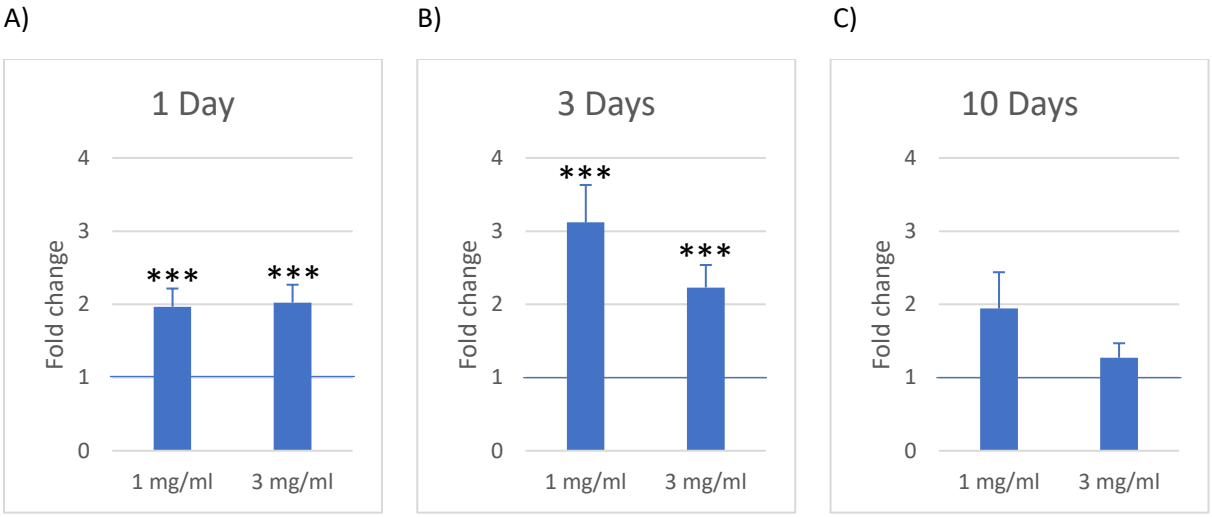

Figure 5.4: Relative gene expression of the proliferation marker Ki67. *Gene expression during PEP treatment for 1 A), 3 B), and 10 C) days. The effects on relative Ki67 gene expression with 1 mg/ml and 3 mg/ml PEP as compared to untreated cells (control). The values were normalised against control cells, set to 1, and each column represents a mean of 3 different experiments seeded out in triplicates, performed in technical triplicates. The graphs show the relative gene expression (fold change) in cells subjected to PEP treatments compared to control cells (which are set to one, baseline indicated with line). Data is presented as mean + SEM. Asterisk denote show significant differences between control and PEP treated cells at the indicated time periods (***p < 0.001).*

5.4 PEP effect on cell differentiation in fibroblasts

Fibroblast cells differentiate to myofibroblast cells. This differentiation can be observed by measuring the α-SMA amount in samples, as this protein is only expressed in myofibroblast cells (Darby et al., 2014). The amount of α-SMA was measured using real-time PCR (mRNA) and western blot (protein) to observe differentiation after 1-, 3- and 10 days of PEP treatment in the fibroblast cell culture. There was no difference in relative gene expression between the negative control and PEP treated cells after 1- and 3 days treatment, and a small decrease in *α-sma* gene expression after 10 days (see figure 5.5). This is in contrast to protein levels of α-SMA during the indicated time periods, in which we observed an increase after 1 day of treatment, and significant decrease after 3 days (see figure 5.6). Following 10 days, no significant variations were observed.

A) B) C)

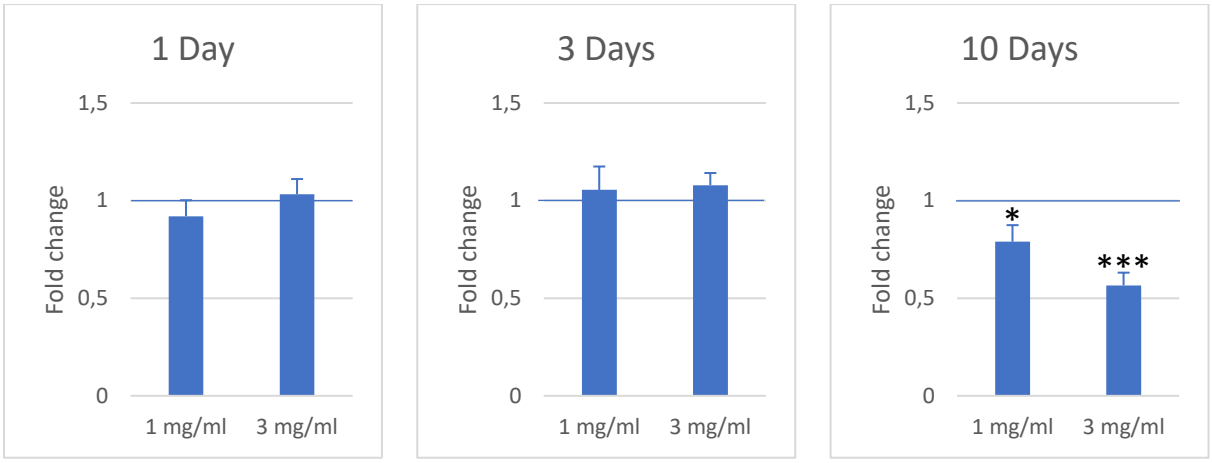

Figure 5.5: Relative gene expression of the differentiation marker α-sma. *Gene expression during PEP treatment for one A), three B), and ten C) days. The effects on relative α-sma gene expression with 1 mg/ml and 3 mg/ml PEP as compared to untreated cells (control). The values were normalised against control cells, set to 1, and each column represents a mean of 3 different experiments seeded out in triplicates, performed in technical triplicates. The graphs show the relative gene expression (fold change) in cells subjected to PEP treatments compared to control cells (which are set to one, baseline indicated with line). Data is presented as mean + SEM. Asterisk denote show significant differences between control and PEP treated cells at the indicated time periods (*p < 0.05, ***p < 0.001).*

A)

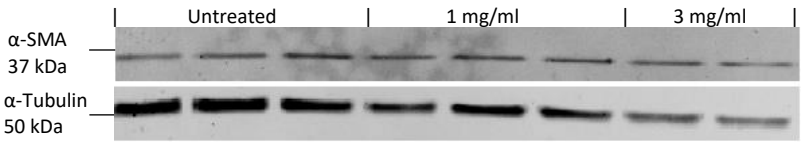

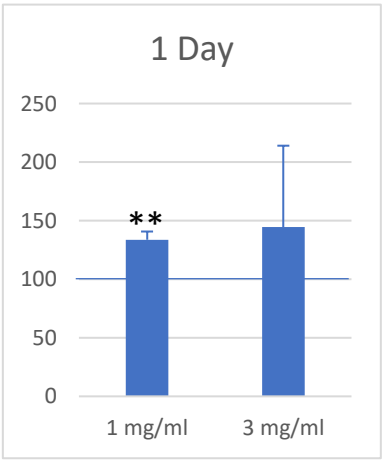

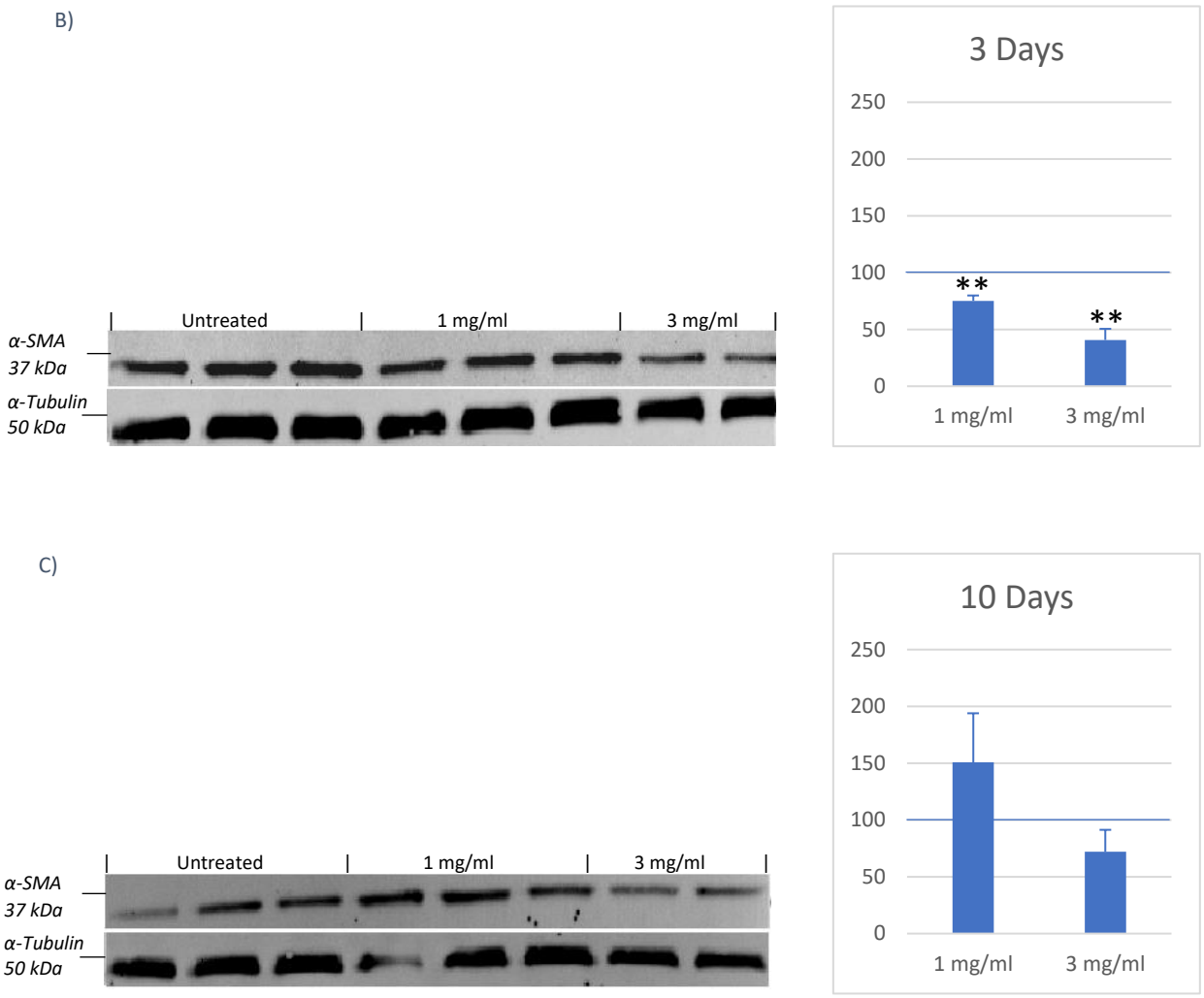

Figure 5.6: Protein expression of differentiation marker α-SMA. *A representative western blot image shown in 1 day of PEP treatment A), 3 days of PEP treatment B), 10 days of PEP treatment C). The upper images display the bond of α-SMA, while the lower images display the bond of the reference protein, α-tubulin. These images were quantified and the corresponding values were substracted against the reference protein values. To the right are the corresponding graphs of the relative protein expression in cells subjected to PEP treatments compared to control cells (which are set to 100, baseline indicated with line). Data is presented as mean + SEM. Asterisk denote show significant differences between control and PEP treated cells at the indicated time periods (**p < 0.01).*

5.5 PEP effect of Hsp70 expression in fibroblast cells

Hsp70 is a chaperone protein commonly expressed in higher rate during wound healing (Atalay et al., 2009). The amount of Hsp70 was measured using real-time PCR (mRNA) and western blot (protein) to observe effects in expression after 1-, 3- and 10 days of PEP treatment in the fibroblast cell culture. There is an increase in relative gene expression when comparing all PEP treated cells with the negative control (untreated cells). There is an increased difference compared to the negative control with increased PEP amount and increased treatment period (figure 5.7). This is in contrast to protein levels (figure 5.8), which shows a significant increase in expression at 1 day of PEP treatment compared to

negative control. At 3 days of PEP treatment there is a similar Hsp70 protein expression for cell treated with PEP and negative control. At 10 days of PEP treatment, there is a significant decrease in Hsp70 protein expression compared to negative control.

A) B) C)

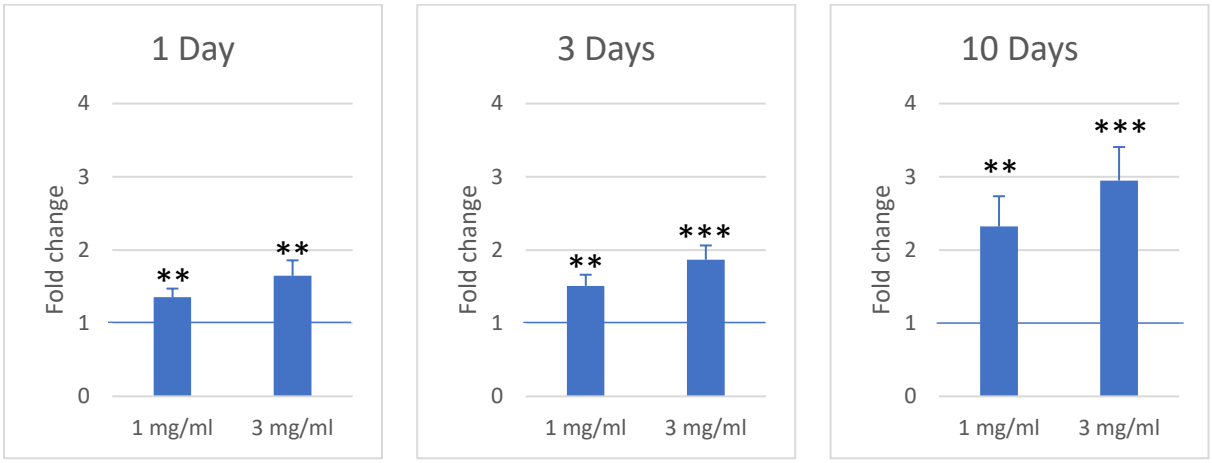

Figure 5.7: Relative gene expression of hsp70. *Gene expression during PEP treatment for one A), three B), and ten C) days. The effects on relative hsp70 gene expression with 1 mg/ml and 3 mg/ml PEP as compared to untreated cells (control). The values were normalised against control cells, set to 1, and each column represents a mean of 3 different experiments seeded out in triplicates, performed in technical triplicates. The graphs show the relative gene expression (fold change) in cells subjected to PEP treatments compared to control cells (which are set to one, baseline indicated with line). Data is presented as mean + SEM. Asterisk denote show significant differences between control and PEP treated cells at the indicated time periods (**p < 0.01, ***p < 0.001).*

A)

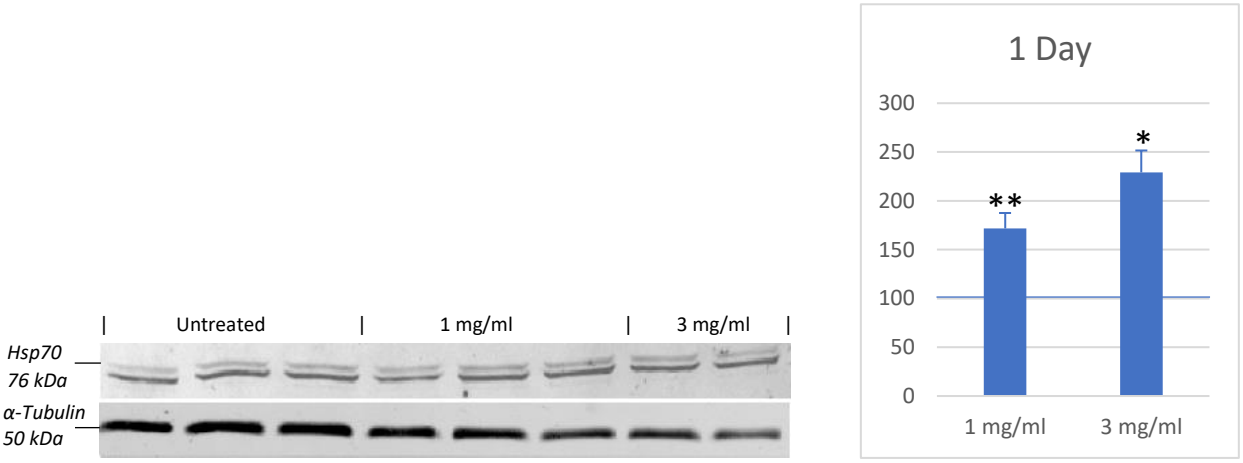

B)

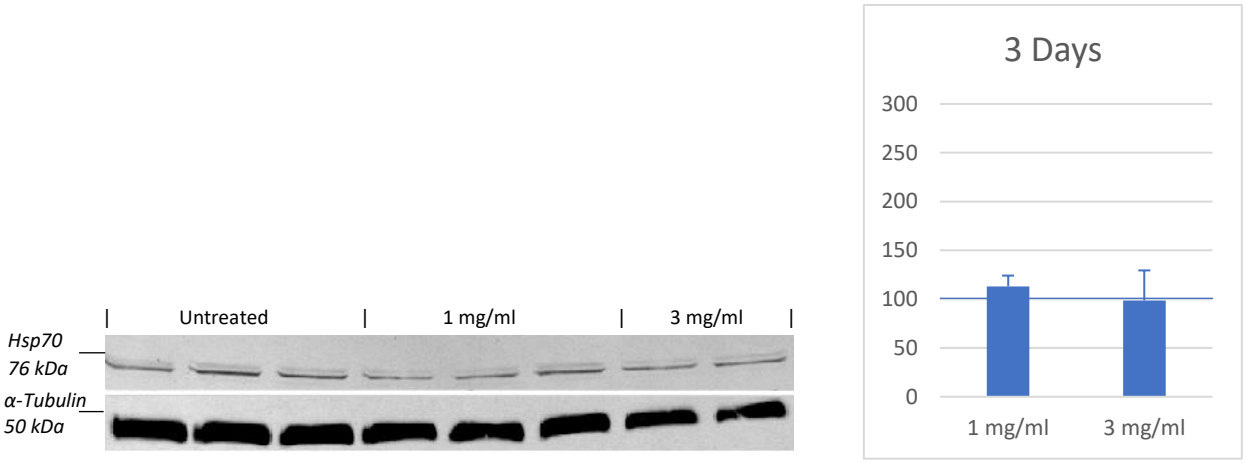

C)

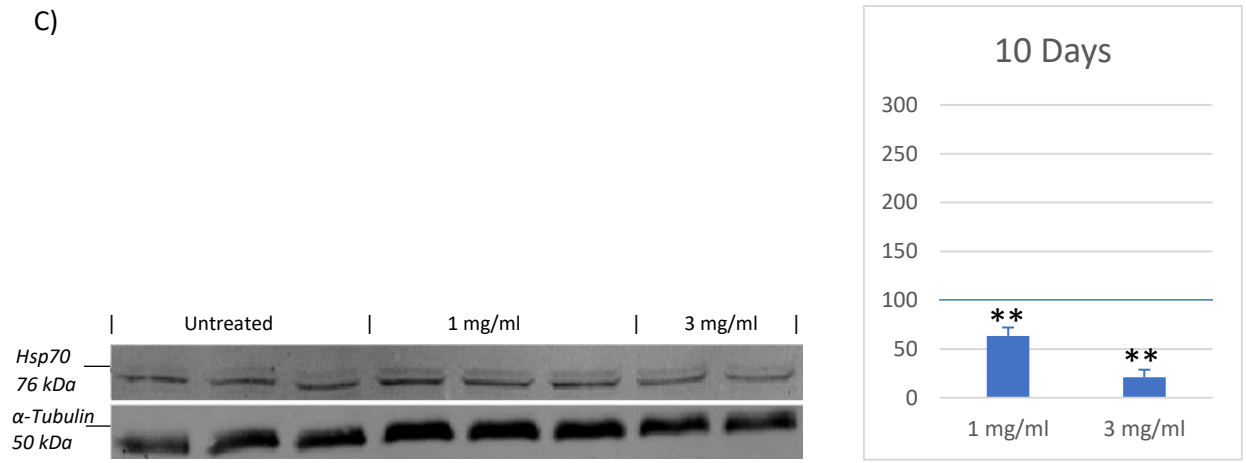

Figure 5.8: Protein expression of Hsp70. *A representative western blot image shown in 1 day of PEP treatment A), 3 days of PEP treatment B), 10 days of PEP treatment C). The upper images display the bond of Hsp70, while the lower images display the bond of the reference protein, α-tubulin. These images were quantified and the corresponding values were substracted against the reference protein values. To the right are the corresponding graphs of the relative protein expression in cells subjected to PEP treatments compared to control cells (which are set to 100, baseline indicated with line). Data is presented as mean + SEM. Asterisk denote show significant differences between control and PEP treated cells at the indicated time periods (*p < 0.05, **p < 0.01).*

5.6 Effect of PEP on expression of ECM production

During wound healing, there are numerous components generated by fibroblast cells to create the ECM. In order to observe how the addition of ESM to fibroblast cells would affect this process, three mRNA precursors for structural proteins known to be part of this process was measured. The gene expression level of *collagen 1* (see figure 5.9), *collagen 3* (see figure 5.10) and *elastin* (see figure 5.11)

was measured using real-time PCR to observe differentiation after 1-, 3- and 10 days of PEP treatment in the fibroblast cell culture. There appears to be no significant difference in the expression of these genes, with some exceptions. There is an increase in expression of *collagen 1* and *collagen 3* following ten days of treatment with 3 mg/ml PEP, and a decrease in expression in *collagen 3* and *elastin* following three days of treatment with 1 mg/ml PEP. There is also a significant decrease of *collagen 3* expression following one day of treatment with 1 mg/ml PEP.

5.6.1 Collagen 1

A) B) C)

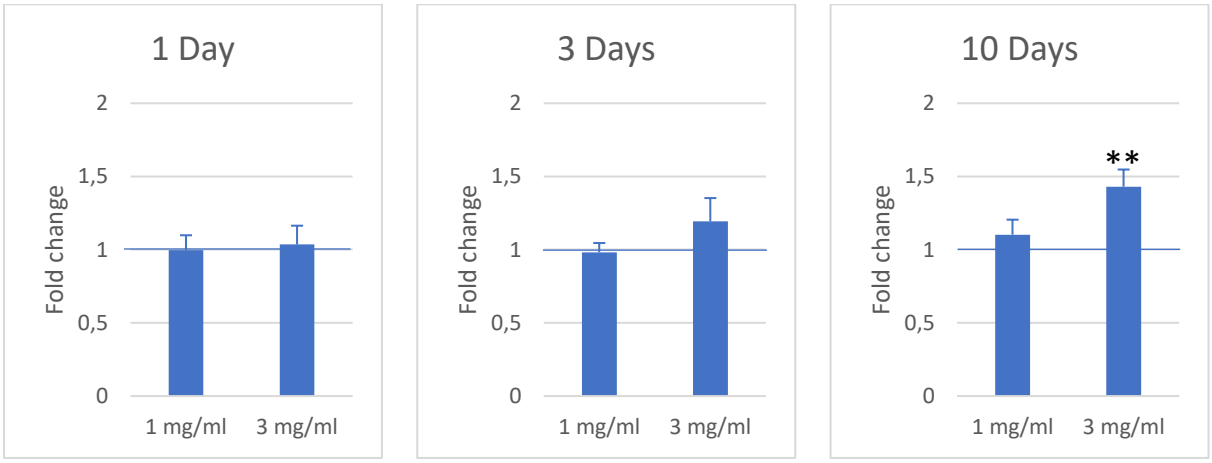

Figure 5.9: Relative gene expression of collagen 1. *Gene expression during PEP treatment for one A), three B), and ten C) days. The effects on relative collagen 1 gene expression with 1 mg/ml and 3 mg/ml PEP as compared to untreated cells (control). The values were normalised against control cells, set to 1, and each column represents a mean of 3 different experiments seeded out in triplicates, performed in technical triplicates. The graphs show the relative gene expression (fold change) in cells subjected to PEP treatments compared to control cells (which are set to one, baseline indicated with line. Data is presented as mean + SEM. Asterisk denote show significant differences between control and PEP treated cells at the indicated time periods (**p < 0.01).*

5.6.2 Collagen 3

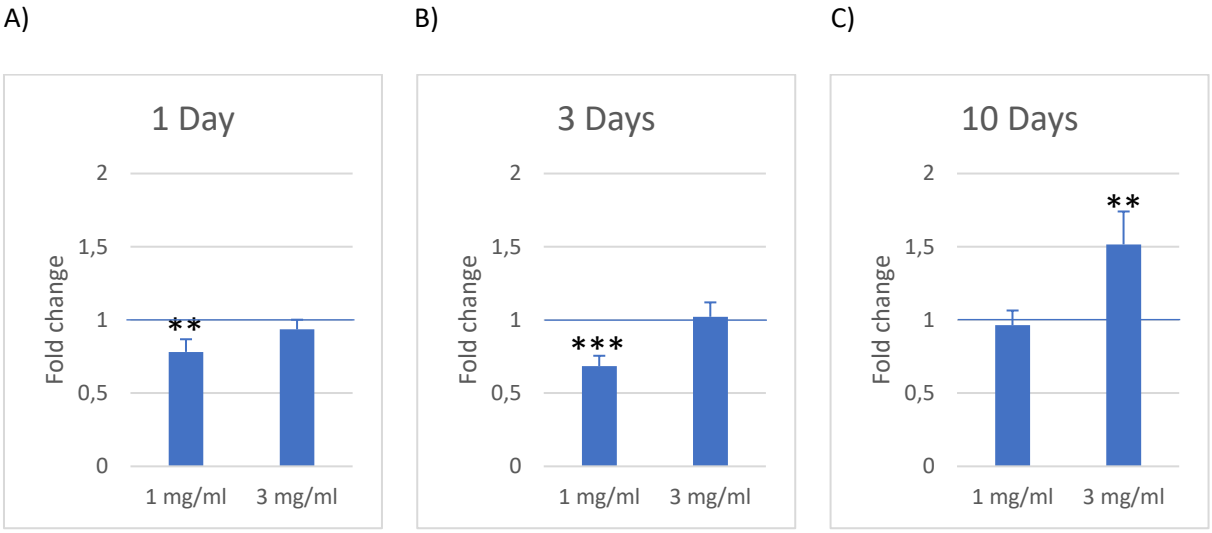

Figure 5.10: Relative gene expression of collagen 3. *Gene expression during PEP treatment for one A), three B), and ten C) days. The effects on relative collagen 3 gene expression with 1 mg/ml and 3 mg/ml PEP as compared to untreated cells (control). The values were normalised against control cells, set to 1, and each column represents a mean of 3 different experiments seeded out in triplicates, performed in technical triplicates. The graphs show the relative gene expression (fold change) in cells subjected to PEP treatments compared to control cells (which are set to one, baseline indicated with line. Data is presented as mean + SEM. Asterisk denote show significant differences between control and PEP treated cells at the indicated time periods (**p < 0.01, ***p < 0.001).*

5.6.3 Elastin

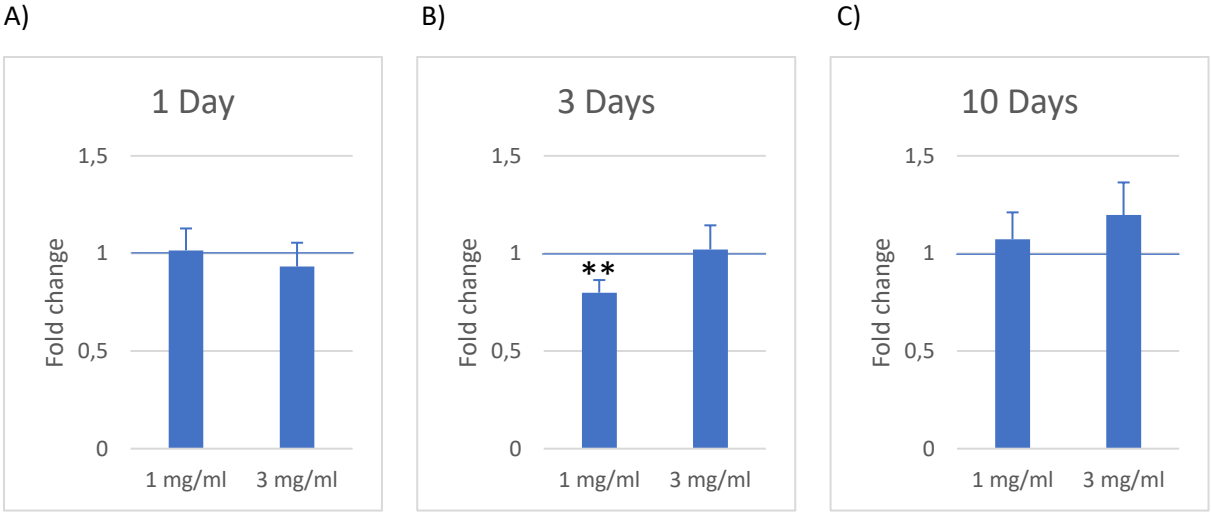

Figure 5.11: Relative gene expression of elastin. *Gene expression during PEP treatment for one A), three B), and ten C) days. The effects on relative elastin gene expression with 1 mg/ml and 3 mg/ml PEP as compared to untreated cells (control). The values were normalised against control cells, set to 1, and each column represents a mean of 3 different experiments seeded out in triplicates, performed in technical triplicates. The graphs show the relative gene expression (fold change) in cells subjected to PEP treatments compared to control cells (which are set to one, baseline indicated with line. Data is presented as*

*mean + SEM. Asterisk denote show significant differences between control and PEP treated cells at the indicated time periods (**p < 0.01).*

5.7 Structural characterisation of scaffolds (SEM)

SEM was used to visualize the difference in structure between the scaffolds, and to observe how the different components would integrate to the matrix. An image of each scaffold was taken at 50x and 500x magnification. The images show how the inclusion of ESM into a 3D scaffold will generate a more irregular surface, which may assist in cell adhesion. PEGDA appears to make the structural integrity of the scaffold more rigid, and the passages within the scaffolds smaller. It is uncertain whether this provides a positive effect other than scaffold stability.

5.7.1 Biovotec Control Scaffold

The Biovotec control scaffold has been pre-sterilized and contains 0.75% collagen. No ESM or PEGDA is present in this scaffold.

A)

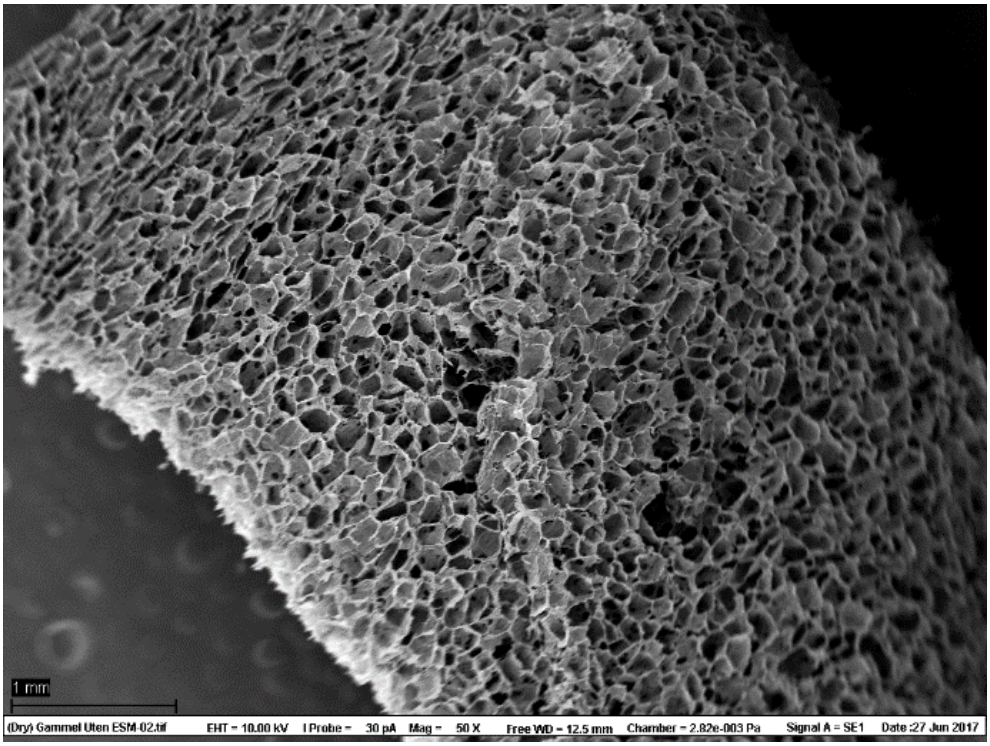

B)

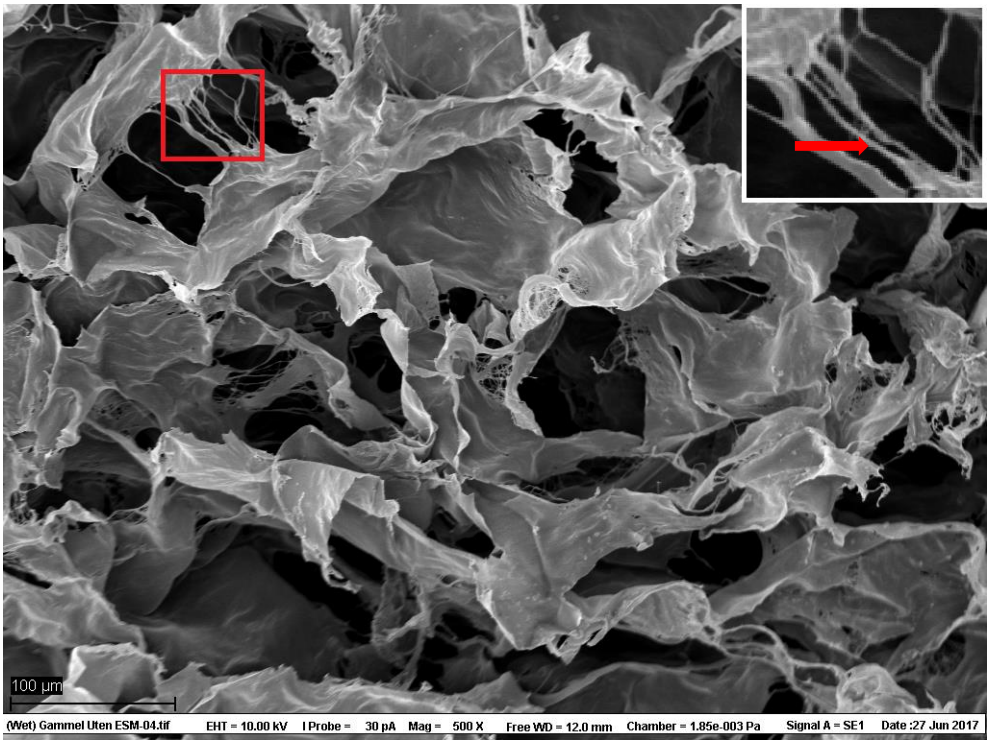

Figure 5.12: Structural imaging of Biovotec Control Scaffold. *Images captured of Biovotec control scaffold using SEM with a A) magnification of 50x, and with B) a magnification of 500x. The boxed area is presented at high magnification in the upper right corner. The red arrows indicate collagen accumulation.*

5.7.2 Biovotec ESM Scaffold

The Biovotec ESM scaffold has been pre-sterilized and contains 0.75% collagen and 3% ESM. No PEGDA is present in this scaffold.

A)

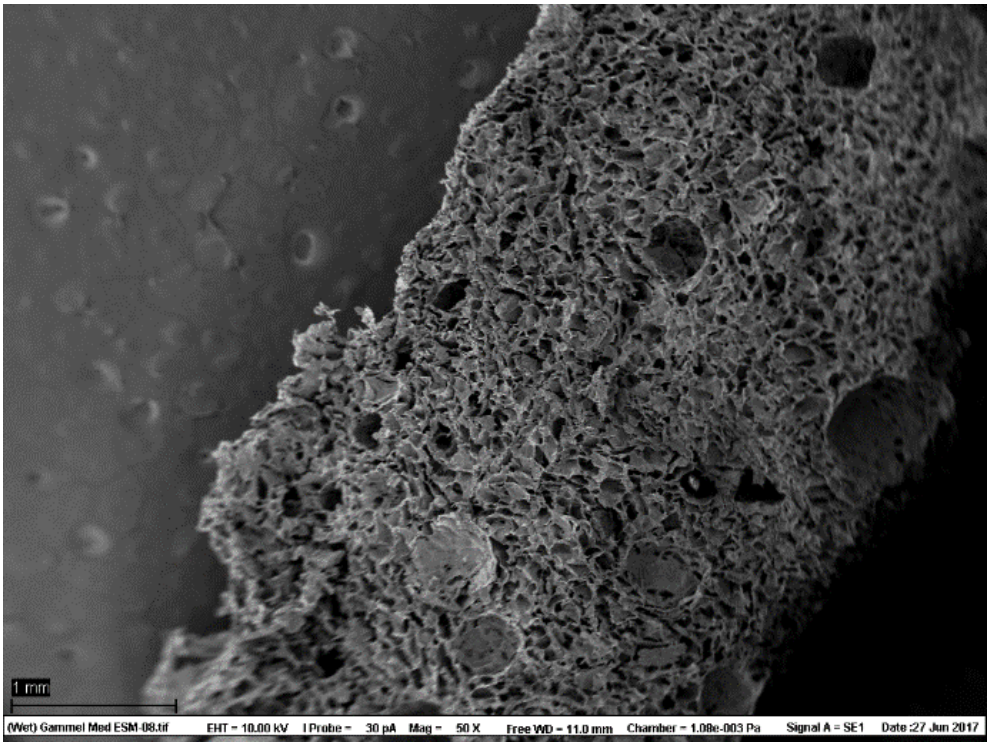

B)

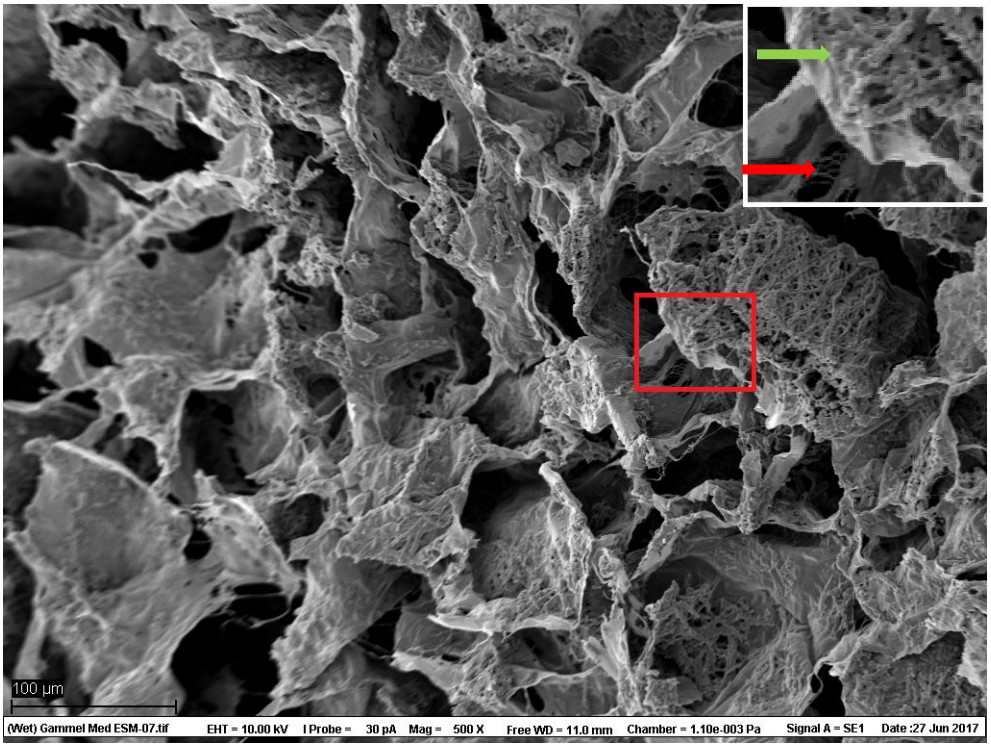

Figure 5.13: Structural imaging of Biovotec ESM scaffold. *Images captured of Biovotec ESM scaffold using SEM with a A) magnification of 50x, and with B) a magnification of 500x. The boxed area is presented at high magnification in the upper right corner. The red arrows indicate collagen accumulation. The green arrows indicate ESM accumulation.*

5.7.3 Cryogel 5

The Cryogel 5 scaffold was sterilized using 70% EtOH and washed with D-PBS. It contains 200 mg/ml PEGDA, 2 mg/ml collagen and 50 mg/ml ESM.

A)

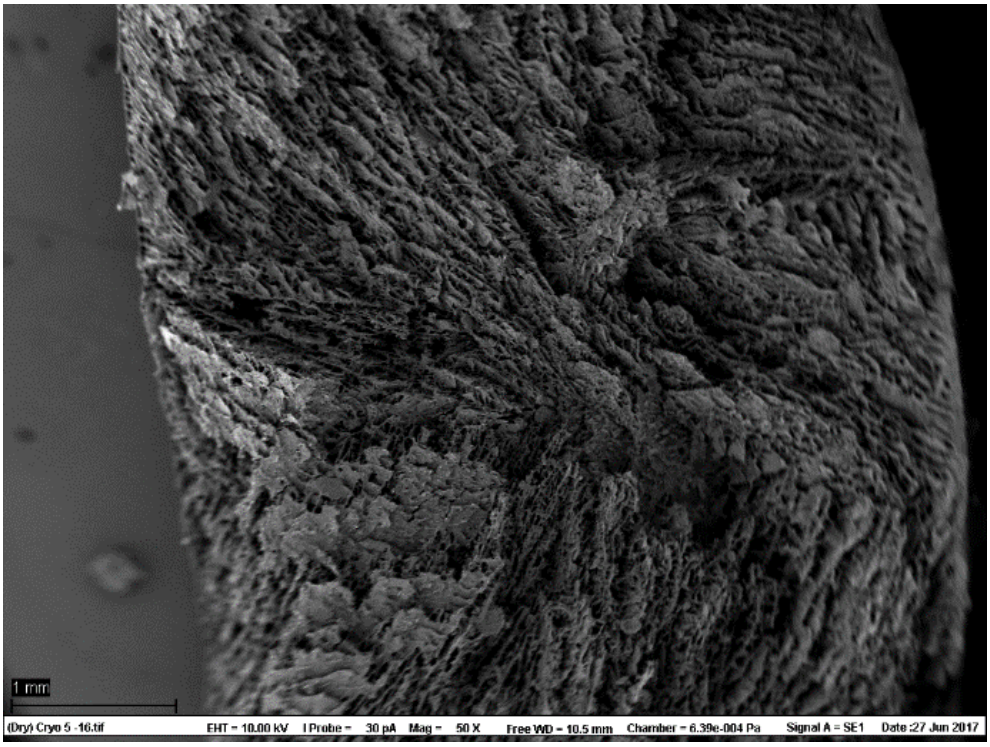

B)

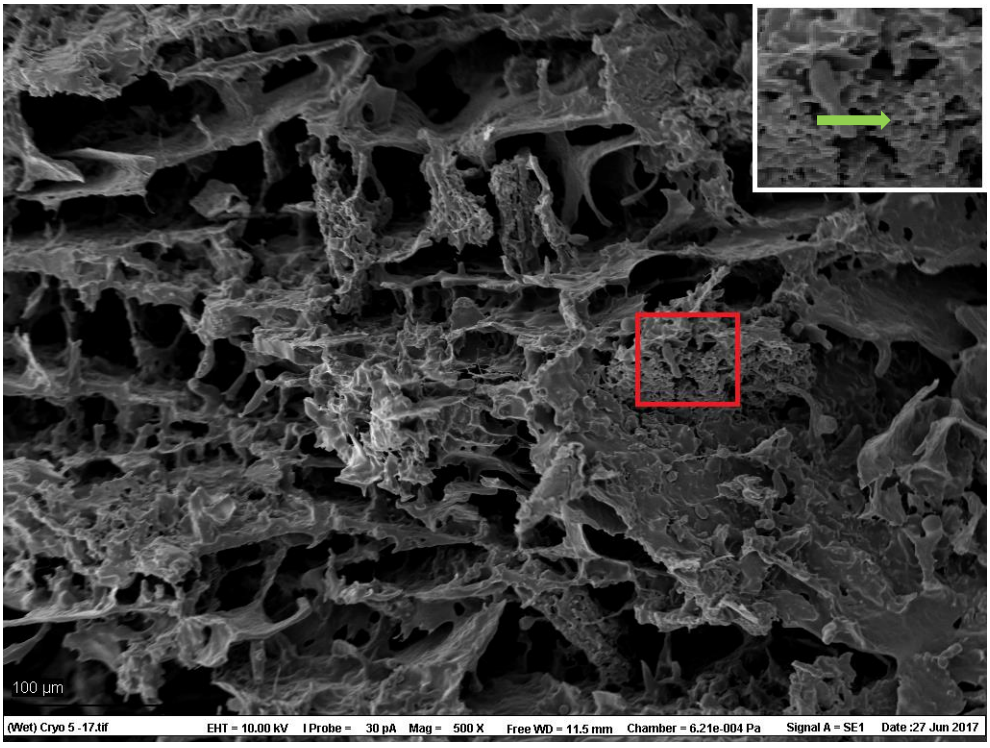

Figure 5.14: Structural imaging of Cryogel 5 Scaffold. *Images captured of Cryogel 5 scaffold using SEM with a A) magnification of 50x, and with B) a magnification of 500x. The boxed area is presented at high magnification in the upper right corner. The green arrows indicate ESM accumulation.*

5.7.4 Cryogel 6

The Cryogel 6 scaffold was sterilized using 70% EtOH and washed with D-PBS. It contains 200 mg/ml PEGDA, 2 mg/ml collagen and 12,5 mg/ml ESM. Cryogel 6 contains accumulations of ESM, albeit far smaller and less concentrated than those found in Cryogel 5 and Biovotec ESM scaffolds. The blue arrow shown indicate what is believed to be PEGDA congestions. However, as these structures are not present in Cryogel 5 and Cryogel 8, which contains an identical concentration of PEGDA, it uncertain whether this is the case.

A)

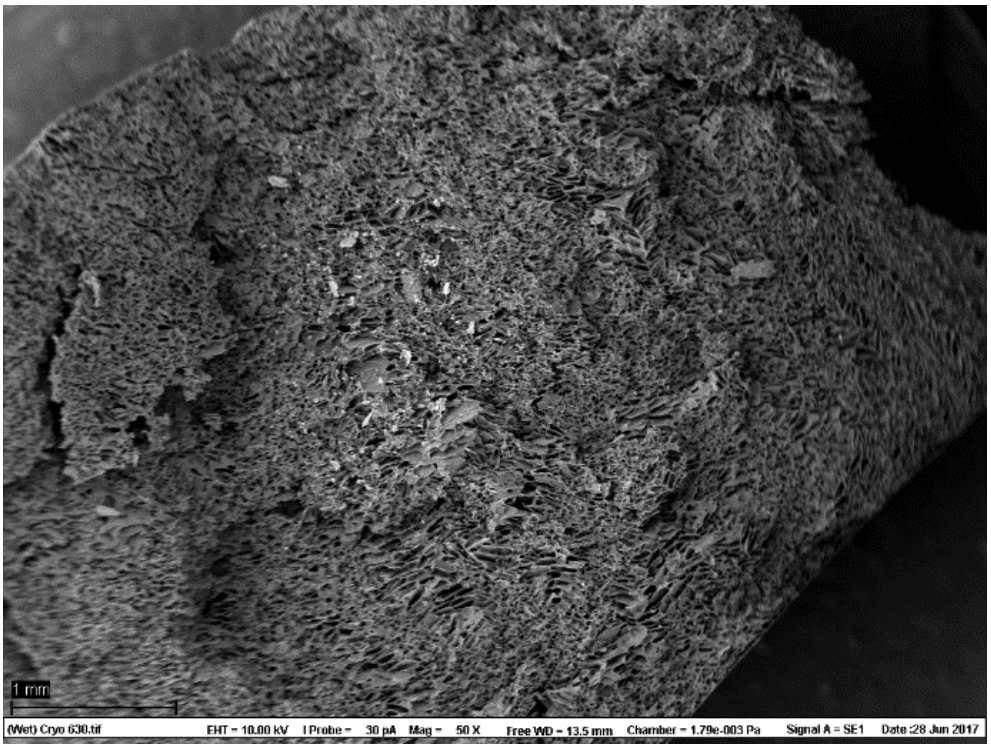

B)

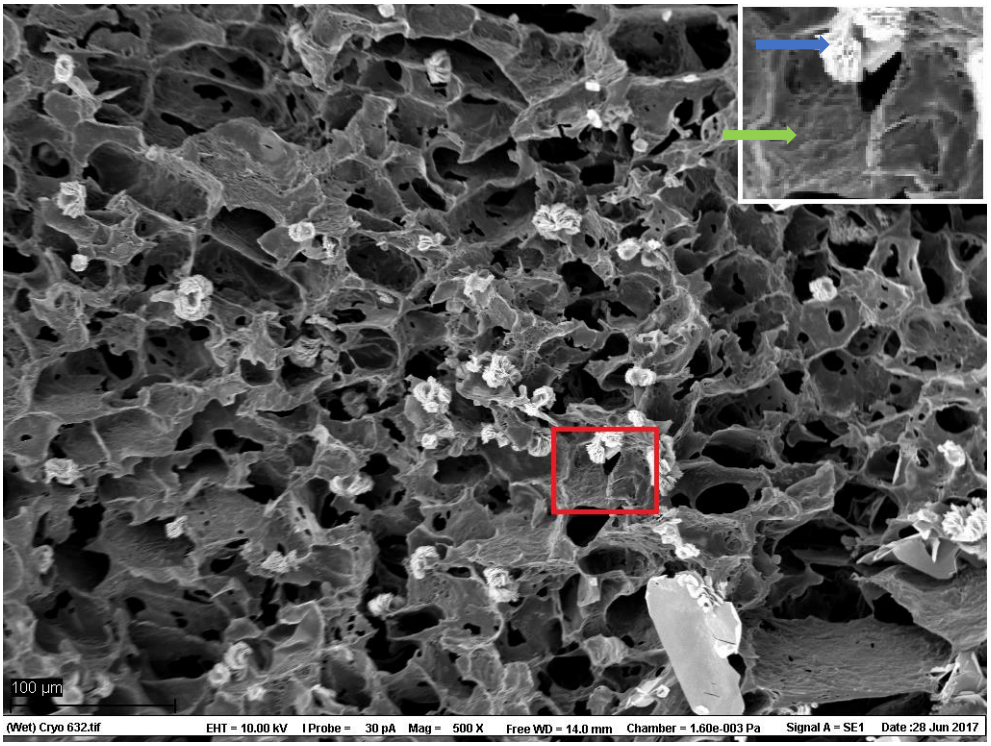

Figure 5.15: Structural imaging of Cryogel 6 Scaffold. *Images captured of Cryogel 6 scaffold using SEM with a A) magnification of 50x, and with B) a magnification of 500x. The boxed area is presented at high magnification in the upper right corner. The green arrows indicate ESM accumulation. The blue arrows indicate what is believed to be PEGDA accumulation.*

5.7.5 Cryogel 8

The Cryogel 8 scaffold was sterilized using 70% EtOH and washed with D-PBS. It contains 200 mg/ml PEGDA and 2 mg/ml collagen. There is no ESM present in this scaffold. In comparison to Biovotec control scaffold, there is a reduced amount of collagen accumulation to be found in this scaffold.

A)

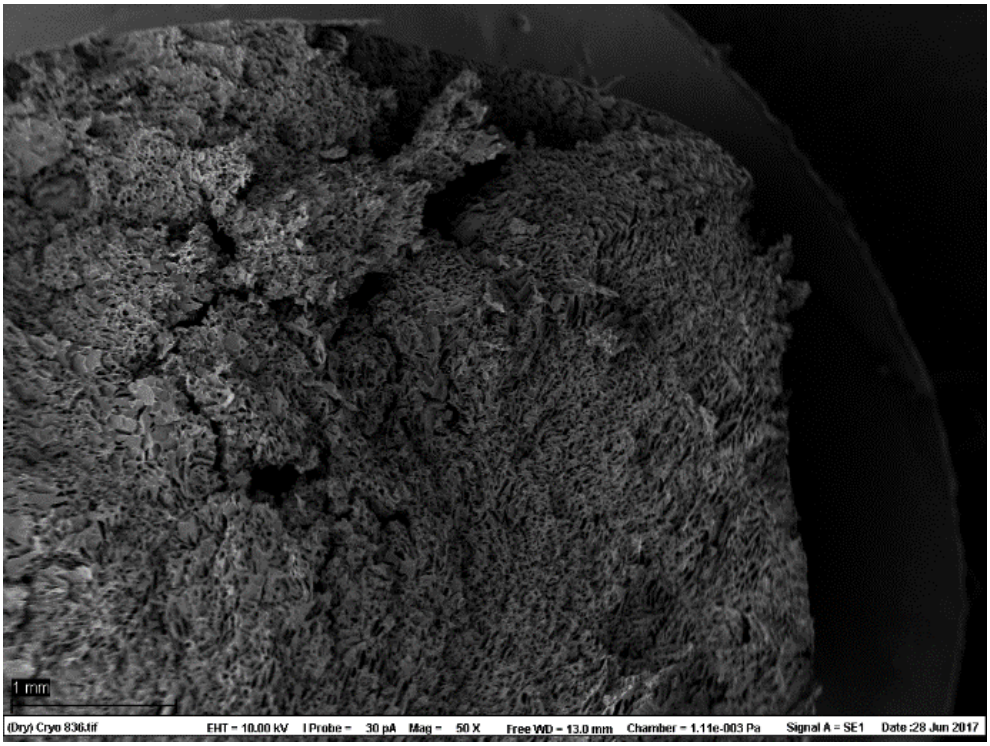

B)

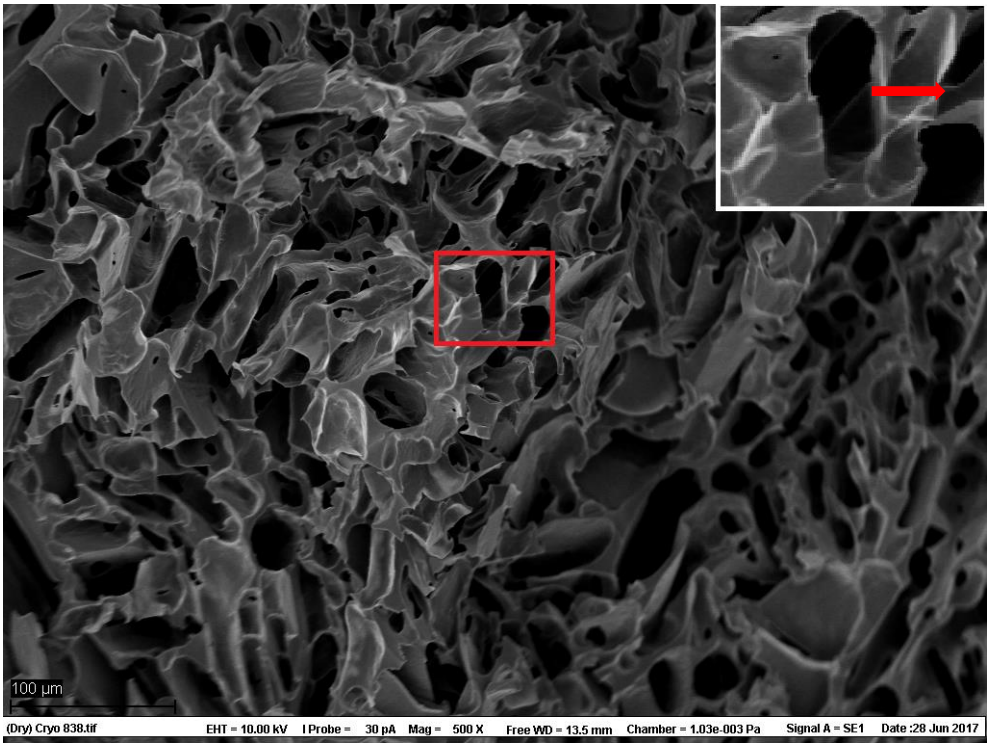

Figure 5.16: Structural imaging of Cryogel 8 Scaffold. *Shown are images captured of Cryogel 8 scaffold using SEM with a A) magnification of 50x, and with B) a magnification of 500x. The boxed area is presented at high magnification in the upper right corner. The red arrows indicate collagen accumulation.*

5.8 Live/Dead Imaging of cells grown in scaffold

The red dye EthD-1 was used to colour dead cells, while the green dye calceinAM was used to colour living cells. Through fluorescent microscopy the cells were observed in the scaffolds to qualitatively determine if cells could adhere and proliferate into the different scaffolds. EthD-1 also reacted with PEGDA in the scaffolds, but it was still possible to differentiate between unspecific staining and the dead cells. Calcein also reacted with some components in the scaffolds, including ESM, but it was still possible to differentiate between them and the living cells. The image stacks show that fibroblast cells are present throughout the scaffolds. There appears to be a somewhat higher cell number in the scaffolds containing ESM. However, this is not a quantitative analysis, and therefore not enough to determine significant variation.

5.8.1 Live/Dead imaging of Biovotec control Scaffold

When exposed to cells in starvation medium, the scaffold immediately lost its form (fell together). Despite this, when observing cells in the scaffold using fluorescent imaging, there is definite presence of both living and dead cells (see figure 5.17).

A)

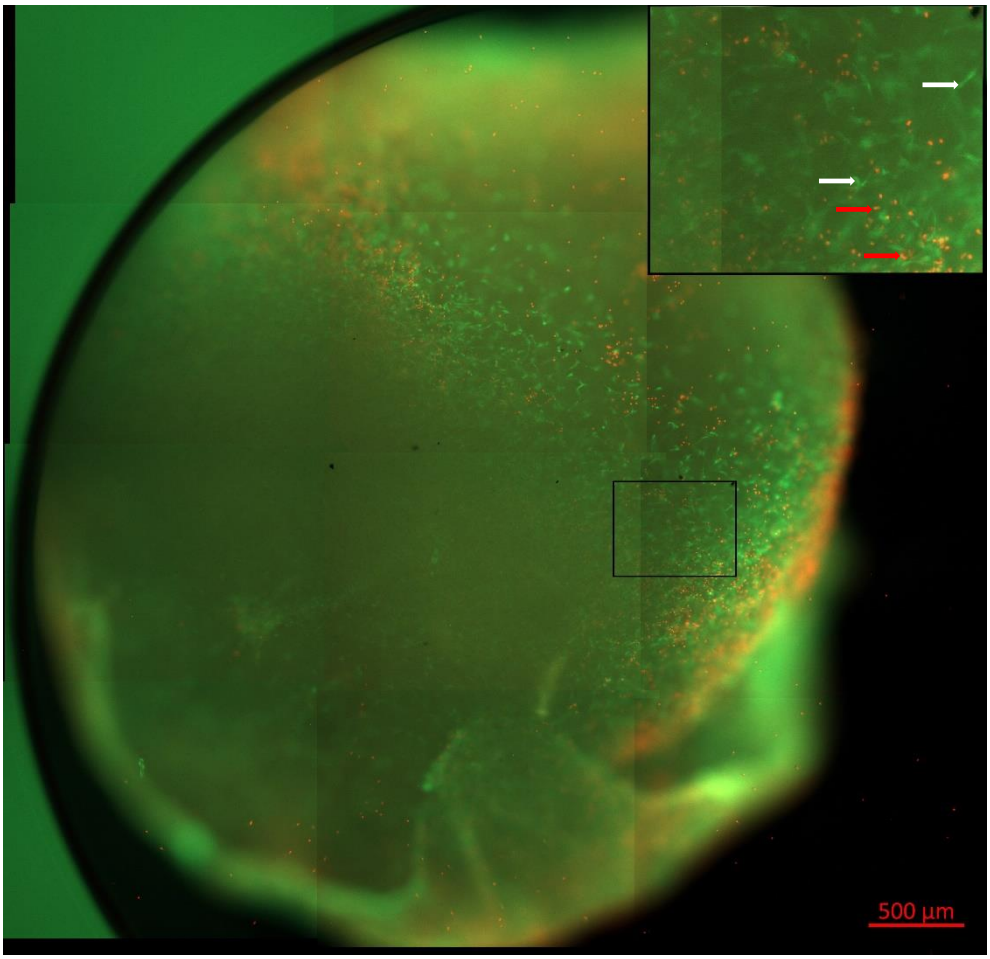

B)

i)

Top Section

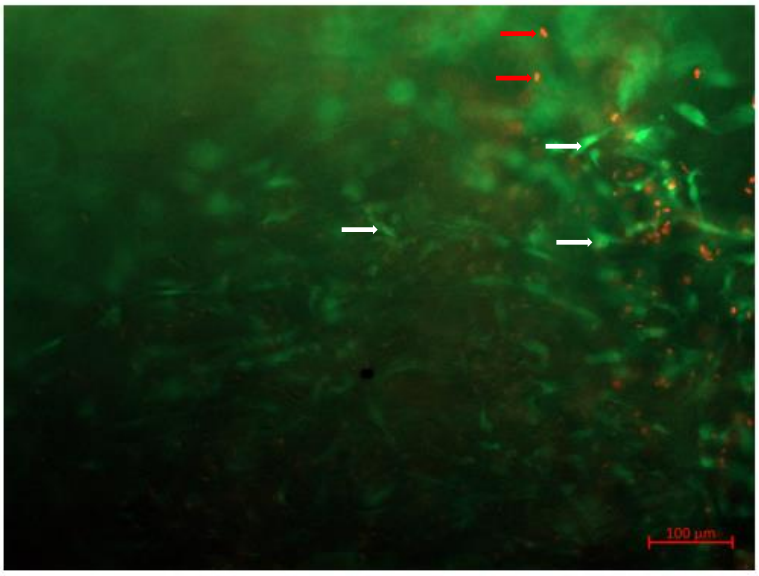

ii)

Middle Section

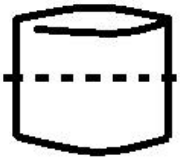

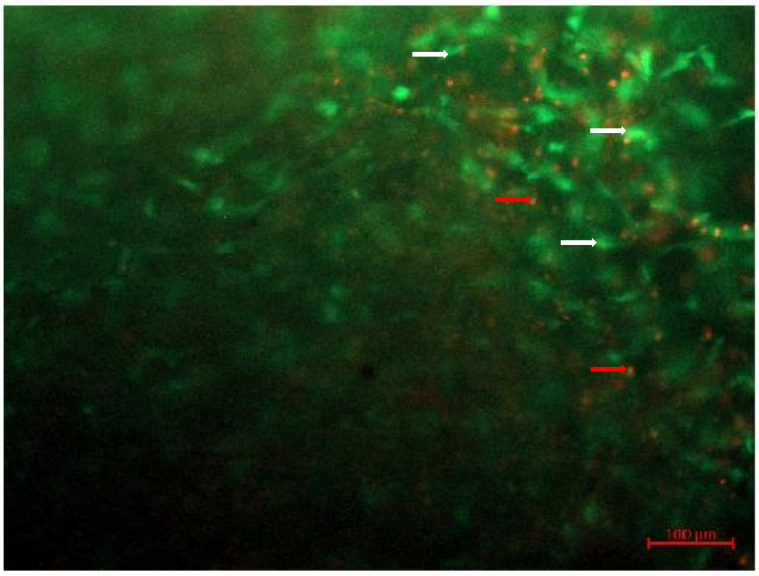

iii)

Lower Section

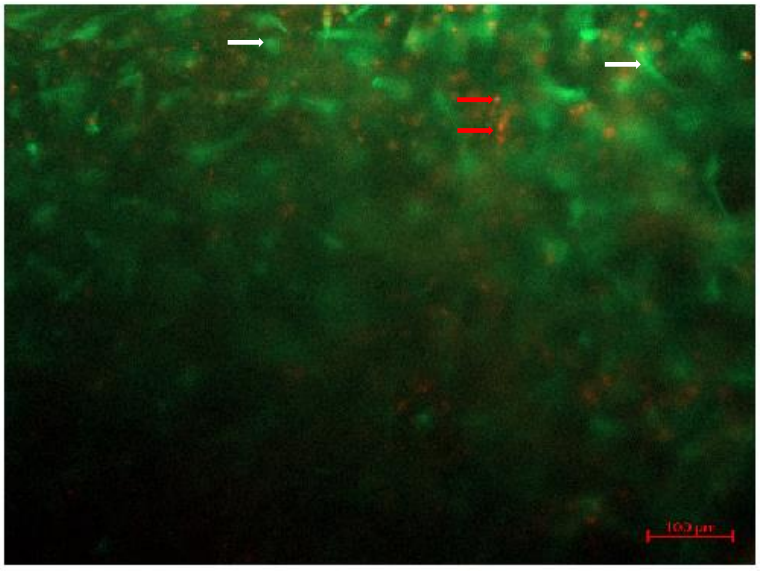

C)

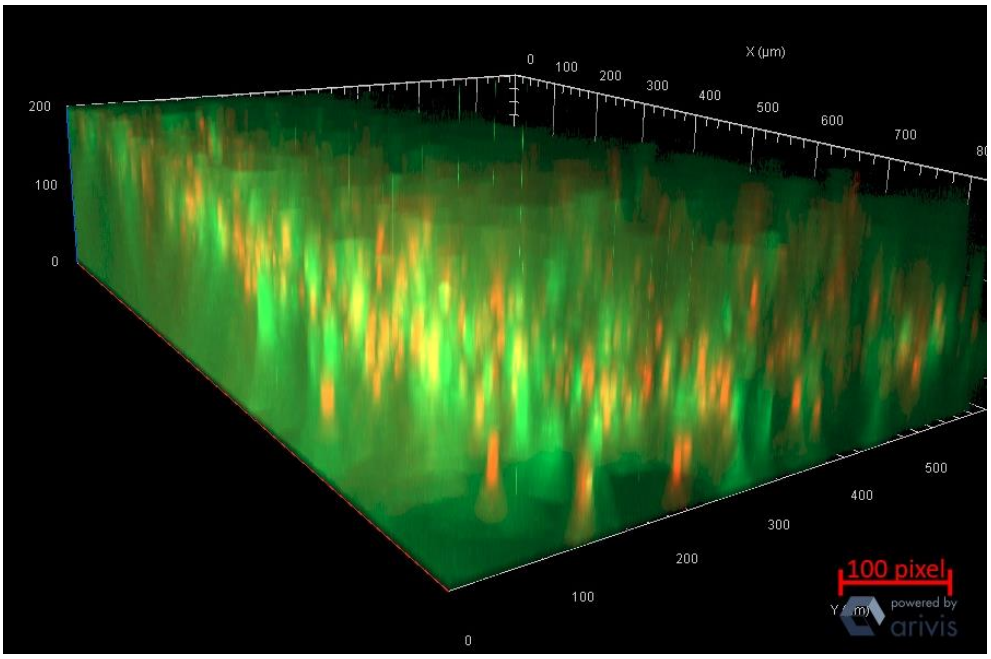

Figure 5.17: Fluorescence microscopy analysis of fibroblast cells in Biovotec control scaffold. *Cells were stained using Live/Dead™ Viability/Cytotoxicity kit to differentiate between living and dead cells. Cells were applied to scaffold and incubated for 2 weeks prior to fluorescent staining. Red arrows point to dead cells. White arrows point to living cells. A) Overview image of the whole scaffold. B) show images taken from a stack of the whole scaffold. To the left are image rendering of the scaffold, that indicates where the image is taken from. Image i) is taken from the upper part of the scaffold, while image ii) is taken from the middle section, and image iii) is taken from the bottom section of the scaffold. C) is a 3D rendering of cells present in scaffold. The images indicate that cell growth is present throughout the scaffold.*

5.8.2 Live/Dead imaging of Biovotec ESM Scaffold

When exposed to cells in starvation medium, the scaffold maintained most of its form. When observing cells in the scaffold using fluorescent imaging, there is definite presence of both living and dead cells (see figure 5.18).

A)

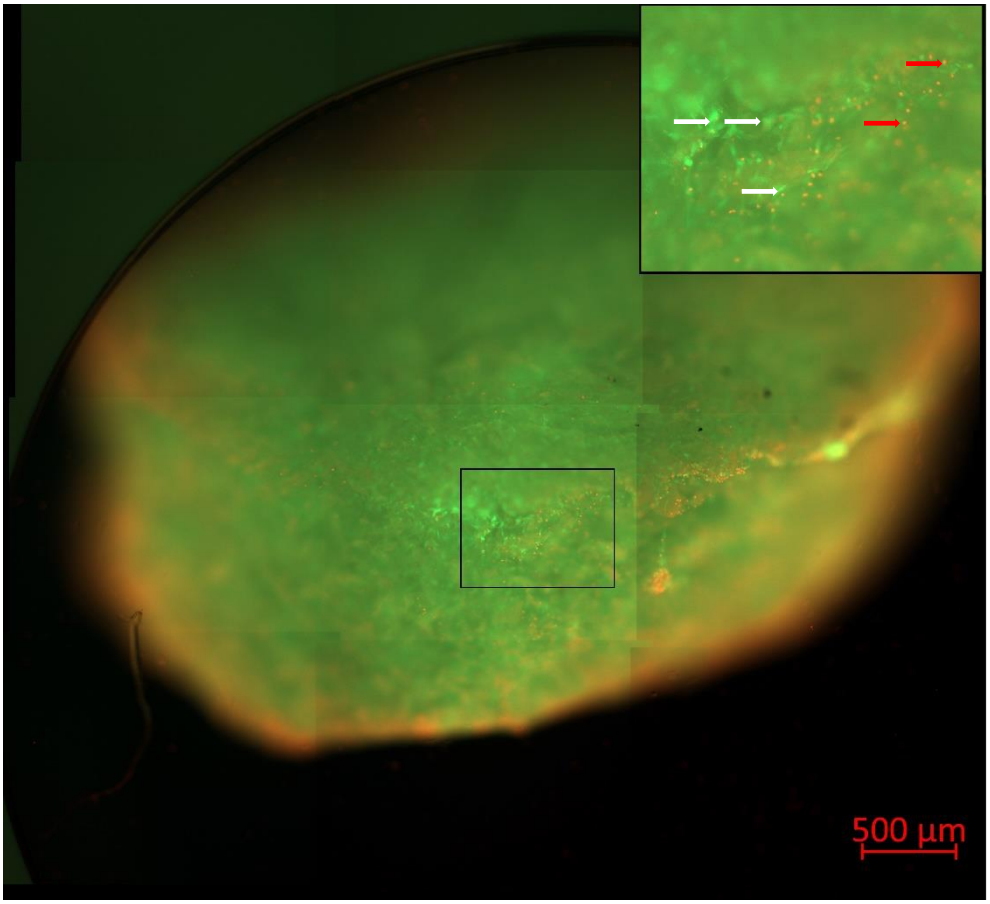

B)

i)

Top Section

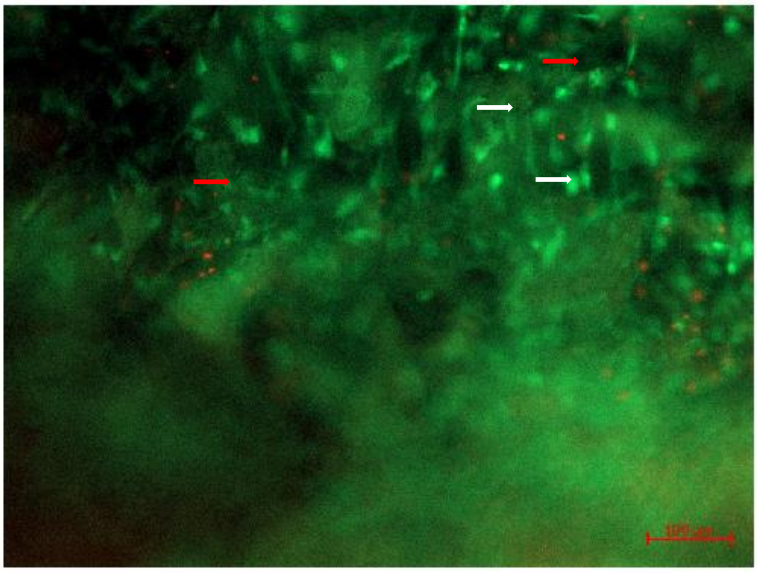

ii)

Middle Section

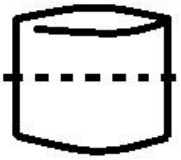

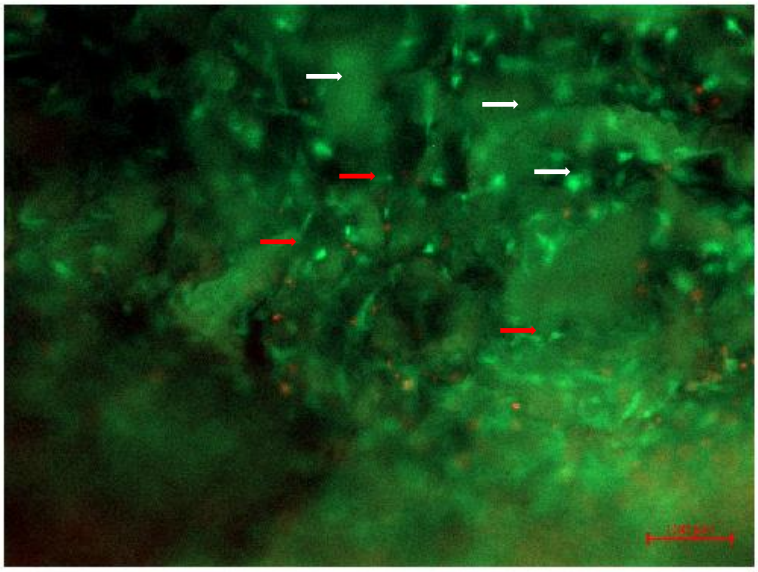

iii)

Lower Section

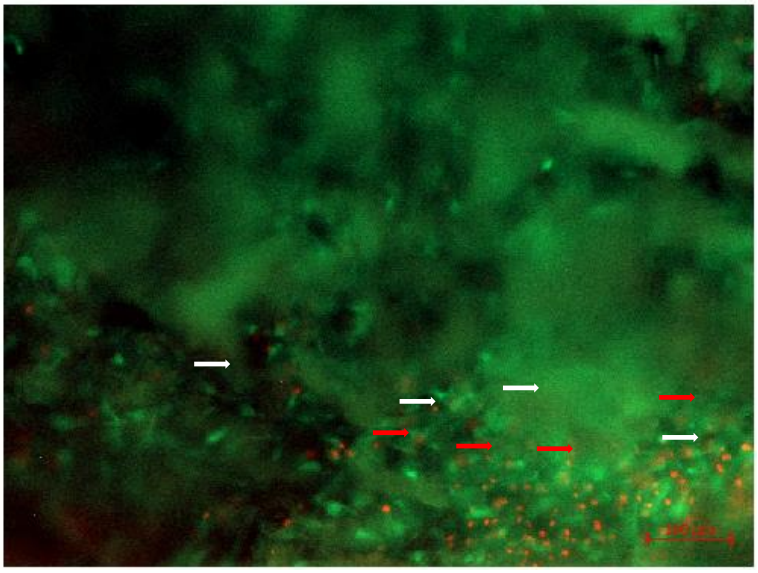

C)

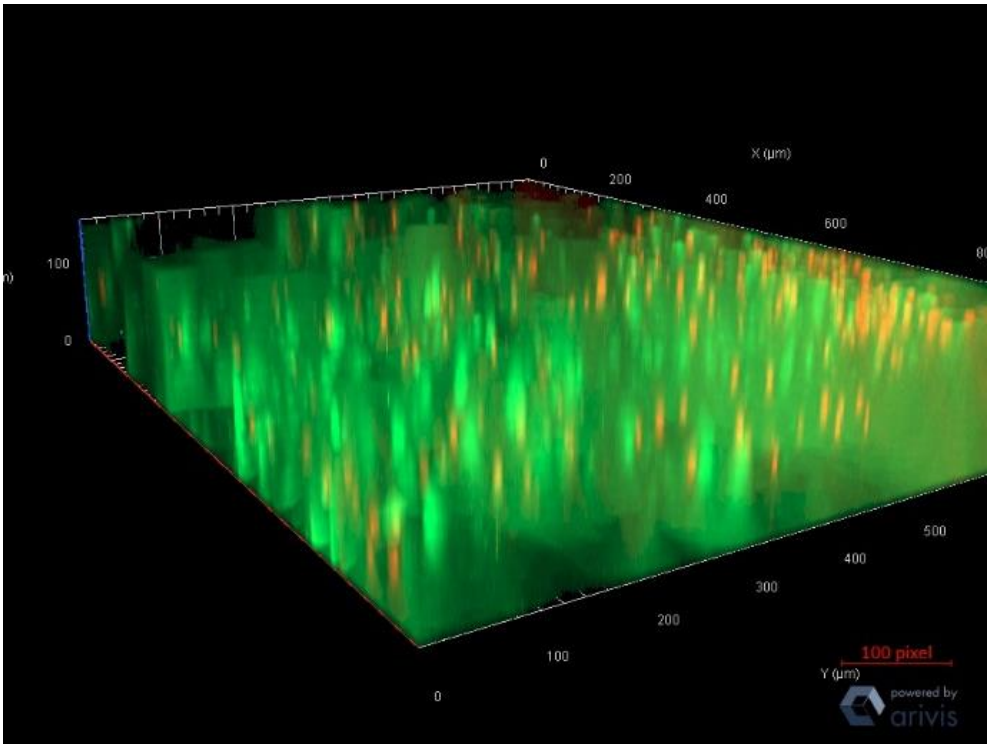

Figure 5.18: Fluorescence microscopy analysis of fibroblast cells in Biovotec ESM scaffold. *Cells were stained using Live/Dead™ Viability/Cytotoxicity kit to differentiate between living and dead cells. Cells were applied to scaffold and incubated for 2 weeks prior to fluorescent staining. Red arrows point to dead cells. White arrows point to living cells. A) Overview image of the whole scaffold. B) show images taken from a stack of the whole scaffold. To the left are image rendering of the scaffold, that indicates where the image is taken from. Image i) is taken from the upper part of the scaffold, while image ii) is taken from the middle section, and image iii) is taken from the bottom section of the scaffold. C) is a 3D rendering of cells present in scaffold. The images indicate that cell growth is present throughout the scaffold.*

5.8.3 Live/Dead imaging of Cryogel 5 Scaffold

When exposed to cells in starvation medium, the scaffold maintained its form. When observing cells in the scaffold using fluorescent imaging, there is definite presence of both living and dead cells (see figure 5.19).

A)

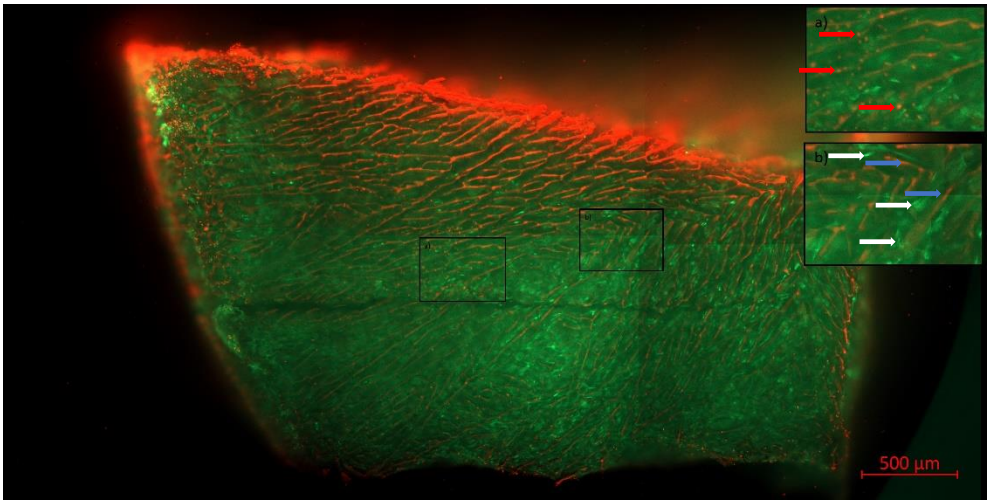

B)

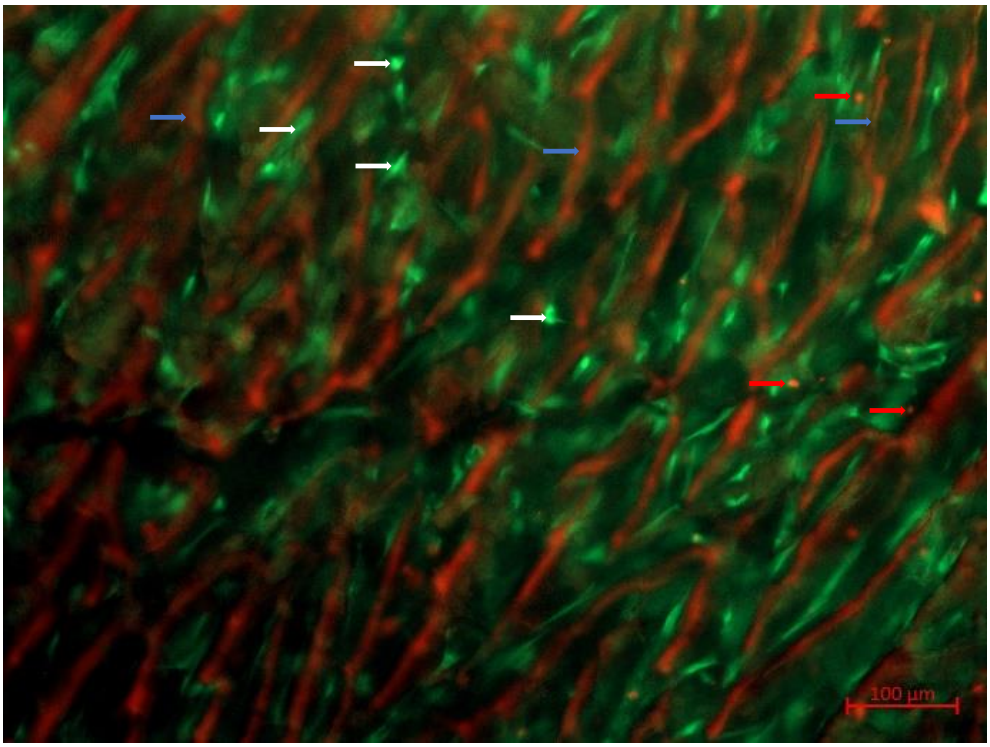

Figure 5.19: Fluorescence microscopy analysis of fibroblast cells in Cryogel 5 scaffold. *Cells were stained using Live/Dead™ Viability/Cytotoxicity kit to differentiate between living and dead cells. Cells were applied to scaffold and incubated for 2 weeks prior to fluorescent staining. Red arrows point to dead cells. White arrows point to living cells. Blue arrows point to staining of the PEGDA scaffold component. A) Overview image of the whole scaffold. B) Closeup image of scaffold.*

5.8.4 Live/Dead imaging of Cryogel 6 Scaffold

When exposed to cells in starvation medium, the scaffold maintained its form. When observing cells in the scaffold using fluorescent imaging, there is definite presence of both living and dead cells (see figure 5.20).

A)

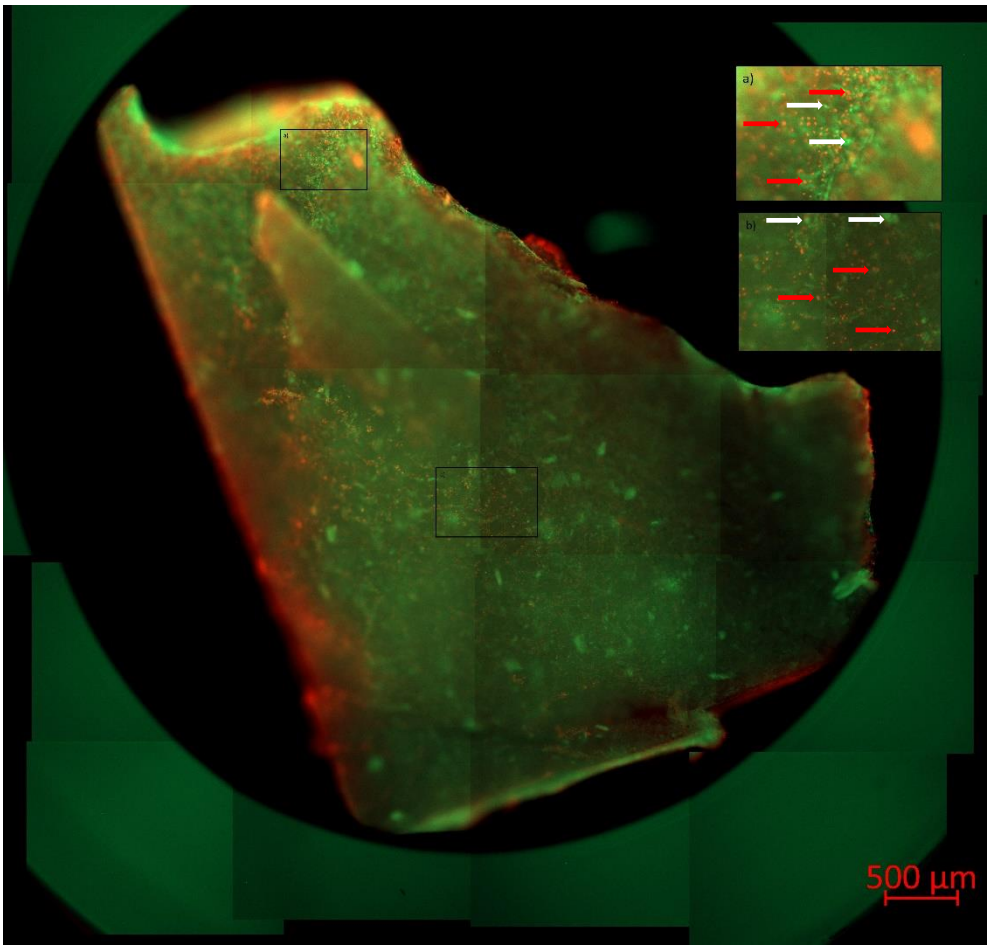

B)

i)

Top Section

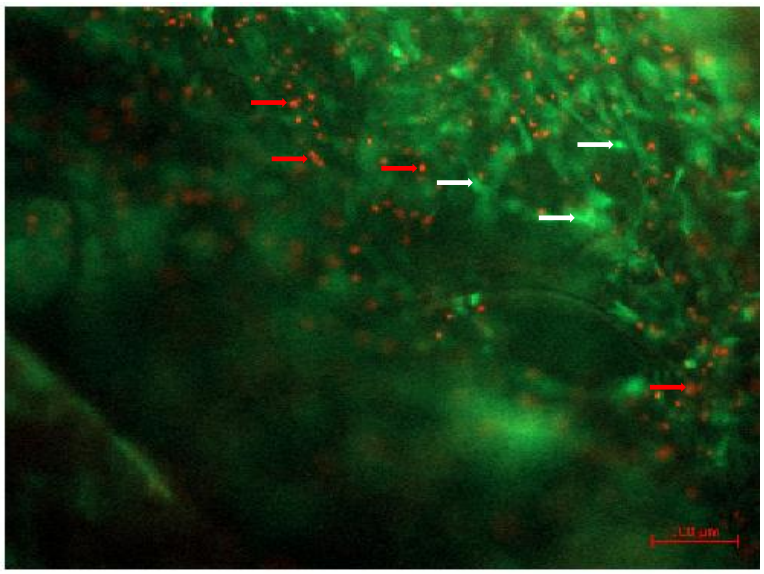

ii)

Middle Section

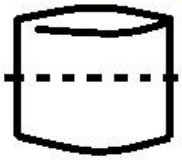

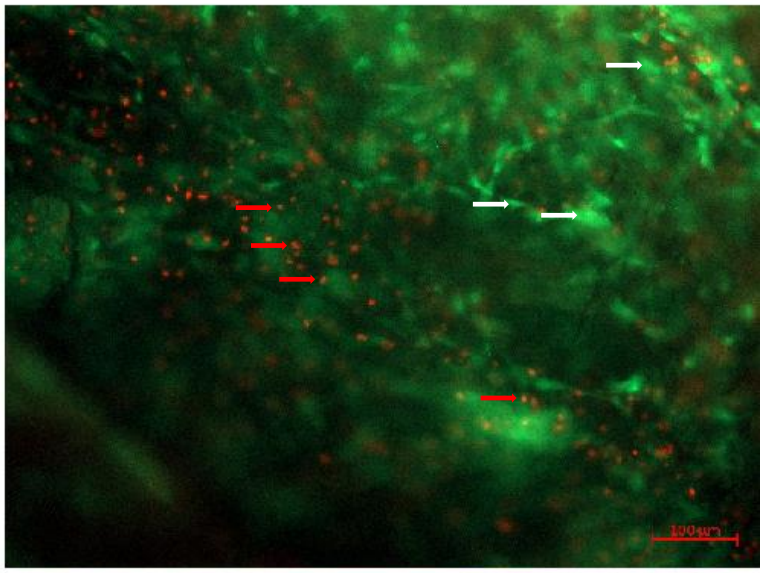

iii)

Lower Section

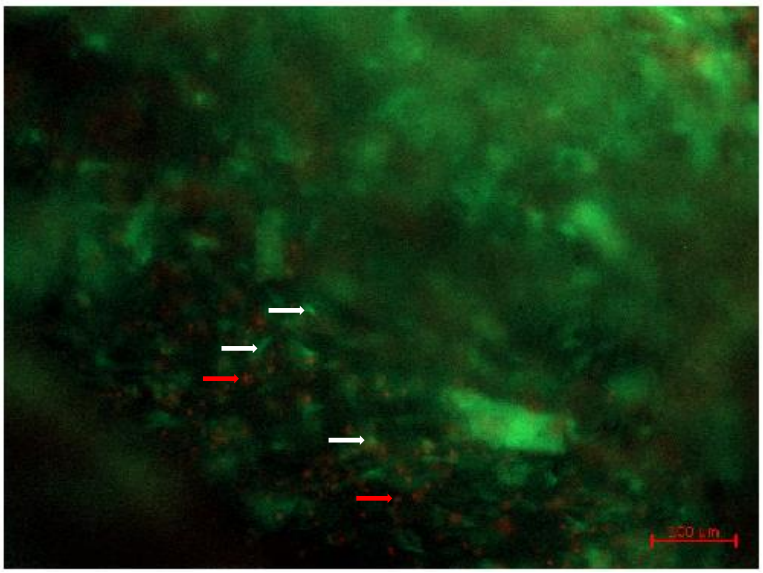

C)

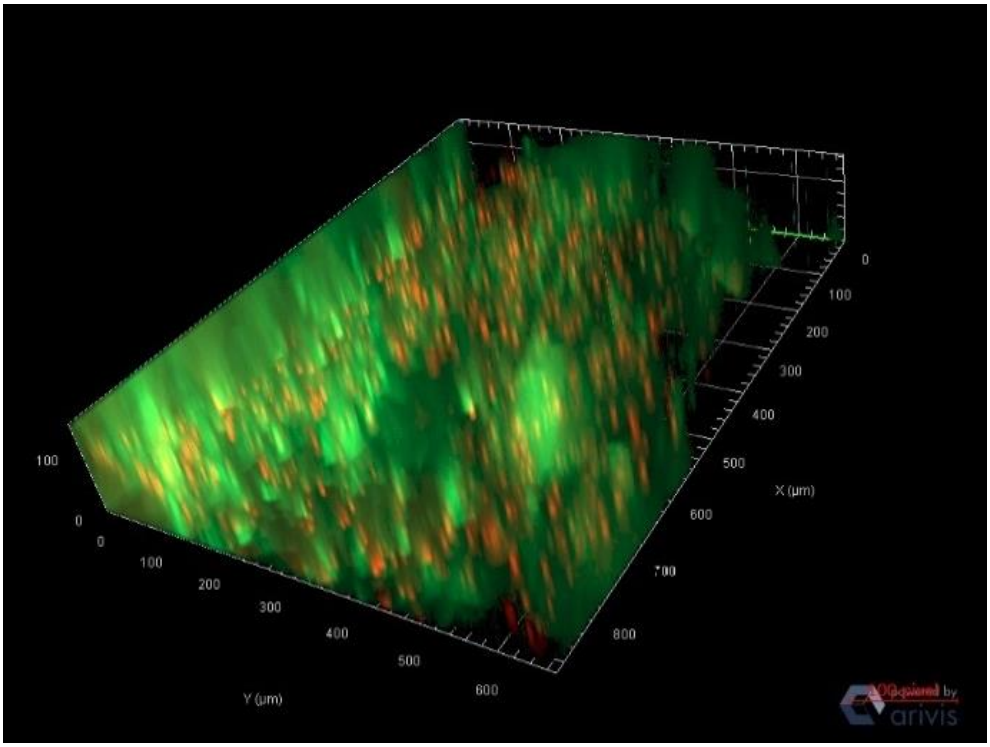

Figure 5.20: Fluorescence microscopy analysis of fibroblast cells in Cryogel 6 scaffold. *Cells were stained using Live/Dead™ Viability/Cytotoxicity kit to differentiate between living and dead cells. Cells were applied to scaffold and incubated for 2 weeks prior to fluorescent staining. Red arrows point to dead cells. White arrows point to living cells. A) Overview image of the whole scaffold. B) show images taken from a stack of the whole scaffold. To the left are image rendering of the scaffold, that indicates where the image is taken from. Image i) is taken from the upper part of the scaffold, while image ii) is taken from the middle section, and image iii) is taken from the bottom section of the scaffold. C) is a 3D rendering of cells present in scaffold. The images indicate that cell growth is present throughout the scaffold.*

5.8.5 Live/Dead imaging of Cryogel 8 Scaffold

When exposed to cells in starvation medium, the scaffold maintained its form. When observing cells in the scaffold using fluorescent imaging, there is definite presence of both living and dead cells (see figure 5.21).

A)

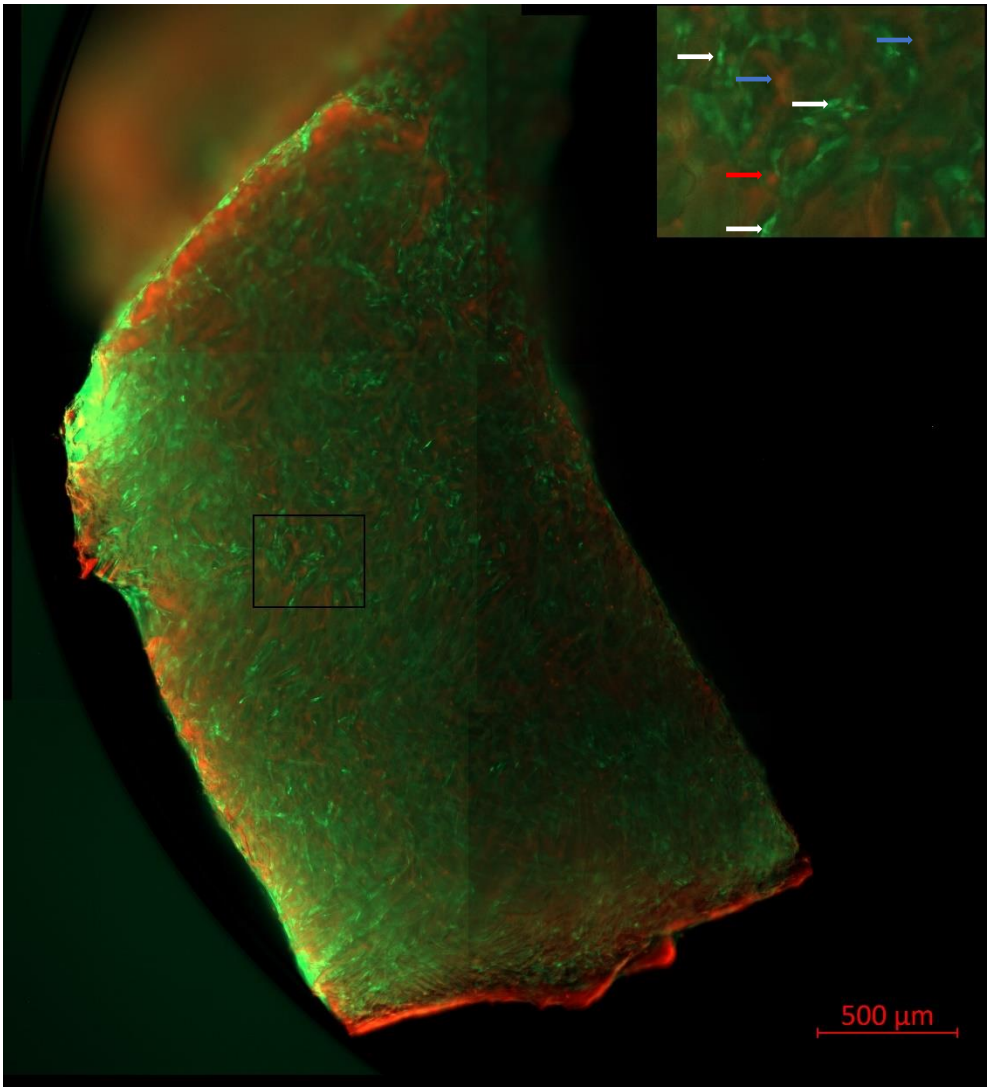

B)

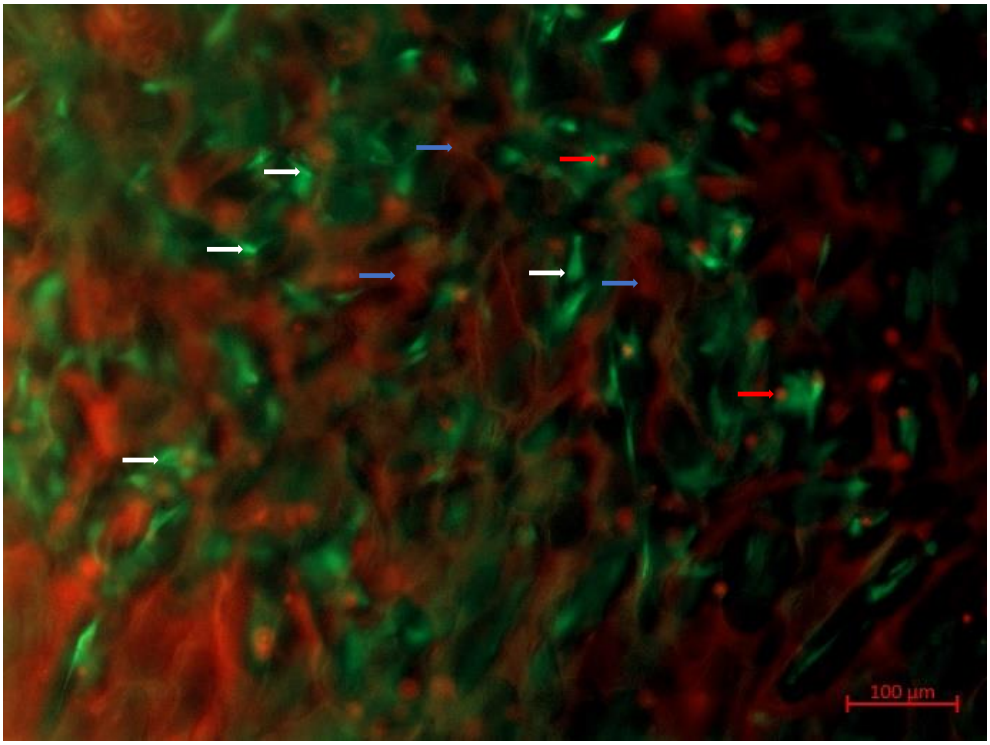

Figure 5.21: Fluorescence microscopy analysis of fibroblast cells in Cryogel 8 scaffold. *Cells were stained using Live/Dead™ Viability/Cytotoxicity kit to differentiate between living and dead cells. Cells were applied to scaffold and incubated for 2 weeks prior to fluorescent staining. Red arrows point to dead cells. White arrows point to living cells. Blue arrows point to staining of the PEGDA scaffold component. A) Overview image of the whole scaffold. B) Closeup image of scaffold.*

6. Discussion

The ongoing challenges in prevention or treatment of chronic wounds is a global health issue problem, and the economic pressure this puts on nations is immense. In addition to the economic impact it represents, the reduced life quality of individuals suffering from these illnesses makes it urgent to develop new and improved products that may be an alternative to the expensive products available on the marked today (Järbrink et al., 2017). Such innovation in the field of wound healing can in turn potentially reduce healthcare costs and improve the quality of life for numerous patients (Frykberg & Banks, 2015). An ideal wound healing material should not only accelerate wound healing, but also reduce loss of proteins and fluids from the wound, and should be cheap and minimise any risk of infection.

The use of ESM to improve wound healing is far from a new concept, and has been used in medicinal applications in several eastern countries for hundreds of years (Jia et al., 2011; Sah & Rath, 2016). In western culture however, ESM has been considered a waste material, and large amounts of ESM is disposed of annually (Jia et al., 2011). The use of ESM has been lacking a scientific understanding of effectiveness and molecular mechanism to properly explain how and if it holds a significant benefit in both general wound healing and appliance to chronic wounds (Sah & Rath, 2016). Fibroblast cells are abundant in human skin, and play a vital role in wound healing (Rittiè, 2016). ESM can potentially provide an extracellular matrix environment for the cells and enhance wound healing. Although previous studies have shown promising results, further research is sorely needed to determine in what extent ESM can contribute in facing the global health challenge of effective wound healing.

6.1 The effect of PEP on fibroblast activity

6.1.1 Fibroblast proliferation and matrix production

Fibroblast cells are important cells during the wound healing process. They possess a unique capability to produce components of the ECM, that hold importance for replacement of the injured matrix as well as wound contraction and closure. In normal skin tissue, fibroblast cells are quiescent, but following tissue injury they are activated and proliferates in the peri-wound stroma. Fibroblast cells migrate from the collagen-rich connective tissue into the provisional matrix of the wound. The cells are responsible for exchanging the initial fibrin clot with ECM structural components (Bainbridge, 2013). In addition the migration and differentiation into myofibroblast cells is vital for the formation of the granulation tissue (T. T. Vuong, 2017). As fibroblast cells are responsible for a variety of tasks,

the need for high proliferative ability to multiply is vital for rapid and healthy wound healing (Guo & DiPietro, 2010).

To determine how PEP would affect fibroblast activity, the first step was determining how high PEP concentration it was possible to use, without disrupting vital cellular mechanisms that would lead to cell death. A previous study showed no effect on cell viability when treated with ESM for a period of 3 days. This study was conducted with concentrations ranging from 0,5-3 mg/ml (T. T. Vuong, 2017). This is in line with our results, where no negative effect on cell viability (see figure 5.1) at 3 mg/ml was observed. Similar effects were also observed after 1 day stimulation. Our experiments further showed that PEP stimulation led to increased cell proliferation at both 1 and 3 days of stimulation, reflecting highly proliferating and viable cells at the time points tested (see figure 5.3). The increase in proliferation was present in all concentrations tested. However, it was determined that 1 mg/ml and 3 mg/ml of PEP would be the concentrations most suitable for further study in 2D experimentation, as these concentrations displayed only a minor toxic effect on fibroblasts (see figure 5.2), while achieving a high proliferating effect. The measurements performed on the proliferation marker Ki67 support the findings of increased proliferation (see figure 5.4) (Scholzen & Gerdes, 2000). The relative gene expression of *ki67* increased when stimulated with PEP compared with control cells at 1- and 3 days of treatment. Although both cell proliferation and *ki67* gene expression showed a significant increase in cell proliferation, we were unable to determine the optimal concentration of PEP, as *ki67* showed a higher relative gene expression following 3 days of 1 mg/ml PEP treatment, while cell proliferation measurements showed that higher concentrations resulted in higher cell proliferation. A reason for this could be that the cells used in the experiment may have consisted of a heterogenous population, and cells may have different phenotypes when experimented on at different passages. As such, some cell cultures may have a different expression rates than others (Kaur & Dufour, 2012). Although the attempt was to homogenize the cells prior to the experiments, using starvation medium, the fibroblasts were on some occasions tested at different passages between experimental repetitions. The increase in cell proliferation could be explained by the high amount of hyaluronic acid (HA) found in ESM (Tram T. Vuong et al., 2017). HA has been noted to improve cell proliferation and influence collagen synthesis (Hu et al., 2014). Collagen fibres have also been found to affect cell proliferation, which could further facilitate the increase observed (Tracy et al., 2016). Although there is debated as to whether HA does have a direct effect on fibroblast proliferation, studies has shown that there are high amounts of HA present during cell mitosis. Inhibition of HA is also found to prevent cell proliferation and mitosis (Ohara et al., 2010). In regards to HA having an indirect effect on proliferation through collagen synthesis, PEP stimulation showed no significant effect on *collagen I* gene expression (see figure 5.9), and in some instances, a negative effect on *collagen III* gene expression (see figure

5.10) during 1- and 3 days of stimulation. However, collagen V is also present in ESM, and deficiency of this protein has been shown to decrease fibroblast proliferation (DeNigris, Yao, Birk, & Birk, 2016; Tram T. Vuong et al., 2017). As the expression of collagen V was not tested in this thesis, it might be that synthesis of collagen V could have increased as a response to the high amount of HA, leading to an increase in proliferation. Another factor which may influence fibroblast proliferation is fibronectin. High levels of fibronectin has been shown to reduce fibroblast proliferation, while in contrast, fibronectin coupled with TGF-β1 increase proliferation (Sapudom et al., 2015). As there is presence of fibronectin in ESM, and TGF-β1 is expressed by myofibroblasts this could be a supporting factor for cell proliferation (Ahmed et al., 2017; Baum & Duffy, 2011). The GAG chondroitin sulphate (CS) which is also present in ESM, albeit at a far lower concentration than HA, has also been shown to have some proliferative effect on cells (Sirko, von Holst, Wizenmann, Götz, & Faissner, 2007). The high increase in proliferation found in this thesis may be the result of many factors, and to fully comprehend the process behind it, further research is required.

As fibroblast cells are responsible for the deposition and production of various ECM components, we wanted further to investigate whether PEP stimulation would affect gene expression of essential ECM components (Darby et al., 2014; Hu et al., 2014; Tram T. Vuong et al., 2017).

The ratio of collagen I and collagen III is found to affect scar tissue formation, as higher concentration of collagen III is found in fetal wound healing, which results in scarless repair (Hu et al., 2014). An inadequate or defective collagen I and III expression are commonly associated with tissue fragility and delayed wound healing and as such, could be important components to either directly insert into wound sites, or indirectly promote synthesis (Tracy et al., 2016). Our results showed little difference in the *collagen I* and *collagen III* ratio when treated with PEP, with a few exceptions and mainly in the direction of increased *collagen I* expression. The increase in *collagen I* and *collagen III* following 10 days of treatment (see figure 5.9 and figure 5.10) may be due to a larger amount of fibroblast cells having undergone differentiation. Disregarding the significant change in expression of the ECM components in some of the conditions tested, which is mainly seen through low treatment concentrations during shorter treatment periods, or during the longer treatment periods mentioned above, there is less change seen through PEP treatment than would be expected. The lack of effect on *elastin* expression (see figure 5.11) may be because elastin expression control is extensively performed at the posttranscriptional level (Mithieux & Weiss, 2005). As such, it may be better to look at the protein expression to observe any potential effect of PEP treatment. Both *collagen I* and *collagen III* may be unresponsive to PEP treatment due to insolubility of collagen proteins (Ahmed et al., 2017), making it harder for fibroblast cells to react with them. The results found is in contrast to findings from Ohto-Fujita et al., who reported that the expression pattern of ECM molecules when treated with low

concentrations of a water-soluble alkaline-digested form of eggshell membrane (ASESM) resembled the early phase of wound healing, while a high dose resembled the late phase. They found that *collagen III*, in addition to other ECM molecules not included in the testing of this thesis, had a high expression at lower concentrations, with a downward expression when treated with higher concentrations (Ohto-Fujita et al., 2011). Ohto-Fujita *et al.* also found no change in *elastin* expression level when treating fibroblast cells with ASESM, which supports the earlier statement regarding high posttranscriptional control on *elastin* expression (Mithieux & Weiss, 2005; Ohto-Fujita et al., 2011).

The results provided in this thesis (see figure 5.10), display a different trend, where lower concentrations of ESM result in a lower expression of *collagen III*, in addition to other ECM molecules. The reason for these conflicting results might be that hydrolyzation of ESM results in a higher availability of ESM components for fibroblast cells to react with. As such, to perform tests on fibroblast-ESM interactions with different methods of ESM processing may yield different results than those found in this thesis. Integrins are receptors that function as a mediator for fibroblasts to adhere to the ECM (Schwartz, 2010). As such, for future studies it may be beneficial to observe the expression of integrins to determine the potential of reaction between fibroblast cells and ESM.

6.1.2 Myo-fibroblast differentiation, stress indication and migration

Fibroblast cells will in most cases differentiate into myofibroblasts when exposed to TGF-β (Darby et al., 2014). Once differentiated they will assist in generating ECM and promote wound contraction (Bainbridge, 2013). As only myofibroblasts express α-SMA, this is often used as an indicator of the amount of differentiated fibroblast cells in a sample, and can be measured through expression of both gene and protein expression to account for any posttranscriptional modifications (Li & Wang, 2011). As such, measurement of α-SMA was used to observe whether PEP would inhibit or promote differentiation of fibroblast cells.

When comparing gene expression (see figure 5.5) with protein expression (see figure 5.6), they were inconsistent. There was large variation within protein measurements themselves, and as such large variation when compared to *α-sma* gene expression. According to Greenbaum *et al.* the reasons for observing high variations between gene and protein expression can be divided into three sections. One reason may be due to an abundance of post-transcriptional mechanisms that may affect the amount of mRNA sequences which actually undergo translation, resulting in an incomparable amount of proteins. Another reason may be due to the fact that proteins may have substantially different *in vivo* half-lives. Finally, there may be lacking suitable methods of measurement, where background noise and inaccurate experimentation may result in receiving an incorrect comparison (Greenbaum, Colangelo, Williams, & Gerstein, 2003). In regards to mRNA expression measured using real-time PCR,

any fractional difference in substrates may cause large variance in measurements. In regards to protein expression measurement using western blotting, quantification of blots may be affected by numerous factors such as background noise, uneven blots or other factors, in addition to differences between samples. In regards to the variance within the protein expression measurements, there was a lack of data to properly determine whether the mean actually showed a sufficiently correct amount, or in some cases, even determine a trend. When observing such inconsistency between results, a common factor to question the capability of the marker chosen. However, it has been stated in several studies that α-SMA is a suitable indicator for fibroblast differentiation, which leads us to believe the issue resides elsewhere (Baum & Duffy, 2011; Hinz, Celetta, Tomasek, Gabbiani, & Chaponnier, 2001). Another potential reason could be that the fibroblast cells experimented on were of a heterogeneous population, which could result in high variation in the stages of (myo)fibroblasts prior to testing.

Once successfully migrated to the wound site, myofibroblasts will secrete cytokines (TGF-β and IL-1β) that interact with receptors on the fibroblast cell membrane. This in turn activates a signalling pathway that increases transcription of α-SMA and upregulates differentiation (Baum & Duffy, 2011). Further α-SMA expression in myofibroblasts is regulated by multiple general and tissue-specific proteins that form complex combinatorial interactions with each other (Tomasek, McRae, Owens, & Haaksma, 2005). This complexity of α-SMA expression may result in a highly biphasic pattern which in turn could explain the high variations we have witnessed in this thesis (Baum & Duffy, 2011). Measuring these cytokines expressed by the myofibroblasts could assist in providing us with a further indication as to how ESM affects differentiation. To determine exactly to what extent PEP affects differentiation, further testing is necessary.

Migration of fibroblast cells into the wound site is vital for wound closure (Bielefeld et al., 2013). The chaperone protein Hsp70 is a factor in cell migration, it can be used as a marker to indicate migration (T. T. Vuong, 2017). The reduction of Hsp70 protein expression following 10 days of treatment can indicate reduced migration as a result of higher differentiation at longer treatment periods. This indication does not coincide with the results presented in α-SMA expression in this thesis, as it displays a reduction compared with the negative control. However, previous experiments performed by the research group achieved results which indicated an increase in α-SMA expression following ten days of PEP treatment, which would coincide with this hypothesis (T. T. Vuong, 2017). Hsp70 is utilized in an abundance of tasks during wound healing. As such, it may be difficult to make specific statements as to what their expression may cause. In future experiments, more specific indicators/markers might be better for determining exact effect of PEP treatment.

When introducing a foreign substance to cells, the cells will often respond to stress by activating a series of mechanisms. The Hsp70 protein is one of the proteins that is commonly expressed at a higher rate during this cellular response. It is commonly used in the cell to regulate proteins through folding, but during a stress response it can inhibit factors that would otherwise lead to apoptosis (Mayer & Bukau, 2005). As such, an increase in this protein and its mRNA preface is used as an indicator for observing the magnitude of the stress responses activated in the fibroblast cells. These include modulating inflammation, removing wound debris, enhancing cell proliferation and collagen synthesis, as well as assisting in migration (Atalay et al., 2009). As Hsp70 is expressed as a result of so many responsive mechanisms due to tissue damage, it is well suited to function as a marker to determine the level of stress response in cells. Although the gene expression showed a higher divergency of stress symptoms during longer exposure to PEP when compared to negative control, the fact that the protein expression was substantially reduced indicate that posttranscriptional modifications have down regulated the stress response. As such, it is feasible to assume that prolonged exposure to PEP does not result in a high stress reaction of the cells.

As Hsp70 is used as a stress response marker, it is important for a variety of mechanisms during wound healing. However, when measuring Hsp70 in chronic wounds there is little to no expression (Singh et al., 2015). According to an older study which found similar results in protein expression, the mRNA values did not show the same correlation, suggesting that chronic wounds have a post-transcriptional effect on *hsp70* (Oberringer et al., 1995). Singh et al. mentions that type 2 diabetes mellitus (T2DM), an illness that commonly displays chronic ulcers, have regulatory effects on HSP synthesis, which suggests that posttranscriptional downregulation of *hsp70* may negatively influence wound healing (Singh et al., 2015). As treatment with PEP had a large influence on immediate Hsp70 protein expression following 1 day of treatment (see figure 5.8A), this suggests that PEP could have implications in assisting chronic wound healing.

6.2 Including ESM in 3D tissue engineering

A suitable scaffold for tissue engineering should hold certain characteristics; it should be biocompatible so cells can adhere, migrate into and finally proliferate in the scaffold; it should be biodegradable; it should possess certain architectural characteristics with pore structure and porosity to ensure efficient diffusion of nutrients to the cells (O'Brien, 2011). In addition to ESM, the inclusion of PEGDA and collagen to 3D scaffolds was also observed, to see how these components affected the morphology of the scaffolds. The cryogels supplied by Innovent displayed smaller pockets through the scaffolds (see figure 5.14 – 5.16), which should provide a more rigid morphology. This coincides with the structural integrity PEGDA is meant to introduce to the scaffolds (Wartenberg et al., 2017). In addition to this,

we observed that when the cryogel scaffolds were introduced to medium, the cryogels maintained their structure (data not shown), unlike the scaffolds lacking PEGDA incorporation. As ESM also provide some structural integrity, the biovotec control scaffold which lack both PEGDA and ESM completely fell together when exposed to any form of liquid. This deviates from the Biovotec ESM scaffold, which maintained majority of its structural integrity, albeit somewhat less than the cryogel scaffolds. Interestingly, scaffolds which contained high amounts of ESM in addition to PEGDA displayed a far more directed structure, with thin, long wall-like structures throughout the scaffold. Although there is a chance this is an effect of cutting the scaffold prior to imaging, this can be seen in both SEM imaging (see figure 5.14) and fluorescent imaging (see figure 5.19). These images were taken at different times and from different scaffolds. As such, it is plausible that this is the result of the composition of PEGDA and high amounts of ESM, resulting in a far more rigid structure than the other scaffolds tested. As PEGDA is included primarily for structural reasons, if higher concentrations of ESM in a 3D environment is proven to have little effect on cell viability, PEGDA may prove to be obsolete. However, further testing is required before this can be determined.

The cross-linked fibrillary structure that the ESM provides may be considered a suitable biomaterial to include in scaffold aimed for tissue engineering, and has been known to provide a suitable ECM environment for fibroblast cells (Chaudhari et al., 2016; Tram T. Vuong et al., 2017). The incorporation of ESM into 3D scaffolds introduces several new challenges for experimentation, that were not present in 2D testing using PEP. There are several ways and substrates available to make these scaffolds, but to make them optimal for wound treatment, they must fulfil a variety of properties and no method is without disadvantages (Chaudhari et al., 2016). To construct an optimal scaffold, there is the issue of space distribution to enable migration through the scaffold, oxygen, nutrient and waste accessibility as well as several other factors known to hold importance for proper tissue development (Duval et al., 2017). One issue we faced was the distribution of nutrients into the scaffold. During the early testing of fibroblast seeding to 3D scaffolds, we observed no cellular activity within the scaffolds when studying both through SEM and fluorescent microscope. After several failed attempts, it was decided that we would substantially reduce the size of the scaffolds, and this resulted in cellular growth in the scaffolds (see figures 5.17-5.21). Although the medium was able to permeate into the 3D scaffolds once they were reduced about 2 mm in length, the problem still persisted when larger scaffolds were required. To overcome this challenge, a form of engineered circulatory system may need to be implemented. Working with 3D models also hold definite advantages. The increase in dimensionality will provide a better insight to the *in vivo* cellular behaviour, and has been shown to affect cell proliferation, differentiation and cell viability (Duval et al., 2017). One determining factor which showed a substantial change when transferring the experimentation to a 3D cell culture was the cell

viability of the fibroblasts when exposed to ESM. In a 2D environment, it was determined that 3 mg/ml PEP was the upper limit for testing. However, when observing ESM incorporated into a 3D model, the concentrations were as high as 50 mg/ml, and although this thesis is unable to provide any quantitative data on cell viability in a 3D scaffold, it was evident that fibroblast cells were shown to adhere and proliferate within all the scaffolds. By observing the scaffolds through fluorescent imaging, the cells appeared to properly infiltrate each of the scaffolds. Although it is difficult to make any quantitative verification as to which scaffold constitution provided the most optimal conditions for the fibroblast cells to adhere and proliferate, there seems to be a higher population of living cells in the scaffolds containing ESM. A reason to why it is difficult to make quantitative measurements from these images is that the dyes used also cross-reacted to certain compositions of the scaffolds, making it harder to differentiate between scaffold and cells at a quantitative level. However, as the red fluorescent dye also coloured the PEGDA components in the cryogel scaffolds, it enabled a unique visualization of how the fibroblast cells organize within the scaffold (see figure 5.19 and 5.21). As this thesis is situated in an early phase of understanding how the inclusion of ESM in a 3D scaffold may affect fibroblast cells, further testing will be required to determine what the optimal applicable concentration may be in a 3D model and how the supplementation of ESM might affect wound healing.

6.3 Current developments in tissue engineering

There has been an increasing focus around the tissue engineering over the last decade, and the field has seen much progress. The increased appreciation for the use of 3D scaffolds in tissue engineering has brought forth the understanding for the specificity required of a scaffold. Many different types and methods are being tested, and we are beginning to see an emergence of tissue specific scaffolds, that focuses on mimicking the characteristics of the designated ECM composition in ways that optimises its effects in wound healing (Ho, Walsh, Yue, Dardik, & Cheema, 2017). The use of scaffold in tissue engineering has achieved such attention that they were described at a National Science foundation workshop as the best materials for restoring, maintaining and improving tissue function. Although the use of 3D scaffolds in tissue engineering is producing remarkable results, there are still several factors that require improvement, and the optimal compositions of scaffolds are far from achieved. To optimize a mixture between biodegradability, biocompatibility and mechanical strength further research is still required (Chaudhari et al., 2016). Research is needed to complete a high-quality, universal bio-engineered scaffold that provides rapid wound healing with minimum scarring. As the field of bio-scaffold fabrication improves, it is highly probable that tissue-engineering techniques will become a standard tool in the future (Ho et al., 2017).

6.4 Methodical issues

The results achieved in this thesis assist in further understanding how ESM affect fibroblast cells in both 2D and 3D environments. The following chapter take into consideration the systematic and random errors to the methodological approach, due to random variation in the sample size, and potential faults in design and instruments.

The values achieved in real-time RT-PCR to observe gene expression had several obvious outliers that were not included in the final mean values. In addition to this, there were several values that by themselves did not demonstrate obvious sample errors, and were therefore included, resulting in large errors of means. Although real-time RT-PCR is a powerful method for detecting and quantifying gene expressions in cells (Pfaffl, 2012), the specificity of the method may generate large errors of mean as a result of minor differences in samples and sample preparation. Due to the difficultly of this method, an abundance of data was collected to generate a proper mean and error of mean. Although this did help reduce the spread, there is still some presence of variance within the results.

When analysing the data achieved from both real-time PCR and western blot, each time period is treated as a separate entity. To gain a greater understanding of how PEP affected fibroblast cells, it would be advantageous to compare the data of each measurement to untreated samples taken following one day of PEP treatment.

Although both gene- and protein expression was tested for 1, 3 and 10 days of PEP treatment, experiments on cell viability, cell proliferation and cytotoxic effect to ESM, were only conducted for 1 and 3 days of PEP treatment. The two time periods enabled us to see some form of trend. However, in retrospect it may have been optimal to perform these three experiments with the same time periods as real-time PCR and western blot to achieve a more complete overview and to enable the research group to better compare the results.

Both SEM and fluorescence imaging were conducted several times with the inclusion of cell culture imbedded into the scaffolds to observe how they reacted. With the exception of the two final runs using fluorescent microscopy, there was very little to no cell culture to be observed during imaging. As the method was inconsistent, the research group however discovered that the cause was due to the medium being unable to properly penetrate the scaffolds, and provide nutrients to the cells. To overcome this challenge, the scaffolds were cut into smaller pieces prior to adding cell culture. However, because of a fixed timeframe set to this thesis, we were unable to perform another run of SEM imaging with the inclusion of cell culture into the scaffolds.

7. Conclusion

This thesis has given insight to the effects ESM and its derivate PEP have on fibroblast cells and its ability to enhance and improve the wound healing mechanism in the cells. Optimal concentrations in 2D experimentation was found where PEP provided high proliferative effects, without compromising cell viability.

Through quantitative PCR measurements, we concluded that PEP assists in upregulating Hsp70, which may assist in chronic wound treatment. Measurements performed on differentiation of fibroblasts and expressions of various ECM components showed results conflicting with previous published articles and opens the field for further study into how this may have occurred.

Through testing, a critical element for enabling ESM in 3D scaffolds was explored. We were able to culture cells in all 3D scaffolds presented to them, although a higher number of cells were observed in scaffolds containing ESM. Through trial and error, it has been found that a steady influx of nutrients in the entirety of the scaffold is required for the fibroblast cells to proliferate and inhabit the environment presented for them. As such, there is a future requirement of generating an engineered circulatory system within the scaffolds, as any scaffold exceeding ~2mm in size may have problems with nutrient accessibility. Although there has been some progress as to finding the optimal composition of scaffolds, this is far from concluded, and further research will be required.

8. Further Research

Further testing will be required to properly determine exactly how ESM affects the differentiation of fibroblasts, either through another marker, or through a higher number of samples in western blot to account for posttranscriptional modifications of α-SMA. In regards to gene expression, it will be important to maintain a homogenous cell culture. Although data was accumulated for 3 different time periods, there was not enough time to analyse the data against an untreated, initial measurement (negative control, 1 day). Given enough time, a further understanding of how treatment with PEP would affect fibroblast cells over time in regards to proliferation, differentiation, stress response and ECM production could be discovered.

As earlier mentioned, the increase in dimensionality will provide a better insight to the *in vivo* cellular behaviour, and has been shown to affect cell proliferation, differentiation and cell viability (Duval et al., 2017). In the future, further testing to optimize the correct composition of scaffold components is required. The research group will require additional scaffolds, with smaller variations in their composition to observe which holds the highest merit. To achieve this, a more specific dye composition may be required to enable quantitative measurements of living/dead cells within the scaffolds.

9. References

Ahmed, T. A. E., Suso, H.-P., & Hincke, M. T. (2017). In-depth comparative analysis of the chicken eggshell membrane proteome. *Journal of Proteomics, 155*(Supplement C), 49-62. doi:https://doi.org/10.1016/j.jprot.2017.01.002

Atalay, M., Oksala, N., Lappalainen, J., Laaksonen, D. E., Sen, C. K., & Roy, S. (2009). HEAT SHOCK PROTEINS IN DIABETES AND WOUND HEALING. *Current protein & peptide science, 10*(1), 85-95.

Augustin, M. (2013). Cumulative life course impairment in chronic wounds. *Curr Probl Dermatol, 44*, 125-129. doi:10.1159/000350789

Bainbridge, P. (2013). Wound healing and the role of fibroblasts. *J Wound Care, 22*(8), 407-408, 410-412. doi:10.12968/jowc.2013.22.8.407

Baum, J., & Duffy, H. S. (2011). Fibroblasts and Myofibroblasts: What are we talking about? *Journal of cardiovascular pharmacology, 57*(4), 376-379. doi:10.1097/FJC.0b013e3182116e39

Bielefeld, K. A., Amini-Nik, S., & Alman, B. A. (2013). Cutaneous wound healing: recruiting developmental pathways for regeneration. *Cellular and Molecular Life Sciences, 70*(12), 2059-2081. doi:10.1007/s00018-012-1152-9

Biosystems, A. (2008). Guide to performing relative quantitation of gene expression using real-time quantitative PCR. In (pp. 52-59): Applied Biosystems.

Chan, B. P., & Leong, K. W. (2008). Scaffolding in tissue engineering: general approaches and tissue-specific considerations. *European Spine Journal, 17*(Suppl 4), 467-479. doi:10.1007/s00586-008-0745-3

Chaudhari, A. A., Vig, K., Baganizi, D. R., Sahu, R., Dixit, S., Dennis, V., . . . Pillai, S. R. (2016). Future Prospects for Scaffolding Methods and Biomaterials in Skin Tissue Engineering: A Review. *International Journal of Molecular Sciences, 17*(12), 1974. doi:10.3390/ijms17121974

Clark, R. A. (2001). Fibrin and wound healing. *Ann N Y Acad Sci, 936*, 355-367.

Darby, I. A., Laverdet, B., Bonté, F., & Desmoulière, A. (2014). Fibroblasts and myofibroblasts in wound healing. *Clin Cosmet Investig Dermatol, 7*, 301-311. doi:10.2147/ccid.s50046

Dario, P., Laschi, C., Micera, S., Vecchi, F., Zecca, M., Menciassi, A., . . . C. Carrozza, M. (2003). *Biologically-Inspired Microfabricated Force and Position Mechano-Sensors*.

DeNigris, J., Yao, Q., Birk, E. K., & Birk, D. E. (2016). Altered dermal fibroblast behavior in a collagen V haploinsufficient murine model of classic Ehlers-Danlos syndrome. *Connective tissue research, 57*(1), 1-9. doi:10.3109/03008207.2015.1081901

Duval, K., Grover, H., Han, L.-H., Mou, Y., Pegoraro, A. F., Fredberg, J., & Chen, Z. (2017). Modeling Physiological Events in 2D vs. 3D Cell Culture. *Physiology, 32*(4), 266-277. doi:10.1152/physiol.00036.2016

Fischer, E. R., Hansen, B. T., Nair, V., Hoyt, F. H., & Dorward, D. W. (2012). Scanning Electron Microscopy. *Current Protocols in Microbiology, CHAPTER*, Unit2B.2-Unit2B.2. doi:10.1002/9780471729259.mc02b02s25

Frantz, C., Stewart, K. M., & Weaver, V. M. (2010). The extracellular matrix at a glance. *Journal of Cell Science, 123*(24), 4195-4200. doi:10.1242/jcs.023820

Frykberg, R. G., & Banks, J. (2015). Challenges in the Treatment of Chronic Wounds. *Adv Wound Care (New Rochelle), 4*(9), 560-582. doi:10.1089/wound.2015.0635

Gould, L., Abadir, P., Brem, H., Carter, M., Conner-Kerr, T., Davidson, J., . . . Schmader, K. (2015). Chronic Wound Repair and Healing in Older Adults: Current Status and Future Research. *Journal of the American Geriatrics Society, 63*(3), 427-438. doi:10.1111/jgs.13332

Greenbaum, D., Colangelo, C., Williams, K., & Gerstein, M. (2003). Comparing protein abundance and mRNA expression levels on a genomic scale. *Genome Biology, 4*(9), 117. doi:10.1186/gb-2003-4-9-117

Guo, S., & DiPietro, L. (2010). Factors Affecting Wound Healing. *J Dent Res, 89*(3), 219-229. doi:10.1177/0022034509359125

Haddon, C. M., & Lewis, J. H. (1991). Hyaluronan as a propellant for epithelial movement: the development of semicircular canals in the inner ear of Xenopus. *Development, 112*(2), 541-550.

Heid, C. A., Stevens, J., Livak, K. J., & Williams, P. M. (1996). Real time quantitative PCR. *Genome Res, 6*(10), 986-994.

Hinz, B., Celetta, G., Tomasek, J. J., Gabbiani, G., & Chaponnier, C. (2001). Alpha-Smooth Muscle Actin Expression Upregulates Fibroblast Contractile Activity. *Molecular Biology of the Cell, 12*(9), 2730-2741.

Hinz, B., Mastrangelo, D., Iselin, C. E., Chaponnier, C., & Gabbiani, G. (2001). Mechanical Tension Controls Granulation Tissue Contractile Activity and Myofibroblast Differentiation. *The American Journal of Pathology, 159*(3), 1009-1020.

Ho, J., Walsh, C., Yue, D., Dardik, A., & Cheema, U. (2017). Current Advancements and Strategies in Tissue Engineering for Wound Healing: A Comprehensive Review. *Adv Wound Care (New Rochelle), 6*(6), 191-209. doi:10.1089/wound.2016.0723

Hu, M. S., Maan, Z. N., Wu, J. C., Rennert, R. C., Hong, W. X., Lai, T. S., . . . Lorenz, H. P. (2014). Tissue engineering and regenerative repair in wound healing. *Ann Biomed Eng, 42*(7), 1494-1507. doi:10.1007/s10439-014-1010-z

Jia, J., Guo, Z., Yu, J., & Duan, Y. (2011). A New Candidate for Guided Tissue Regeneration: Biomimetic Eggshell Membrane. *Journal of Medical Hypotheses and Ideas*.

Järbrink, K., Ni, G., Sönnergren, H., Schmidtchen, A., Pang, C., Bajpai, R., & Car, J. (2017). The humanistic and economic burden of chronic wounds: a protocol for a systematic review. *Systematic Reviews, 6*, 15. doi:10.1186/s13643-016-0400-8

Karp, G. (2010). *Cell and molecular biology: Concepts and experiments*.

Kaur, G., & Dufour, J. M. (2012). Cell lines: Valuable tools or useless artifacts. *Spermatogenesis, 2*(1), 1-5. doi:10.4161/spmg.19885

Krafts, K. P. (2010). Tissue repair: The hidden drama. *Organogenesis, 6*(4), 225-233. doi:10.4161/org.6.4.12555

Kumar, A., Mishra, R., Reinwald, Y., & Bhat, S. (2010). Cryogels: Freezing unveiled by thawing. *Materials Today, 13*(11), 42-44. doi:https://doi.org/10.1016/S1369-7021(10)70202-9

Li, B., & Wang, J. H. C. (2011). Fibroblasts and Myofibroblasts in Wound Healing: Force Generation and Measurement. *Journal of tissue viability, 20*(4), 108-120. doi:10.1016/j.jtv.2009.11.004

Lindahl U, C. J., Kimata K, et al. . (2017). *Proteoglycans and Sulfated Glycosaminoglycans* (3 ed.). Cold Spring Harbor (NY).

Mahmood, T., & Yang, P.-C. (2012). Western Blot: Technique, Theory, and Trouble Shooting. *North American Journal of Medical Sciences, 4*(9), 429-434. doi:10.4103/1947-2714.100998

Martin, P. (1997). Wound healing--aiming for perfect skin regeneration. *Science, 276*(5309), 75-81.

Mayer, M. P., & Bukau, B. (2005). Hsp70 chaperones: Cellular functions and molecular mechanism. *Cellular and Molecular Life Sciences, 62*(6), 670-684. doi:10.1007/s00018-004-4464-6

Menke, N. B., Ward, K. R., Witten, T. M., Bonchev, D. G., & Diegelmann, R. F. (2007). Impaired wound healing. *Clin Dermatol, 25*(1), 19-25. doi:10.1016/j.clindermatol.2006.12.005

Mithieux, S. M., & Weiss, A. S. (2005). Elastin. *Adv Protein Chem, 70*, 437-461. doi:10.1016/s0065-3233(05)70013-9

Mustoe, T. A., O'Shaughnessy, K., & Kloeters, O. (2006). Chronic wound pathogenesis and current treatment strategies: a unifying hypothesis. *Plast Reconstr Surg, 117*(7 Suppl), 35s-41s. doi:10.1097/01.prs.0000225431.63010.1b

Nicot, N., Hausman, J. F., Hoffmann, L., & Evers, D. (2005). Housekeeping gene selection for real-time RT-PCR normalization in potato during biotic and abiotic stress. *J Exp Bot, 56*(421), 2907-2914. doi:10.1093/jxb/eri285

O'Brien, F. J. (2011). Biomaterials & scaffolds for tissue engineering. *Materials Today, 14*(3), 88-95. doi:https://doi.org/10.1016/S1369-7021(11)70058-X

Oberringer, M., Baum, H. P., Jung, V., Welter, C., Frank, J., Kuhlmann, M., . . . Hanselmann, R. G. (1995). Differential expression of heat shock protein 70 in well healing and chronic human wound tissue. *Biochem Biophys Res Commun, 214*(3), 1009-1014. doi:10.1006/bbrc.1995.2386

Ohara, H., Ichikawa, S., Matsumoto, H., Akiyama, M., Fujimoto, N., Kobayashi, T., & Tajima, S. (2010). Collagen-derived dipeptide, proline-hydroxyproline, stimulates cell proliferation and hyaluronic acid synthesis in cultured human dermal fibroblasts. *J Dermatol, 37*(4), 330-338. doi:10.1111/j.1346-8138.2010.00827.x

Ohto-Fujita, E., Konno, T., Shimizu, M., Ishihara, K., Sugitate, T., Miyake, J., . . . Atomi, Y. (2011). Hydrolyzed eggshell membrane immobilized on phosphorylcholine polymer supplies extracellular matrix environment for human dermal fibroblasts. *Cell Tissue Res, 345*(1), 177-190. doi:10.1007/s00441-011-1172-z

Pankov, R., & Yamada, K. M. (2002). Fibronectin at a glance. *J Cell Sci, 115*(Pt 20), 3861-3863.

Pfaffl, M. W. (2012). Quantification strategies in real-time polymerase chain reaction. *Martin Filion, Hg., Quantitative real-time PCR in Applied Microbiology*, 53-62.

Rittiè, L. (2016). Cellular mechanisms of skin repair in humans and other mammals. doi:DOI 10.1007/s12079-016-0330-1

Rose, M. L., & Hincke, M. T. (2009). Protein constituents of the eggshell: eggshell-specific matrix proteins. *Cell Mol Life Sci, 66*(16), 2707-2719. doi:10.1007/s00018-009-0046-y

Rozario, T., & DeSimone, D. W. (2010). The Extracellular Matrix In Development and Morphogenesis: A Dynamic View. *Developmental biology, 341*(1), 126-140. doi:10.1016/j.ydbio.2009.10.026

Rønsen, J. H. (2012). *Kostnader for behandling av kroniske leggsår i hjemmesykepleien.* (Master), UIO, Retrieved from https://www.duo.uio.no/handle/10852/34211

Sah, M. K., & Rath, S. N. (2016). Soluble eggshell membrane: A natural protein to improve the properties of biomaterials used for tissue engineering applications. *Materials Science and Engineering: C, 67*(Supplement C), 807-821. doi:https://doi.org/10.1016/j.msec.2016.05.005

Sapudom, J., Rubner, S., Martin, S., Thoenes, S., Anderegg, U., & Pompe, T. (2015). The interplay of fibronectin functionalization and TGF-[small beta]1 presence on fibroblast proliferation, differentiation and migration in 3D matrices. *Biomaterials Science, 3*(9), 1291-1301. doi:10.1039/C5BM00140D

Schaefer, L., & Schaefer, R. M. (2010). Proteoglycans: from structural compounds to signaling molecules. *Cell Tissue Res, 339*(1), 237-246. doi:10.1007/s00441-009-0821-y

Schmittgen, T. D., & Livak, K. J. (2008). Analyzing real-time PCR data by the comparative CT method. *Nature protocols, 3*(6), 1101-1108.

Scholzen, T., & Gerdes, J. (2000). The Ki-67 protein: from the known and the unknown. *J Cell Physiol, 182*(3), 311-322. doi:10.1002/(sici)1097-4652(200003)182:3<311::aid-jcp1>3.0.co;2-9

Schwartz, M. A. (2010). Integrins and Extracellular Matrix in Mechanotransduction. *Cold Spring Harb Perspect Biol, 2*(12), a005066. doi:10.1101/cshperspect.a005066

Singh, K., Agrawal, N. K., Gupta, S. K., Mohan, G., Chaturvedi, S., & Singh, K. (2015). Decreased expression of heat shock proteins may lead to compromised wound healing in type 2 diabetes mellitus patients. *Journal of Diabetes and its Complications, 29*(4), 578-588. doi:https://doi.org/10.1016/j.jdiacomp.2015.01.007

Sirko, S., von Holst, A., Wizenmann, A., Götz, M., & Faissner, A. (2007). Chondroitin sulfate glycosaminoglycans control proliferation, radial glia cell differentiation and neurogenesis in neural stem/progenitor cells. *Development, 134*(15), 2727-2738. doi:10.1242/dev.02871

Sotiropoulou, P. A., & Blanpain, C. (2012). Development and homeostasis of the skin epidermis. *Cold Spring Harb Perspect Biol, 4*(7), a008383. doi:10.1101/cshperspect.a008383

Su, Y., & Richmond, A. (2015). Chemokine Regulation of Neutrophil Infiltration of Skin Wounds. *Adv Wound Care (New Rochelle), 4*(11), 631-640. doi:10.1089/wound.2014.0559

Thomas, M. G., Marwood, R. M., Parsons, A. E., & Parsons, R. B. (2015). The effect of foetal bovine serum supplementation upon the lactate dehydrogenase cytotoxicity assay: Important

considerations for in vitro toxicity analysis. *Toxicology in Vitro, 30*(1, Part B), 300-308. doi:https://doi.org/10.1016/j.tiv.2015.10.007

Tomasek, J. J., McRae, J., Owens, G. K., & Haaksma, C. J. (2005). Regulation of α-Smooth Muscle Actin Expression in Granulation Tissue Myofibroblasts Is Dependent on the Intronic CArG Element and the Transforming Growth Factor-β1 Control Element. *The American Journal of Pathology, 166*(5), 1343-1351.

Tracy, L. E., Minasian, R. A., & Caterson, E. J. (2016). Extracellular Matrix and Dermal Fibroblast Function in the Healing Wound. *Adv Wound Care (New Rochelle), 5*(3), 119-136. doi:10.1089/wound.2014.0561

Vuong, T. T. (2017). *Processed eggshell membrane powder regulates cellular functions and increase MMP-activity important in early wound healing processes*. Nofima.

Vuong, T. T., Rønning, S. B., Suso, H.-P., Schmidt, R., Prydz, K., Lundström, M., . . . Pedersen, M. E. (2017). The extracellular matrix of eggshell displays anti-inflammatory activities through NF-κB in LPS-triggered human immune cells. *Journal of Inflammation Research, 10*, 83-96. doi:10.2147/JIR.S130974

Wartenberg, A., Weisser, J., Thein, S., Suso, H.-P., Schmidt, R., & Schnabelrauch, M. (2017). Cryogels as potential scaffolds for wound healing applications. *Journal of Medical Materials and Technologies*(2), 26-29%V 21. doi:10.24354/medmat.v1i2.20

Werdin, F., Tennenhaus, M., Schaller, H.-E., & Rennekampff, H.-O. (2009). Evidence-based Management Strategies for Treatment of Chronic Wounds. *Eplasty, 9*, e19.

World Health Organization. (2017). Diabetes Fact sheet. Retrieved from http://www.who.int/mediacentre/factsheets/fs312/en/

Wyller, V. B. (2016). *Frisk, Cellebiologi, anatomi, fysiologi* (3 ed. Vol. 3): Cappelen Damm (p. 502-507).

Norges miljø- og biovitenskapelige universitet
Noregs miljø- og biovitskapelege universitet
Norwegian University of Life Sciences

Postboks 5003
NO-1432 Ås
Norway